University of Alberta

Elemental Speciation by Capillary Electrophoresis - Inductively Coupled Plasma Mass Spectrometry

By

Jianqi Wang ©

A thesis submitted to the Faculty of Graduate Studies and Research in partial fulfillment of the requirements for the degree of Doctor of Philosophy

Department of Chemistry

Edmonton, Alberta

Fall, 2001

National Library
of Canada

Acquisitions and
Bibliographic Services

395 Wellington Street
Ottawa ON K1A 0N4
Canada

Bibliothèque nationale
du Canada

Acquisitions et
services bibliographiques

395, rue Wellington
Ottawa ON K1A 0N4
Canada

Your file Votre référence

Our file Notre référence

The author has granted a non-exclusive licence allowing the National Library of Canada to reproduce, loan, distribute or sell copies of this thesis in microform, paper or electronic formats.

L'auteur a accordé une licence non exclusive permettant à la Bibliothèque nationale du Canada de reproduire, prêter, distribuer ou vendre des copies de cette thèse sous la forme de microfiche/film, de reproduction sur papier ou sur format électronique.

The author retains ownership of the copyright in this thesis. Neither the thesis nor substantial extracts from it may be printed or otherwise reproduced without the author's permission.

L'auteur conserve la propriété du droit d'auteur qui protège cette thèse. Ni la thèse ni des extraits substantiels de celle-ci ne doivent être imprimés ou autrement reproduits sans son autorisation.

0-612-69013-X

Canada

University of Alberta

Library Release Form

Name of Author:	Jianqi Wang
Title of Thesis:	Elemental Speciation by Capillary Electrophoresis - Inductively Coupled Plasma Mass Spectrometry
Degree:	Doctor of Philosophy
Year this Degree Granted:	2001

Permission is hereby granted to the University of Alberta Library to reproduce single copies of this thesis and to lend or sell such copies for private, scholarly or scientific research purposes only.

The author reserves all other publication and other rights in association with the copyright in the thesis, and except as herein before provided, neither the thesis nor any substantial portion thereof may be printed or otherwise reproduced in any material form whatever without the author's prior written permission.

Jianqi Wang

337-3158 Cardenas Terrace
Fremont, California
USA 94536

Date: Sept.28, 2001

University of Alberta

Faculty of Graduate Studies and Research

The undersigned certify that they have read, and recommend to the Faculty of Graduate Studies and Research for acceptance, a thesis entitled **Elemental Speciation by Capillary Electrophoresis - Inductively Coupled Plasma Mass Spectrometry** submitted by **Jianqi Wang** in partial fulfillment of the requirements for the degree of **Doctor of Philosophy**.

Gary Horlick
Dr. Gary Horlick, Supervisor

CAL
Dr. Frederick F. Cantwell

Dr. Charles A. Lucy

steven Bergens
Dr. Steve H. Bergens

Gregg Taylor
Dr. Greg J. Taylor

ED Salin
Dr. Eric D. Salin, External Examiner

Date: Oct 1, 2001

To Simin and Romy

Abstract

The quantitative speciation of Cr, V, Sb and As was studied in this thesis by coupling capillary electrophoresis (CE) with inductively coupled plasma mass spectrometry (ICP-MS) using a lab-built direct injection nebulizer (DIN) interface.

The quantitative speciation of Cr(III) / Cr(VI) and V(IV) / V(V) was achieved based on the fact that different oxidation states of the two species bear the opposite charges under certain pH conditions and migrate to the opposite directions in an electrical field. Separation was performed using a sample stacking technique to focus the two species of opposite polarity to the opposite ends of a sample plug. Both sensitivity and resolution of Cr(III) / Cr(VI) and of V(IV) / V(V) peaks increased with increasing the length of the sample plug. The presence of a suction-induced flow toward the detector did not cause any significant band broadening; rather it allowed the simultaneous separation of both species in a single run in a shorter analysis time, without the need for sample pre-complexation or conversion. The method showed good repeatability and linearity in addition to a wide linear dynamic range (3 to 4 orders of magnitude). Concentration detection limits at the ppb levels and absolute detection limits at the pg levels were realized.

The quantitative speciation of Sb(III) / Sb(V) and As(III) / As(V) was achieved using a sample stacking technique with removal of the sample matrix. The problem of broadened peak shape of Sb(III)-tartrate complex, $[Sb_2(C_4H_2O_6)_2]^{2-}$, a standard for Sb(III), was solved by converting it into an EDTA complex, $Sb(EDTA)^-$. The optimal conditions for speciation of Sb(III) / Sb(V) and As(III) / As(V) were established by a systematic optimization of the various parameters. Linear dynamic range extended over two orders of magnitude. Concentration detection limits were at the ~0.2 ppb level and the absolute

detection limits were at the ~0.1 pg level. The concentration detection limits can be reduced further to the low ppt level by using a modified method of field-amplified electrokinetic injection. The accuracy of the method was verified by determination of Sb(III) and Sb(V) in synthetic standard mixtures using both internal and external standardization.

Acknowledgements

I would like to thank my supervisor, Professor Gary Horlick for his invaluable advice and guidance during the course of this work. I would also like to thank Mr. Youbin Shao for his assistance and valuable suggestions. Thanks to all members of the research group for their comments and helpful discussions.

I would also like to acknowledge the professional staff of electronics, machining, and glass shops of the Chemistry Department for their first rate support.

Finally, I would like to thank the Department of Chemistry for financial support and for providing an excellent environment for graduate study.

TABLE OF CONTENTS

CHAPTER PAGE

1. Introduction 1
    - 1.1 Elemental Speciation 1
    - 1.2 Capillary Electrophoresis 2
        - 1.2.1 Electrophoretic Mobility 3
        - 1.2.2 Electroosmotic Flow 4
        - 1.2.3 Efficiency and Resolution 7
        - 1.2.4 Sample Injection and Detection 9
    - 1.3 Inductively Coupled Plasma Mass Spectrometry 11
        - 1.3.1 Inductively Coupled Plasma (ICP) 11
        - 1.3.2 Mass Spectrometer (MS) 13
        - 1.3.3 ICP-MS-Advantages and Limitations 16
    - 1.4 Interfacing CE with ICP-MS 17
        - 1.4.1 Interfaces Based on Conventional Concentric Nebulizer 17
        - 1.4.2 Interfaces Based on High Efficiency Nebulizer 18
        - 1.4.3 Interfaces Based on Microconcentric Nebulizer 18
        - 1.4.4 Interfaces Based on Ultrasonic Nebulizer 19
        - 1.4.5 Interfaces Based on Direct Injection Nebulizer 20
    - 1.5 References 21
2 Instrumentation 24
    - 2.1 Introduction 24
    - 2.2 Instrumental Setup 24
        - 2.2.1 CE Unit 24
        - 2.2.2 CE-ICP-MS Interface 26

2.2.3 Optimization of the CE-ICP-MS Interface 28
2.2.3.1 Optimization of the Positioning of the Sheath Flow Capillary 30
2.2.3.2 Optimization of the Nebulizer Gas Flow 30
2.2.3.3 Optimization of the Sheath Liquid Flow 31
2.2.3.4 Optimization of the Makeup Gas Flow 34
2.2.3.5 Stability of the CE-DIN-ICP-MS Coupling 34
2.2.4 ICP-MS 37
2.3 References 43
3 Quantitative Speciation of Chromium 44
3.1 Introduction 44
3.2 Experimental 51
3.2.1 Chemical Reagents 51
3.2.2 Instrumentation 51
3.2.3 Sample Injection 53
3.3 Results and Discussion 54
3.3.1 On-line Concentration Method 54
3.3.2 Identification of Chromium Species 58
3.3.3 Optimization of Electrostacking Parameters 58
3.3.3.1 Choice of Background Electrolyte 60
3.3.3.2 Effect of pH of Background Electrolyte on Electrostacking 60
3.3.3.3 Effect of pH of Sample on Electrostacking 61
3.3.3.4 Effect of Applied Voltages on Electrostacking 63
3.3.3.5 Effect of Injection Volume on Electrostacking 69
3.3.4 Quantitative Speciation 72
3.3.4.1 Calibration Curves 72

3.3.4.2 Limits of Detection 75
3.3.4.3 Matrix Effects 75
3.4 Conclusions 77
3.5 References 80
4 Quantitative Speciation of Vanadium 83
4.1 Introduction 83
4.2 Experimental 93
4.2.1 Chemical Reagents 93
4.2.2 Instrumentation 95
4.2.3 Sample Injection 95
4.3 Results and Discussion 96
4.3.1 Optimization of Sample Stacking Parameters 96
4.3.1.1 Choice of Background Electrolyte 96
4.3.1.2 Choice of Applied Voltage and Injection Volume 97
4.3.1.3 Effect of pH of Sample on Vanadium Speciation 97
4.3.2 Quantitative Speciation 103
4.3.2.1 Calibration Curves 103
4.3.2.2 Limits of Detection 105
4.3.3 Multi-element (Chromium and Vanadium) Speciation 108
4.4 Conclusions 110
4.5 References 113
5 Quantitative Speciation of Antimony 117
5.1 Introduction 117
5.2 Experimental 122
5.2.1 Chemical Reagents 122
5.2.2 Instrumentation 122

5.2.3 Sample Injection 124

5.3 Results and Discussion 125

5.3.1 Development of CE Procedure 125

5.3.1.1 Sample Stacking without Sample Matrix Removal 125

5.3.1.2 Sample Stacking with Sample Matrix Removal 128

5.3.2 Optimization of CE Parameters 132

5.3.2.1 Choice of CE Buffer 132

5.3.2.2 Effect of the Addition of EDTA to Sample on Antimony Separation 134

5.3.2.3 Effect of Stacking and Separation Voltage on Antimony Separation 139

5.3.2.4 Effect of pH of Sample on Antimony Separation 142

5.3.2.5 Effect of pH of CE Buffer on Antimony Separation 146

5.3.2.6 Effect of Suction-induced Flow on Antimony Separation 149

5.3.2.7 Effect of Injection Volume on Antimony Separation 150

5.3.3 Quantitative Speciation 157

5.3.3.1 Calibration Curves 157

5.3.3.2 Limits of Detection 157

5.3.3.3 Speciation of Antimony in Synthetic Standard Mixtures 159

5.4 Conclusions 162

5.5 References 163

6 Quantitative Speciation of Arsenic 167

6.1 Introduction 167

6.2 Experimental 173

6.2.1 Chemical Reagents 173

6.2.2 Instrumentation 175
6.2.3 Sample Injection 176
6.3 Results and Discussion 176
6.3.1 Choice of pH of Sample and Buffer 176
6.3.2 Sample Stacking without Removal of Sample Matrix 177
6.3.3 Sample Stacking with Removal of Sample Matrix 179
6.3.3.1 Effect of Stacking and Separation Voltage on the Arsenic Separation 180
6.3.3.2 Effect of Injection Volume on the Arsenic Separation 182
6.3.3.3 Calibration Curves 186
6.3.3.4 Limits of Detection 189
6.3.4 On-line Concentration by Field-amplified Electrokinetic Injection 189
6.4 Conclusions 196
6.5 References 197
7 Summary and Future Work 202
7.1 Summary 202
7.1.1 DIN Interface for CE-ICP-MS 202
7.1.2 Speciation of Chromium and Vanadium 203
7.1.3 Speciation of Antimony and Arsenic 204
7.2 Future Work 205
7.3 References 207

LISTS OF TABLES

TABLE PAGE

2.01 Effect of the nebulizer gas flow rate on the suction-induced flow rate 32

2.02 Effect of the sheath liquid flow rate on the suction-induced flow rate 32

2.03 ICP-MS operating parameters 42

3.01 Effect of applied voltages on peak area, peak height, peak width, and peak separation 68

3.02 Effect of injection volume on peak area, peak height, peak width, and peak separation 71

3.03 Analytical figures of merit for the speciation of chromium by CE-DIN-ICP-MS 76

4.01 Summary of methods for vanadium speciation 85

4.02 Vanadium (V) species and formation constants (β) in aqueous solution 90

4.03 Analytical figures of merit for the speciation of vanadium by CE-DIN-ICP-MS 107

5.01 Summary of methods for antimony speciation 119

5.02 Effect of stacking voltage on antimony speciation 140

5.03 Effect of sample pH on migration time, peak area, peak width, and peak separation 144

5.04 Effect of buffer pH on migration time, peak area, peak width, and peak separation 148

5.05 Effect of injection volume on peak area, peak height, peak width, and peak separation 154

5.06 Analytical figures of merit for the speciation of antimony (III) and antimony (V) by CE-DIN-ICP-MS 160

5.07 Quantitative speciation of Sb (III) and Sb (V) in synthetic standard mixtures 161

6.01 Summary of CE methods for speciation of As (III) and As (V) 170

6.02 Effect of injection volume on peak area, peak height, peak width, and peak separation 185

6.03 Analytical figures of merit for arsenic speciation by CE-DIN-ICP-MS after sample stacking with sample matrix removal 190

6.04 Analytical figures of merit for arsenic speciation by CE-DIN-ICP-MS with field-amplified electrokinetic injection 195

LISTS OF FIGURES

FIGURE **PAGE**

1.01 Schematic diagram of the electric double layer and the potential distribution 5

1.02 Schematic diagram of the arrangement of a quadrupole mass filter 14

1.03 a-q stability diagram of a quadrupole mass filter 14

2.01 Schematic diagram of the instrumental setup 25

2.02 Schematic diagram of the DIN interface for coupling CE with ICP-MS (not drawn to scale) 27

2.03 Schematic diagram showing position of the DIN interface inside the ICP torch 29

2.04 Dependence of signal intensities of Rh (in sheath liquid) and Y(in CE background electrolyte) on the sheath liquid flow rate. Nebulizer gas flow rate: 0.55 L/min. Makeup gas flow rate: 0.66 L/min 33

2.05 Dependence of signal intensities of Rh (in sheath liquid) and Y (in CE background electrolyte) on the makeup gas flow rate. Nebulizer gas flow rate: 0.55 L/min. Sheath liquid flow rate: 30 μL/min 35

2.06 Plots of signal intensities of Rh (in sheath liquid) and Y (in CE background electrolyte) vs. time with and without the applied voltage. Nebulizer gas flow rate: 0.55 L/min. Makeup gas flow rate: 0.66 L/min. Sheath liquid flow rate: 30 μL/min 36

2.07 Schematic diagram of the main components of Perkin-Elmer SCIEX ELAN 5000A ICP-MS system used in this thesis 38

3.01 Fractional composition diagram for chromium(III) as a function of pH 50

3.02 Dependence of Cr(VI) species distribution on pH and total chromium concentration of (a) 10^{-3} M and (b) 10^{-5} M 52

3.03 Schematic diagram showing the stacking processes: (a) sample injection by suction, (b) capillary transfer, (c) application of voltage (+10 kV) and suction, (d) analyte stacking 55

3.04 Electropherogram for a sample solution containing Cr(III) and Cr(VI) at 1 ppm each. Conditions: background electrolyte, 50 mM $Ca(NO_3)_2$ at pH 2.0; sample pH, 3.0; applied voltage, +10 kV; injection volume, 0.60 µL 57

3.05 Electropherograms for (a) 1 ppm Cr(III), (b) 1 ppm Cr(VI) and (c) sample containing Cr(III) and Cr(VI) at 1 ppm each. Conditions as in Fig. 3.04 59

3.06 Electropherograms of 1 ppm each Cr(III) and Cr(VI) solution with a background electrolyte pH of (a) 6.0 and (b) 2.0. Other conditions as in Fig. 3.04 62

3.07 Electropherograms of 1 ppm each Cr(III) and Cr(VI) sample solution with pH of (a) 5.0 and (b) 3.0. Other conditions as in Fig. 3.04 64

3.08 Electropherograms of 1 ppm each Cr(III) and Cr(VI) sample solution with pH of (a) 5.0 and (b) 3.0. Conditions as in Fig. 3.04 except 50 mM HNO_3 (pH 1.3) was used as the background electrolyte 65

3.09 Electropherograms of 1ppm each Cr(III) and Cr(VI) solutions with different applied voltages (6-15 kV). Conditions: background electrolyte, 50 mM $Ca(NO_3)_2$ at pH 2.0; sample pH, 3.0; injection volume, 0.60 µL; 67

3.10 Electropherograms of 1ppm each Cr(III) and Cr(VI) solutions with different injection volume (0.20-1.0 µL). Conditions: background electrolyte, 50 mM $Ca(NO_3)_2$ at pH 2.0; sample pH, 3.0; applied voltage, +10 kV 70

3.11 Plots of peak area (a) and peak height (b) versus injection volume. Conditions as in Table 3.02 73

3.12 Calibration curves for Cr(III) and Cr(VI). Conditions: background electrolyte, 50 M $Ca(NO_3)_2$ at pH 2.0; sample pH, 3.0; applied voltage, +10 kV; injection volume,0.60 µL 74

3.13 Electropherograms of 1ppm each Cr(III) and Cr(VI) solutions with sample matrix of (a) 1mM HNO_3, (b) 10 mM HNO_3 and (c) 10 mM $NaNO_3$. Conditions: background electrolyte, 50 mM $Ca(NO_3)_2$ at pH 2.0; applied voltage,+10 kV; injection volume, 0.60 μL 78

4.01 Species distribution of vanadium (IV) as a function of pH for a total vanadium concentration of 10^{-5} M. Dashed lines were estimated where reliable equilibrium data are not available [39] 89

4.02 Predominant vanadium (V) species as a function of total vanadium concentration and pH. (a) From Ref.[45]. (b)From Ref.[54] 91

4.03 Fractional composition diagram for vanadium (V) as a function of pH in very dilute aqueous solution 94

4.04 Electropherograms of (a) 1 ppm V(IV) and (b) 1 ppm V(V) at sample pH 1.7. Conditions: background electrolyte, 50 mM $Ca(NO_3)_2$ at pH 2.0; injection volume, 0.60 μL; applied voltage, +10 kV 99

4.05 Electropherograms of (a) 1 ppm V(IV) and (b) 1 ppm V(V) and (c) 1 ppm V(IV)/V(V) at sample pH 2.2. Conditions as in Figure 4.04 101

4.06 Electropherograms of (a) 1 ppm V(IV) and (b) 1 ppm V(V) and (c) 1 ppm V(IV)/V(V) at sample pH 3.1. Conditions as in Figure 4.04 102

4.07 Electropherogram for a sample solution containing V(IV) and V(V) at 1 ppm each. Conditions: background electrolyte, 50 mM $Ca(NO_3)$2 at pH 2. Sample pH,3.1; applied voltage, +10kV; injection volume, 0.60 μL 104

4.08 Calibration curves V(IV) and V(V). Conditions: background electrolyte, 5 mM $Ca(NO_3)_2$ at pH 2.0; sample pH, 3.1; applied voltage, +10 kV; injection volume, 0.60 μL 106

4.09 Electropherograms for a sample solution containing V(IV), V(V), Cr(III) and Cr(VI) at 1 ppm each. Conditions: background electrolyte, 50 mM $Ca(NO_3)_2$ at pH 2.0; sample pH, 3.0; applied voltage, +10kV;

injection volume, 0.60 µL 109

4.10 Electropherograms for a sample solution containing V(IV) and Cr(VI) at 1 ppm (20 µM) each. Conditions as in Figure 4.09 111

5.01 Fractional composition diagram for antimony (V) as a function of pH in very dilute aqueous solution 123

5.02 Electropherograms for solutions containing (a) 1 ppm Sb(V) and (b) 1 ppm Sb(III). Conditions: buffer, 20 mM $(NH_4)H_2PO_4$ at pH 4.6; sample pH, 5.2; injection volume, 0.63 µL; applied voltage, +20 kV 126

5.03 Structure of the Sb(III)-tartrate complex anion 127

5.04 Electropherograms for solutions containing (a) 1 ppm Sb(V)/Sb(III) and (b) 1 ppm Sb(V) /Sb(III) and 0.4 mM Na_2H_2EDTA. Conditions as in Fig.5.02 129

5.05 Schematic diagram showing the electrostacking with sample matrix removal: (a) sample injection by suction, (b) application of voltage (–20 kV) and no suction, (c) pumping sample matrix out of capillary by EOF while the anions stack up at the boundary, (d) voltage polarity switching (–20 kV→+20 kV), (e) normal CE separation with suction flow 131

5.06 Electropherograms for solutions containing (a) 1 ppm each Sb(III)/Sb(V), (b) 1 ppm Sb(III) and (c) 1 ppm Sb(V). Conditions: buffer, 20 mM EDTA at pH 4.6; sample, 0.4 mM EDTA at pH 5.6; injection volume, 0.63 µL; stacking voltage, –20 kV; separation voltage, +20 kV 133

5.07 Electropherograms for sample solutions containing Sb(III) and Sb(V) (1 ppm each) and 0.4 mM EDTA using (a) 20 mM phthalate and (b) 15 mM plus 5 mM EDTA as the running buffer. Other conditions as in Fig. 5.06 135

5.08 Electropherograms for sample solutions containing Sb(III) and Sb(V) (1 ppm each) with different EDTA concentration added in the sample.

Other conditions as in Fig.5.06 137

5.09 Plots of peak areas (arbitrary units) for Sb(III) and Sb(V) as a function of EDTA concentration added in the sample. Conditions as in Fig.5.06 138

5.10 Electropherograms for sample solutions containing Sb(III) and Sb(V) (1 ppm each) and 0.4 mM EDTA with different separation voltage (15-25 kV) applied. Other conditions as in Fig.5.06 141

5.11 Electropherograms for solutions containing Sb(III) and Sb(V) (1 ppm each) and 0.4 mM EDTA with different sample pH (3.2-11.0). Other conditions as in Fig.5.06 143

5.12 Electropherograms for solutions containing (a) 1 ppm Sb(III), (b) 1ppm Sb(V) , and (c) Sb(III) and Sb(V) (1 ppm each) at sample pH 3.2. Other conditions as in Fig.5.06 145

5.13 Electropherograms for sample solutions containing Sb(III) and Sb(V) (1 ppm each) and 0.4 mM EDTA with different running buffer pH (3.6-5.6). Other conditions as in Fig.5.06 147

5.14 Electropherograms for sample solutions containing Sb(III) and Sb(V) (1 ppm each) in the presence of different suction flow rate: (a),0.26 μL/min; (b), 0.21 μL/min; (c), 0.16 μL/min. Other conditions as in Fig.5.06 151

5.15 Electropherograms of Sb(III) and Sb(V) (1ppm each)solutions with different injection volume (0.11-1.1 μL). Conditions as in Fig.5.06 153

5.16 Plots of peak areas for Sb(III) and Sb(V) versus injection volume. Conditions as in Table 5.05 156

5.17 Calibration curves for Sb(III) and Sb(V). Conditions: running buffer, 20 mM EDTA at pH 4.6; sample, 0.4 mM EDTA at pH 5.6; injection volume, 0.63 μL; stacking voltage, –20 kV; separation voltage, +20 kV 158

6.01 Fractional composition diagrams for arsenic(III) (a) and arsenic(V) (b) as a function of pH in dilute aqueous solution 174

6.02 Electropherogram for a sample solution containing As(III) and As(V) at 1 ppm each. Conditions: running buffer, 20 mM phosphate at pH 11.0; sample pH, 11.0; applied voltage, +20 kV; injection volume, 0.63 μL 178

6.03 Electropherograms for solutions containing (a) 100 ppb each As(III) and As(V), (b) 100 ppb As(III), and (c) 100 ppb As(V). Conditions: running buffer, 20 mM $Na_2B_4O_7$ at pH 10.0; sample pH, 10.0; stacking voltage, −15 kV; separation voltage, +20 kV; injection volume, 0.63 μL 181

6.04 Electropherograms for a test solution containing 100 ppb each As(III) and As(V) with different separation voltages (10-25 kV) applied. Other conditions as in Fig. 6.03 183

6.05 Electropherograms for a test solution containing 100 ppb each As(III) and As(V) with different injection volumes (0.11-1.05 μl). Other conditions as in Fig. 6.03 184

6.06 Plots of peak areas for As(III) and As(V) versus injection volumes. Conditions as in Fig. 6.05 187

6.07 Calibration curves for As(III) and As(V). Conditions as in Fig.6.03. 188

6.08 Schematic diagram showing the modified field-amplified sample injection: (a) hydrodynamic injection of water plug, (b) electrokinetic injection of sample, (c) pumping water plug out of capillary by EOF while the anions stack up at the boundary, (d) EOF balanced with suction flow, (e) normal CE separation after polarity switching 192

6.09 Calibration curves for As(III) and As(V) with the modified field-amplified electrokinetic injection. Conditions: running buffer, 20 mM $Na_2B_4O_7$ at pH 10.0, sample pH, 10.0; suction flow rate, 0.21 μL/min; injection voltage, −20 kV; injection time, 60 s; separation voltage, +20 kV 194

6.02 Electropherogram for a sample solution containing As(III) and As(V) at 1 ppm each. Conditions: running buffer, 20 mM phosphate at pH 11.0; sample pH, 11.0; applied voltage, +20 kV; injection volume, 0.63 µL 178

6.03 Electropherograms for solutions containing (a) 100 ppb each As(III) and As(V), (b) 100 ppb As(III), and (c) 100 ppb As(V). Conditions: running buffer, 20 mM $Na_2B_4O_7$ at pH 10.0; sample pH, 10.0; stacking voltage, −15 kV; separation voltage, +20 kV; injection volume, 0.63 µL 181

6.04 Electropherograms for a test solution containing 100 ppb each As(III) and As(V) with different separation voltages (10-25 kV) applied. Other conditions as in Fig. 6.03 183

6.05 Electropherograms for a test solution containing 100 ppb each As(III) and As(V) with different injection volumes (0.11-1.05 µl). Other conditions as in Fig. 6.03 184

6.06 Plots of peak areas for As(III) and As(V) versus injection volumes. Conditions as in Fig. 6.05 187

6.07 Calibration curves for As(III) and As(V). Conditions as in Fig.6.03. 188

6.08 Schematic diagram showing the modified field-amplified sample injection: (a) hydrodynamic injection of water plug, (b) electrokinetic injection of sample, (c) pumping water plug out of capillary by EOF while the anions stack up at the boundary, (d) EOF balanced with suction flow, (e) normal CE separation after polarity switching 192

6.09 Calibration curves for As(III) and As(V) with the modified field-amplified electrokinetic injection. Conditions: running buffer, 20 mM $Na_2B_4O_7$ at pH 10.0, sample pH, 10.0; suction flow rate, 0.21 µL/min; injection voltage, −20 kV; injection time, 60 s; separation voltage, +20 kV 194

Chapter 1

Introduction

1.1 Elemental Speciation

Elemental speciation can be defined as the identification and quantification of the different chemical forms and oxidation states an element can take within a given sample. Its importance arises from the fact that the toxicity and biological activity of an element is strongly dependent on its chemical forms and oxidation states. Determination of these specific forms and oxidation states would be more meaningful than that of the total element content to predict the possible impact on the environment and human health. Elemental speciation also plays an important role in environmental studies since the accumulation, transport and removal of metal pollutants are highly species dependent. Recognition of these facts has motivated a strong interest in elemental speciation over the past decade, as reflected by the increasing number of reports of applications in the toxicological, biomedical, and environmental sciences. More recently four analytical journals have published special issues devoted to speciation [1-4].

Requirements for elemental speciation have led to the development of various analytical techniques. Gas chromatography (GC) and high performance liquid chromatography (HPLC) coupled with atomic absorption spectrometry (AAS), inductively coupled plasma atomic emission (ICP-AES) or mass spectrometry (ICP-MS) are frequently used approaches [5-10]. ICP-MS is one of the most sensitive element selective techniques, with multi-element detection capability, relatively few chemical interferences and good tolerance to difficult sample matrices [11]. ICP-MS as an element-specific detector has proven to be well suited for HPLC, making HPLC-ICP-MS one of the most popular methods for elemental speciation [10].

Over the past decade, capillary electrophoresis (CE) has gained great acceptance as a powerful separation technique for inorganic species [12-24]. Recently the potential and usefulness of CE for metal speciation analysis have been reviewed [25]. Capillary electrophoresis as a separation technique offers several advantages over HPLC, including high separation efficiency, small sample volume requirements, low buffer consumption rate, simple instrumentation and short analysis time [20]. For speciation purpose CE has another important advantage: there are no chemical interactions between the analytes and the stationary phase. In HPLC, those interactions may shift the equilibrium between analytes, which can lead to erroneous results in the quantitative speciation analysis [25]. The superior separation potentials of CE combined with the highly sensitive and element-specific detection capability of ICP-MS, make CE-ICP-MS one of the most promising and powerful analytical techniques in elemental speciation.

1.2 Capillary Electrophoresis

Electrophoresis is the migration of charged species in an electrolyte solution under the influence of an electric field. Cations migrate toward the cathode, and anions migrate toward the anode. Neutral species have no electromigration. Traditional electrophoresis has been performed in a support medium such as a slab gel or paper. An important function of the support media is to reduce the convection and diffusion that leads to band broadening. Nevertheless, only relatively low voltages can be applied before Joule heating effect causes significant loss of resolution. Low applied voltage means the analysis time has to be long in order to achieve the desired separation.

The introduction of glass capillaries in electrophoresis by Jorgensen and Lukacs [26,27] in 1981 brought profound changes to the field of electrophoresis and ultimately led to the development of capillary electrophoresis. Narrow bore (25-100μm) capillaries have high surface-to-volume ratios that enable effective heat dissipation through the capillary walls. This makes it possible to use high voltages to achieve high efficiency separations and short analysis times. Capillary electrophoresis has grown rapidly to become a collection of several related techniques that involve the application of electric fields over narrow bore capillaries to achieve separations. These techniques include capillary zone electrophoresis (CZE), capillary gel electrophoresis (CGE), capillary isoelectric focusing (CIEF), capillary isotachophoresis (CITP), micellar electrokinetic capillary chromatograph (MECC), and capillary electrochromatography (CEC). In the area of elemental speciation, CZE is currently the most used technique among all CE modes. The basic principles underlying this technique will be discussed in this section.

1.2.1 Electrophoretic Mobility

In CZE, separation is based on the differential migration of ions in solution under the influence of an electric field. Different ions have different electrophoretic mobilities and therefore migrate through the capillary at different speeds. For a spherical particle with charge q and radius r moving through a fluid of viscosity η, the electrophoretic mobility (μ_{ep}) is described by Equation (1.1):

$$\mu_{ep} = \frac{q}{6\pi\eta r} \tag{1.1}$$

The electrophoretic velocity (υ_{ep}) is given by Equation (1.2), where E is the electric field strength.

$$\upsilon_{ep} = \mu_{ep} E \tag{1.2}$$

As seen from Equations (1.1) and (1.2), for a given electric field, the electrophoretic velocities of ions in solution depend on their charge/size ratio.

1.2.2 Electroosmotic Flow

Capillary electrophoresis is commonly performed in fused silica capillaries. The inside wall of a fused silica capillary is covered with silanol (Si–OH) groups that ionize in contact with a high pH electrolyte solution. The negative surface charge (Si–O$^-$) results in the formation of an electric double layer as shown in Figure 1.01. A tightly adsorbed layer of cations and molecules, called the Stern layer, is established at the wall surface to partially neutralize the negative charge. Ions in this layer are immobile, even under the influence of an electric field. The remaining surface charge is neutralized by the excess cations in the diffuse part of the double layer. Ions in this layer are mobile. When a voltage is applied across the capillary, the excess cations in the diffuse layer start to migrate toward the cathode, and since they are solvated by water, the bulk solution is dragged along with them. The net result is a bulk flow of liquid in the same direction. The movement of liquid by an electric field is called electroosmotic flow (EOF). The magnitude of EOF is given by Smoluchowski Equation [28]:

$$\upsilon_{eo} = \frac{\varepsilon\zeta}{\eta} E \tag{1.3}$$

where υ_{eo} is electroosmotic velocity, ε is the dielectric constant of the electrolyte, η is the viscosity, and ζ is the potential (ψ_1) at the interface between the Stern layer and the diffuse layer as shown in Figure 1.01.

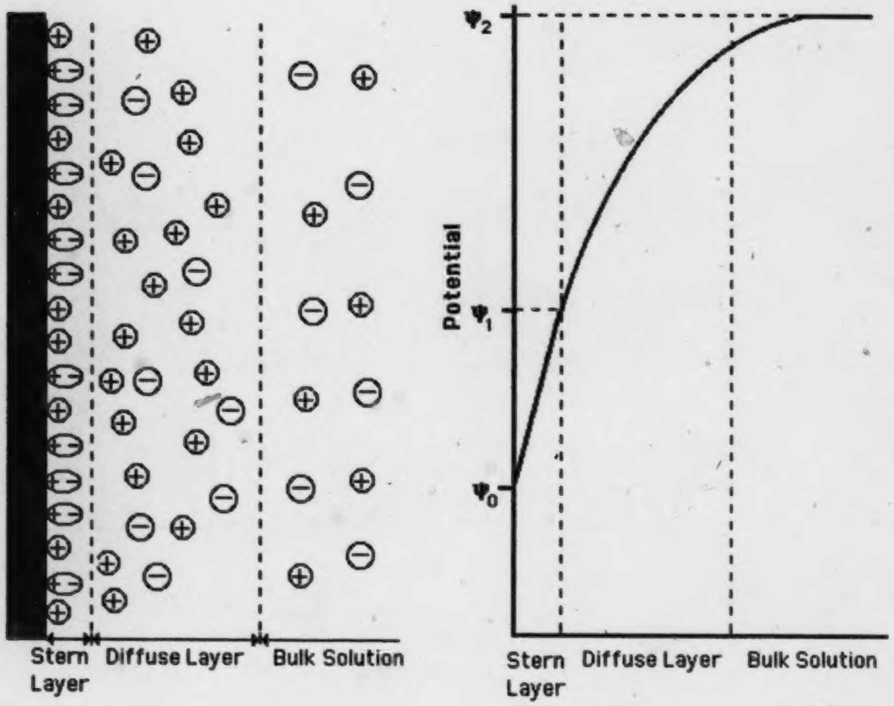
Stern Layer
Diffuse Layer
Bulk Solution
Ψ_2
Ψ_1
Ψ_0
Potential
Stern Layer
Diffuse Layer
Bulk Solution

Figure 1.01 Schematic diagram of the electric double layer and the potential distribution

The magnitude of ζ potential is related to the capillary surface charge density (θ), the dielectric constant (ε) of the buffer, and the thickness of the double layer (1/κ) according to Gouy-Chapman Equation:

$$\zeta = \frac{\theta}{\varepsilon\kappa} \tag{1.4}$$

A combination of Equations (1.3) and (1.4) yields:

$$\upsilon_{eo} = \frac{\theta}{\eta\kappa}E \tag{1.5}$$

As seen from Equation (1.5), the magnitude of EOF is directly proportional to the surface charge density of the capillary wall, and inversely proportional to the buffer viscosity and the Debye-Huckel constant (κ). An increase in the buffer pH will increase the ionization of the silanol groups on the capillary wall and therefore increase the surface charge density and the EOF. At about pH 2, the ionization of all surface silanol groups is completely suppressed, and therefore the EOF should approach zero [12]. An increase in the buffer concentration will increase the κ and decrease the double layer thickness (1/κ) as κ is directly proportional to the square root of ionic strength. As a result, the EOF decreases with increasing the buffer concentration. Other factors that affect the EOF include buffer viscosity, temperature, and organic solvents in the buffer solution.

The EOF is generated by the ζ potential near the wall surface and results in a plug-like flat flow profile. This is in contrast to the laminar flow (hydrodynamic flow) encountered in pumped systems such as HPLC. In laminar flow, the solution is driven by a pressure difference between the ends of the column, resulting in a parabolic flow profile: the solution at the center of the column is moving faster than the solution at the edge of the wall. The uniform flow profile of EOF ensures that all analytes are being carried along at the same rate through the capillary, which minimizes sample dispersion. This is an important factor that contributes to the high resolution and efficiency of capillary electrophoresis.

The existence of EOF in CE has both advantages and disadvantages. The EOF makes possible the simultaneous separation and detection of both cations and anions in a single run, if the EOF is strong enough to sweep anions to the cathode regardless of their charge. Analysis time can also be shortened for analytes moving in the same direction as the EOF. A major disadvantage associated with EOF is the difficulty with obtaining reproducible flow rates, and, therefore, poor reproducibility of migration times for all analytes.

1.2.3 Efficiency and Resolution

The efficiency of CE separation is represented by the number of theoretical plates (N),

$$N = \frac{L^2}{\sigma^2} \qquad (1.6)$$

where L is the length of the capillary from the sample injection end to the point of detection, and σ is the standard deviation of a Gaussian band. Under ideal conditions, the only source of band broadening is assumed to be longitudinal diffusion. The variance (σ^2) caused by diffusion is described by the Einstein equation:

$$\sigma^2 = 2Dt \qquad (1.7)$$

where D is the diffusion coefficient of the analyte, and t is the migration time, which can be calculated from the following equation:

$$t = \frac{L}{v} = \frac{L}{\mu_{app}E} \tag{1.8}$$

where μ_{app} is the apparent mobility, $\mu_{app} = \mu_{ep} + \mu_{eo}$. Combining Equations (1.6), (1.7), and (1.8) with the definition of the electric field (E=U/L, where U is the applied voltage) gives an expression for the number of theoretical plates:

$$N = \frac{\mu_{app}U}{2D} \tag{1.9}$$

Equation (1.9) indicates that the separation efficiency increases with increasing the applied voltage. However, the increase in voltage is ultimately limited by the Joule heating effect, which leads to significant band broadening.

In reality, additional sources of band broadening, including the finite width of the injected zone, adsorption of analytes on the capillary wall, mobility difference between the analyte ion and the buffer ion and laminar flow inside the capillary often lead to fewer plate numbers than Equation (1.9) predicts.

The resolution R between two analyte zones is determined by the following equation according to Giddings [29] and Jorgenson and Lukacs [26]:

$$R = \frac{\sqrt{N}}{4}\frac{\Delta\mu}{\overline{\mu}_{app}} \tag{1.10}$$

where $\Delta\mu$ is the difference in mobility between the two species, $\overline{\mu}_{app}$ is the average apparent mobility, $\overline{\mu}_{app} = \overline{\mu}_{ep} + \mu_{eo}$.

Equation (1.10) suggests that both efficiency (N) and selectivity ($\Delta\mu/\mu_{app}$) affect resolution. Increasing applied voltage will increase the N and the resolution, which is however, limited by Joule heating. Maximizing the difference in mobility of analytes ($\Delta\mu$) is therefore a more effective way to improve resolution. This can be done by proper choice of the CE mode, CE buffer, buffer pH, and buffer additives. Another way of improving resolution is to reduce the apparent mobility (μ_{app}) by reducing the EOF or adjusting the EOF to a direction opposite to the electrophoretic flow. From Equation (1.10) it follows that when μ_{app} is near zero, the resolution will be maximized at the expense of analysis time. This has been demonstrated by Lucy and co-workers [30-32] to achieve isotopic separations of anions such as $^{35}Cl^-/^{37}Cl^-$ and cations such as $^{14}NH_4^+/^{15}NH_4^+$.

1.2.4 Sample Injection and Detection

In CE, there are two major sample injection techniques – hydrodynamic or electrokinetic injection. For hydrodynamic injection, the sample is driven into the capillary by a pressure difference between the two ends of the capillary. The pressure difference can be established by applying either pressure at the injection side sample vial or vacuum on the detector side buffer reservoir, or simply by raising capillary at the sample end to induce gravity flow of sample into the capillary. The sample injection volume (V_{inj}) can be calculated by the Poiseuille Equation [33]:

$$V_{inj} = \frac{\pi r^4 \Delta P t_{inj}}{8\eta L} \tag{1.11}$$

where ΔP is the pressure difference used for injection, r is the internal radius of the capillary, t_{inj} is the injection time, η is the viscosity of the sample and L is the length of the capillary. The quantity of each analyte injected (n, mol) is calculated by:

$$n = \frac{\pi r^4 \Delta P t_{inj}}{8\eta L} C \tag{1.12}$$

where C is the concentration of the analyte.

For electrokinetic injection, a voltage is applied across the capillary. The sample is introduced into the capillary by electromigration. The quantity of each analyte injected is calculated by:

$$n = \pi r^2 (\mu_{ep} + \mu_{eo}) E_{inj} t_{inj} C \tag{1.13}$$

where μ_{ep} and μ_{eo} are the electrophoretic and electroosmotic mobility respectively, E_{inj} is the applied electric field ($=U_{inj}/L$), t_{inj} is the injection time, and C is the concentration of each analyte.

One problem with the electrokinetic injection is that the quantity of each analyte injected depends on the electrophoretic mobility. Analytes of higher mobility are introduced into the capillary at higher rate and the injected sample does not have the same chemical composition as the original sample. Therefore, for quantitative analysis, hydrodynamic injection is the preferred mode of sample introduction in CE. Electrokinetic injection is most useful when hydrodynamic injection cannot be applied or the sensitivity of hydrodynamic injection is low.

Because of the narrow-bore capillaries used in CE and the very small injection volumes, it is normally difficult to achieve satisfactory detection limits in terms of concentration. Therefore, the development of sensitive detection system has been one of the major research efforts in CE.

Because of its simplicity and reliability, UV detection has been extensively used in CE. One problem associated with the UV detection, however, is the limited detection sensitivity due to the short optical pathlength. Furthermore, most inorganic ions are transparent in the UV region; direct detection is possible only when the metal ions are complexed with a chromophore. To solve the latter problem, indirect UV detection is often used [12,34]. The key to indirect detection is the choice of a suitable absorbing co-ion added to the background electrolyte. In the analyte zone, the analyte ions displace the absorbing co-ions, so the background absorbance decreases as the analyte zone passes by the detector. The main advantage of indirect UV direction is the universal application, but the limited detection sensitivity remains to be a problem.

Conductivity detection, as a nearly universal detection mode for small ions, has also been used in CE [35-37]. A direct conductivity detection scheme is often difficult to implement without suppression because of the high conductance of the background electrolyte.

Amperometric detection has been applied for metal ion analysis, showing high sensitivity and good selectivity [38-40]. However, the range of detectable analytes is limited. Since the potential of the electrode is held at one value, only those species that are electroactive at that potential are detected.

Among various detection systems developed for CE, ICP-MS is the most promising detector for rapid, sensitive, multi-element determinations [41-44]. A brief overview of the ICP-MS system is presented in the following section.

1.3 Inductively Coupled Plasma Mass Spectrometry

1.3.1 Inductively Coupled Plasma (ICP)

An ICP is a flame-like electrical discharge formed in a stream of argon gas flowing through a set of three concentric quartz tubes known as the ICP torch. The outer tube of the torch is surrounded by a 3-turn load coil connected to a radio frequency (RF) generator. The RF current through the load coil generates a strong oscillating magnetic field, which in turn couples with the Ar gas stream to produce the plasma. A spark of electrons from the Tesla discharge initiates the plasma by causing collisions between the electrons and Ar atoms. The ionizing collisions induced by the high frequency magnetic field, result in the creation of Ar^+ and release of more electrons and so the process becomes self-sustaining. A stable plasma is formed as long as the magnetic field remains sufficiently high and a proper Ar gas flow is maintained [11].

The ICP was first introduced to the analytical chemistry field by Greenfield [45] and Fassel [46] as an excitation source for atomic emission spectroscopy (AES). It was later recognized that its characteristics also made it an excellent atomic ion source for mass spectrometry (MS). It was estimated that the degree of ionization of most elements of the periodic table is greater than 90% in the Ar ICP [47]. In the ICP, the eddy currents induced by the magnetic field flow more closely to the outer portions of the plasma, thus facilitating the formation of a central channel in the plasma. The presence of an axial channel is an important characteristic, which ensures efficient sample introduction. The sample aerosol passes through the central channel without significant mixing with the surrounding plasma gas, so ions from the sample are essentially confined to this narrow, central channel producing high ion density per unit volume. The sampling cone of a mass spectrometer can be easily positioned along the axial channel to maximize the analyte signal and minimize the background and interfering signals. The presence of a central channel also leads to better stability of the plasma. Since most of the eddy currents flow in the outer layer of the plasma, the impedance of the plasma is relatively unchanged when sample ions and atoms are passing through the central channel, so the stability of the plasma is maintained regardless of the nature and concentration of the sample introduced [11].

In addition to the annular structure, the Ar ICP has other unique features: high gas temperature (4500-8000K), high electron temperature (8000-10000K), and high electron number density (1-3 x 10^{15} cm^{-3}) [11]. The high temperatures aid the efficient vaporization, atomization, excitation and ionization of the sample. The high electron number density partially eliminates the ionization-type interference that presents in the flame spectrometries. Those unique properties make Ar ICP the most effective and widely used ion source for atomic mass spectrometry.

1.3.2 Mass Spectrometry (MS)

The most common type of mass spectrometers used in atomic mass spectrometry is the quadrupole mass spectrometer, which offers the advantages of low manufacturing cost, small space requirements, and high scan speed. A quadrupole consists of four parallel cylindrical rods approximately 8-12 cm in length and 1 cm in diameter arranged as shown in Figure 1.02. Opposite rods are connected electrically, and variable dc voltages (U) and RF ac voltages (V) (the same absolute value but opposite sign) are applied to each pair of rods. The electrical field inside the quadrupole is assumed to be a hyperbolic one. The potential (Φ) in such a field may be expressed by the following equation [48,49]:

$$\Phi = [U + V\cos(\omega t)]\,\frac{x^2 - y^2}{2r_0^{\,2}} \qquad (1.14)$$

where ω is frequency of ac voltage, t is time and r_0 is half distance between opposite rods. The electric field components in the x, y, and z directions are therefore:

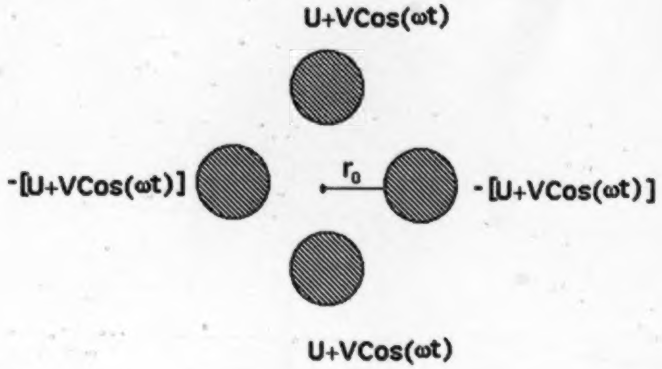
U+VCos(ωt)
-[U+VCos(ωt)]
r_0
-[U+VCos(ωt)]
U+VCos(ωt)

Figure 1.02 Schematic diagram of the arrangement of a quadrupole mass filter.

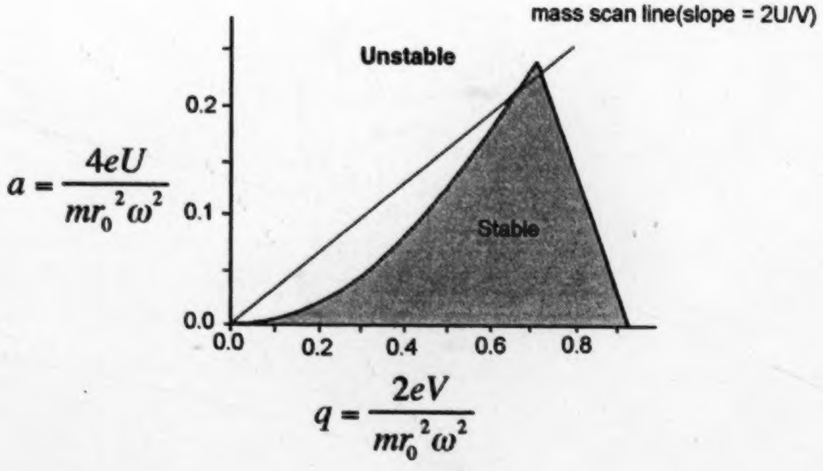

Figure 1.03 a-q stability diagram of a quadrupole mass filter.

$$E_x = -\frac{d\Phi}{dx} = -[U + V\cos(\omega t)]\frac{x}{r_0^2} \tag{1.15}$$

$$E_y = -\frac{d\Phi}{dy} = [U + V\cos(\omega t)]\frac{y}{r_0^2} \tag{1.16}$$

$$E_z = -\frac{d\Phi}{dz} = 0 \tag{1.17}$$

The equations of motion of an ion with mass (m) and charge (e) are:

$$\frac{d^2x}{dt^2} = \frac{eE_x}{m} = -\frac{ex}{mr^2_0}[U + V\cos(\omega t)] \tag{1.18}$$

$$\frac{d^2y}{dt^2} = \frac{eE_y}{m} = \frac{ey}{mr^2_0}[U + V\cos(\omega t)] \tag{1.19}$$

$$\frac{d^2z}{dt^2} = 0 \tag{1.20}$$

By definition:

$$a = \frac{4eU}{\omega^2 r_0^2 m} \tag{1.21}$$

$$q = \frac{2eV}{\omega^2 r_0^2 m} \tag{1.22}$$

Substitution of *a*, *q* into Equations (1.18) and (1.19) and rearrangement yield the following Mathieu Equations:

$$\frac{d^2x}{dt^2} + \frac{\omega^2}{4}[a + 2q\cos(\omega t)]x = 0 \tag{1.23}$$

$$\frac{d^2y}{dt^2} - \frac{\omega^2}{4}[a + 2q\cos(\omega t)]y = 0 \tag{1.24}$$

There are two types of solutions to the Mathieu Equation: (1) bounded solution, describing the stable ion trajectory in which the amplitude of oscillation of an ion is finite. The ion is able to pass the quadrupole filter without touching the rods. (2) unbounded solution, describing the unstable ion trajectory in which the oscillation grows exponentially and ultimately approaches infinity. The ion strikes the rods and is eliminated from the system. The operation of a quadrupole mass filter is often represented using the a-q stability diagram shown in Figure 1.03. The shaded region shows the ion trajectories are stable in both the x and y directions. Outside the stable region, either the x or y motion is unstable. A line with a slope of $a/q = 2U/V$ can be drawn on the stability diagram. This line is known as the mass scan line, representing the situation where the dc voltage U and the ac voltage V are increased simultaneously where their ratio is maintained constant. By scanning the U and V values while holding their ratio constant, ions of different masses are successively brought into the stability region for transmission, so a mass spectrum can be recorded. The resolution of quadrupole mass filter may be varied by simply changing the slope of the mass scan line (a/q ratio).

1.3.3 ICP-MS - Advantages and Limitations

Over the past two decades, ICP-MS has developed into a very powerful technique for trace elemental analysis. Despite the relatively high cost, the technique is gaining increasing popularity because of its unmatched analytical characteristics. ICP-MS offers very low detection limits (ppt level), a broad linear dynamic range (over 7 orders of magnitude), wide elemental coverage (most elements in the periodic table), and isotope ratio analysis. The mass spectra of elements are very simple and unique, making ICP-MS an excellent technique for semi-quantitative elemental analysis.

Like any analytical technique, ICP-MS has its limitations. Spectral interferences and matrix effects do exist [50]. In terms of elemental speciation, ICP-MS can only provide the total concentration of an element and is unable to directly detect molecular forms. The development of coupled techniques that combine the resolving power of separation techniques (e.g. CE) with the sensitivity and specificity of element detectors (e.g. ICP-MS) is therefore necessary for elemental speciation.

1.4 Interfacing CE with ICP-MS

The key to the successful coupling of CE with ICP-MS is the development of an efficient interface [41]. Such an interface must meet two prerequisites: the closing of the CE electrical circuit, and the adaptation of the flow-rate of CE to that of the nebulizer for stable and optimized nebulization. Several interfaces have been described in the literature with varying degree of success [41-43,50-60].

1.4.1 Interfaces Based on Conventional Concentric Nebulizer

Olesik et al. [41] reported the first application of CE with ICP-MS in 1995. The interface was a conventional concentric nebulizer with a conical spray chamber. The outside of the CE capillary end was coated with silver paint and inserted into the center tube of the nebulizer. The silver paint was used to provide an electrical connection between the solution in the CE capillary and the ground. However, silver contamination can occur under some conditions, and the spray chamber caused some band broadening.

Lu et al. [43] described an interface consisted of a Meinhard conventional concentric nebulizer and a conical spray chamber for their CE-ICP-MS studies. A conductive coaxial liquid sheath in the nebulizer provided ground connection to the capillary. A laminar flow was induced inside the CE capillary by the nebulizer suction. A negative pressure was applied to the inlet vial to counterbalance the laminar flow, resulting in the improvement of resolution. In another study, Michalke and Schramel [51,52] used a modified Meinhard concentric nebulizer as the interface for the speciation of Se and Pt, and a possible laminar flow was not detected.

1.4.2 Interfaces Based on High Efficiency Nebulizer

Conventional concentric nebulizers have low sample transport efficiency (typically less than 3%), so there is a need to study other more efficient nebulizers. Kinzer et al.[53] described a CE-ICP-MS interface based on a Meinhard high efficiency nebulizer (HEN) and a conical spray chamber. The HEN has a lower solution uptake rates and higher analyte transport efficiency. The study also demonstrated that the laminar flow rate in the CE capillary could be controlled by regulating the sheath flow rate in the nebulizer. Laminar flow in the direction of the director allows the analysis of positive, negative and neutral species in a single run. By increasing the sheath flow rate, laminar flow in the CE capillary can be eliminated, resulting in the increased resolution at the expense of the analysis time.

1.4.3 Interfaces Based on Microconcentric Nebulizer

A commercial microconcentric nebulizer (MCN) and a cyclonic spray chamber have been used in interfacing CE with ICP-MS for the analysis of metal binding protein [54]. Degradation of separation resolution resulting from nebulizer suction was observed. Two methods of counterbalancing the nebulizer suction were studied. One method was to increase the make-up flow rate, and the other was to apply a negative pressure to the inlet vial. The latter was found to the preferred method for counterbalancing the nebulizer suction, as the sensitivity was not compromised. In another study, Prange and

Schaumloffel [55] developed an CE-ICP-MS interface based on a modified microconcentric nebulizer (MCN 100, CETAC Technologies) with a special, low dead volume spray chamber. The main difference between this modified nebulizer and the MCN 100 is that the nebulizer capillary was changed to a narrower i.d. to increase the flow resistance. Therefore, a minimized negative pressure at the end of the CE capillary was achieved and any laminar flow inside the CE capillary was avoided. The speciation of six arsenic compounds has been accomplished by Holderbeke et al. [56] using a commercial microconcentric nebulizer (MCN 100) to couple CE with ICP-MS.

1.4.4 Interfaces Based on Ultrasonic Nebulizer

All the nebulizers described above are pneumatic nebulizers, using a gas flow stream of high velocity around the sample introduction capillary to break the liquid into fine aerosols. The use of non-pneumatic nebulizer such as an ultrasonic nebulizer (USN) offers two advantages. First, no gas flow is required in the aerosol generation process, eliminating the possibility of nebulizer suction that prevails with pneumatic nebulizers. Second, the nebulization process of an USN is typically 10 times more efficient than that of a concentic pneumatic nebulizer. Lu and Barnes [57] developed an interface to couple CE with ICP-MS using a commercially available USN. Lack of the suction effects resulted in some improvements in resolution, but the detection limits were not improved significantly because of the increased noise in the signal baseline.

Kirlew et al. [58] evaluated the feasibility of using USN as a CE-ICP-MS interface to the analysis of inorganic anions and cations. Both a lab-built USN and a commercially available USN (Cetac U5000AT) were studied. The commercial USN seemed to have better long-term stability and the peak width and shape was improved relative to the lab-built USN. It was found that a stable baseline was difficult to maintain when using USN at low flow rates (10-80 μL/min). The attempt of using the Cetac USN at higher buffer flow rates (1.25 mL/min) for CE-ICP-MS was unsuccessful, as the analytes could not be forced through the capillary under normal CE experimental conditions. A new interface design will be needed for further progress.

1.4.5 Interfaces Based on Direct Injection Nebulizer

All the CE-ICP-MS interfaces described above included a spray chamber. The spray chamber can contribute to band broadening due to convection. A direct injection nebulizer (DIN) is a microconcentric nebulizer that is direct inserted into the ICP torch without using a spray chamber. The DIN offers the advantages of 100% sample transport efficiency, low dead volume, reduced sample washout time, reduced memory effects and improved precision [59,60]. Liu et al. [42] developed a CE-ICP-MS interface based on a modified DIN (Microneb 2000, CETAC Technologies). A coaxial make-up liquid flow was used to provide the ground connection. Excellent efficiency and low detection limits were achieved for the determination of metal species.

A commercial setup (CETAC Technologies) for the DIN is very expensive ($20,000) [11], which is a major limitation for its application to CE-ICP interfacing studies. We have successfully developed a simple, robust and inexpensive DIN for interfacing CE with ICP-MS. The details of the new interface will be described in Chapter 2 of this thesis.

Our research objective is to develop fast, quantitative and reliable elemental speciation technique. As a first step toward this goal, methods to speciate the oxidation states of Cr, V, Sb, and As were developed and presented in this thesis.

1.5 References

1. *J. Anal. At. Spectrom.*, 1996, **11**, No. 12
2. *Analyst,* 1998, **123**, No. 5
3. *Spectrochim. Acta,* 1998, **53B**, No. 2
4. *Fresenius J. Anal. Chem.*, 1999, **363**, No. 5-6
5. Goessler, W., Schlagenhaufen, C., Kuehnelt, D., Greschonig, H., and Irgolic, K. I.,. *Appl. Organomet. Chem.*, 1997, **11**, 327.
6. Lobinski, R., *Appl. Spectrosc.*, 1997, 51, 260A.
7. Ellis, L. A., and Roberts, D. J., *J. Chromatogr. A*, 1997, **774**, 3.
8. Sutton, K., Sutton, R. M. C., and Caruso, J. A., *J. Chromatogr. A*, 1997, **789**, 85.
9. Zoorob, G. K., McKiernan, J. W., and Caruso, J. A., *Mikrochim. Acta*, 1998, **128**, 145.
10. Welz, B., *J. Anal. At. Spectrom.*, 1998, **13**, 413.
11. Montaser, A., Eds, *Inductively Coupled Plasma Mass Spectrometry*, Wiley-VCH, New York, 1998.
12. Jandik, P., and Bonn, G., *Capillary Electrophoresis of Small Molecules and Ions*, VCH, New York, 1993.
13. Timberbaev, A. R., *Electrophoresis*, 1997, **18**, 185.
14. Macka, M., and Haddad, P. R., *Electrophoresis*, 1997, **18**, 2482.
15. Pacakova, V., and Stulik, K., *J. Chromatogr. A*, 1997, **789**, 169.
16. Janos, P., *J. Chromatogr. A*, 1999, **834**, 3.
17. Krivacsy, Z., Gelencser, A., Hlavay, J., Kiss, G., and Sarvari, Z., *J. Chromatogr. A*, 1999, **834**, 21.
18. Timerbaev, A. R., and Buchberger, W., *J. Chromatogr. A*, 1999, **834**, 117.
19. Kaniansky, D., Masar , M., Marak, J., and Bodor, R., *J. Chromatogr. A*, 1999, **834**, 133.

20. Pacakova, V., Coufal, P., and Stulik, K., *J. Chromatogr. A*, 1999, **834**, 257.
21. Liu, B.-F., Liu, L.-B., and Cheng, J.-K., *J. Chromatogr. A*, 1999, **834**, 277.
22. Fukushi, K., Takeda, S., Chayama, K., and Wakida, S.-I., *J. Chromatogr. A*, 1999, **834**, 349.
23. Valsecchi, S. M., and Polesello, S., *J. Chromatogr. A*, 1999, **834**, 363.
24. Timerbaev, A. R., Dabek-Zlotorzynska, E., and van den Hoop, M. A. G. T., *Analyst*, 1999, **124**, 811.
25. Dabek-Zlotorzynska, E., Lai, E. P. C, and Timerbaev, A. R., *Anal. Chim. Acta*, 1998, **359**, 1.
26. Jorgenson, J.W., and Lukacs, K.D., *Anal. Chem.*, 1981, **53**, 1298.
27. Jorgenson, J.W., and Lukacs, K.D., *J. Chromatogr.*, 1981, **218**, 209.
28. Smoluchowski, M.V., *Physik. Z.*, 1905, **6**, 530.
29. Giddings, J.C., *Separation Science*, 1969, **4**, 181.
30. Lucy, C.A., Yeung, K.K-C., Fu, S., and Li, D., Henselwood, T.L. and Underhill, R.S., *Canadian J. Chem.*, 1999, **77**, 281.
31. Lucy, C.A., and McDonald, T.L., *Anal. Chem.* 1995, **67**, 1074.
32. Yeung, K.K-C., and Lucy, C.A., *Anal. Chem.*, 1998, **70**, 3286.
33. Rose, D.J., and Jorgenson J.W., *Anal. Chem.*, 1988, **60**, 642.
34. Jones, W.R., *Handbook of Capillary Electrophoresis*, Landers, J.P., Ed., CRC Press, Boca Raton, FL, 1994.
35. Huang, X., Luckey, J.A., Gordon, M.K., and Zare, R. N., *Anal. Chem.*, 1989, **61**, 766.
36. Huang, X., and Zare, R.N., *Anal.Chem.*, 1991, **63**, 2193.
37. Jones, W.R., Soglia, J., McGlynn, M., Haber, C., Reineck, J., and Krstanovic, C., *Am. Lab.*, 1996, **28**, 25.
38. Lu, W.Z., Cassidy, R.M., and Baranski, A.S., *J. Chromatogr.*, 1993, **640**, 433.
39. Lu, W.Z., and Cassidy, R.M., *Anal.Chem.*, 1993, **65**, 1649.

40. Wen, J., and Cassidy, R. M., *Anal.Chem.*, 1996, **68**, 1047.

41. Olesik, J.W., Kinzer, J. A., and Olesik, S.V., *Anal. Chem.*,1995, **67**, 1.

42. Lu, Y., Lopez-Avila, V., Zhu, J. J., Weiderin, D. R., and Beckert, W. F., *Anal. Chem.*, 1995, **67**, 2020.

43. Lu, Q., Bird, S.M., and Barnes, R.M., *Anal. Chem.*, 1995, **67**, 2949.

44. Tomlinson, M.J., Lin, L., and Caruso, J.A., *Analyst*, 1995, **120**, 583.

45. Greenfield, S., Jones, I. L., and Berry, C.T., *Analyst*, 1964, **89**, 713.

46. Wendt, R.H., and Fassel, V. A., *Anal.Chem.*, 1965, **37**, 920.

47. Houk, R. S., *Anal.Chem.*, 1986, **58**, 97A.

48. Miller, P.E., and Denton, M.B., *J. Chem. Educ.*, 1986, **63**, 617.

49. Leary, J.J. and Schmidt, R.L., *J. Chem. Educ.*, 1996, **73**, 1142.

50. Horlick, G., *Spectroscopy*, 1992, **7**, 22.

51. Michalke, B., and Schramel, P., *Fresenius' J. Anal. Chem.*, 1997, **257**, 594.

52. Michalke, B., and Schramel, P., *Electrophoresis.*,1998, **19**,270.

53. Kinzer, J. A., Olesik, J.W., and Olesik, S.V., *Anal. Chem.*, 1996, **68**, 3250.

54. Taylor, K.A., Sharp, B.L., Lewis, D.J., and Crews, H.M., *J. Anal. At. Spectrom.*,1998, **13**, 1095.

55. Prange, A., and Schaumloffel, D., *J. Anal. At. Spectrom.*, 1999, **14**, 1329.

56. Van Holderbeke, M., Zhao, Y., Vanhaecke, F., Moens, L., Dams, R., and Sandra, P., *J. Anal. At. Spectrom.*, 1999, **14**, 229.

57. Lu, Q., and Barnes, R.M., *Microchem. J.*, 1996, **54**, 129.

58. Kirlew, P.W., Castillano, M.T.M., and Caruso, J. A. , *Spectrochim. Acta*, 1998, **53B**, 221.

59. Lawrence, K.E., Rice, G.W., and Fassel, V.A., *Anal. Chem.*, 1984, **56**, 289.

60. Wiederin, D.R., Smith, F.G., and Houk, R.S., *Anal. Chem.*, 1991, **63**, 219.

Chapter 2

Instrumentation

2.1 Introduction

This chapter presents a detailed discussion of the instrumentation used throughout the research work of this thesis. The discussion can be divided into three parts: the first focuses on the CE system, the second focuses on the design and optimization of the CE-ICP-MS interface, and the third describes the ICP mass spectrometer and optimization of the system.

2.2 Instrumental Setup

A schematic diagram of the entire CE-DIN-ICP-MS system is illustrated in Figure 2.01. The system consists of the CE unit, the CE-ICP interface and the ICP-MS detector. Each part will be discussed individually.

2.2.1 CE Unit

The CE unit was laboratory-built. A fused-silica capillary (76 cm length × 50 μm i.d. × 182 μm o.d.) (Polymicro Technologies Inc., Phoenix, AZ, USA) was used as the electrophoresis capillary. The outlet of this capillary was placed inside the laboratory-constructed direct injection nebulizer (see Section 2.2.2). Electrical contact to ground was accomplished by flowing a coaxial sheath liquid (2% HNO_3) around the CE capillary. A 74900 series syringe pump (Cole-Parmer, Niles, IL, USA) was used to deliver the sheath flow liquid. Voltages applied to the inlet of the CE capillary were provided by a Model

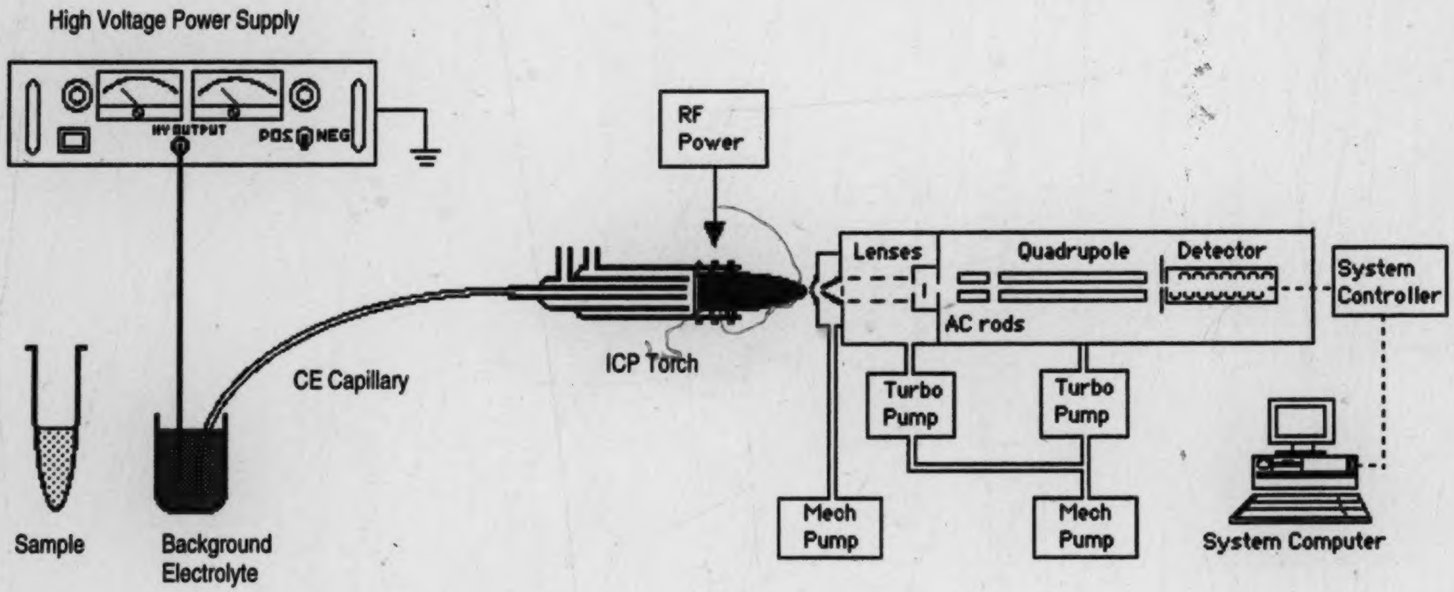
High Voltage Power Supply
HV OUTPUT
POS NEG
Sample
Background
Electrolyte
CE Capillary
RF
Power
ICP Torch
Lenses
Quadrupole
Detector
AC rods
System
Controller
Turbo
Pump
Turbo
Pump
Mech
Pump
Mech
Pump
System Computer

Figure 2.01 Schematic diagram of the instrumental setup

CZE1000R high voltage power supply (Spellman, Hauppauge, NY, USA).

2.2.2 CE-ICP-MS Interface

The CE-ICP-MS interface was a laboratory-made Direct Injection Nebulizer (DIN) (Figure 2.02). The CE capillary (76-cm length × 50 μm i.d. × 182 μm o.d.) was inserted through a PMMA cross connector and into a fused-silica sheath flow capillary (20-cm length × 251 μm i.d. × 360 μm o.d.). Both capillaries were then inserted snugly into a stainless steel supporting capillary to prevent possible vibrations caused by the nebulizer gas flow. This assembly was placed concentrically inside a nebulizer quartz tube that was tapered at the end with tip orifice i.d. of 0.36 mm for the Ar nebulizer gas flow. The CE capillary was sealed in place at the PMMA connector with epoxy. The PMMA connector with the capillary assembly was fixed to a nut through a metal block and a miniature bearing. By turning this nut, the positioning of the sheath flow capillary end relative to the nozzle tip of the nebulizer tube could be adjusted. The capillary assembly can also rotate freely because of the presence of the bearing. Both features made it possible to optimize the nebulization efficiency (aerosol generation) and to achieve the maximum sensitivity. These are major improvements in design compared to a DIN interface reported previously [1].

The sheath liquid flow around the CE capillary at a rate of 20 μL/min has three functions. First, it provides a stable electrical connection at the exit end of the CE capillary to the ground electrode (Pt) at the PMMA connector so that the CE circuit is completed. Second, this sheath liquid also serves the purpose of makeup flow to meet the liquid flow rate requirements of the DIN since the CE buffer flow rate (<1 μL/min) is too small to maintain stable operation of the nebulizer. Third, the flow rate of the sheath liquid ensures that the nebulizing efficiency of the DIN is dominated by the sheath

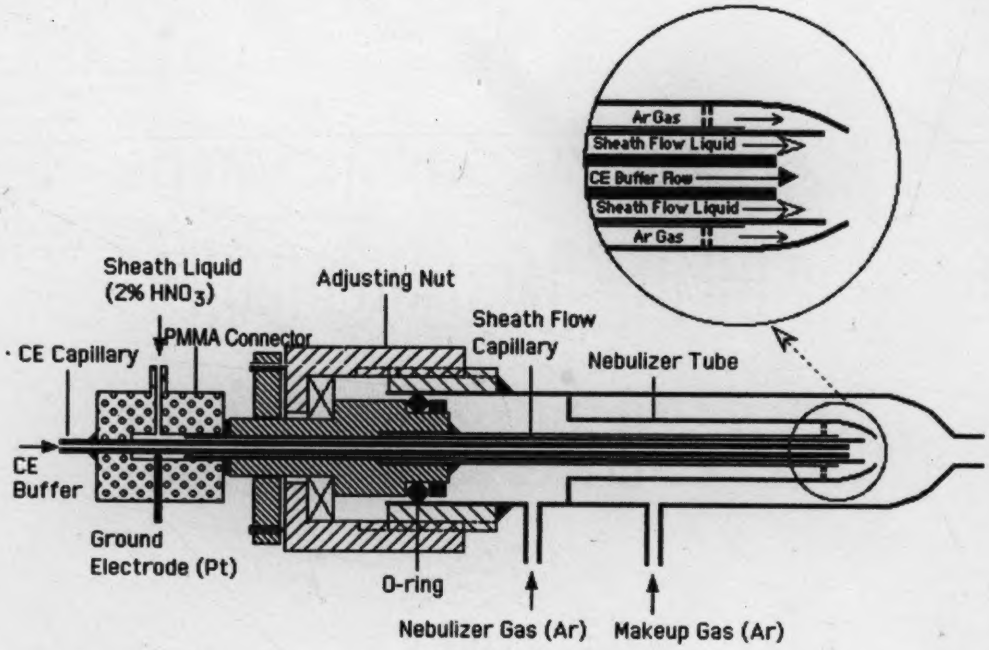
Ar Gas
Sheath Flow Liquid
CE Buffer Flow
Sheath Flow Liquid
Ar Gas
Sheath Liquid
(2% HNO_3)
Adjusting Nut
PMMA Connector
Sheath Flow
Capillary
CE Capillary
Nebulizer Tube
CE
Buffer
Ground
Electrode (Pt)
O-ring
Nebulizer Gas (Ar)
Makeup Gas (Ar)

Figure 2.02 Schematic diagram of the DIN interface for coupling CE with ICP-MS (not drawn to scale)

liquid flow. This provides a constant flow from run to run that is relatively independent of the CE buffer flow.

In order to obtain a stable and reliable electrical connection during nebulization, the exit end of the CE capillary was located 1 mm behind the tip of the sheath flow capillary. The sheath liquid flow and the CE buffer flow were mixed inside this 1-mm section of sheath flow capillary before nebulization (see the inset in Fig. 2.02). The small dead volume (~50 nL) of this 1-mm section of capillary did not appear to cause any significant band broadening and the washout time of this small dead volume was ~ 0.15 sec at the liquid flow rate of 20 µL/min.

As shown in Figure 2.03, the DIN was inserted directly into the ICP torch through an adapter. The sensitivity obtained with the DIN depends strongly on the position of the nebulizer within the torch. The tip of the DIN is usually positioned as close to the base of the plasma as possible in order to achieve the maximum sensitivity [2]. The proximity of the nebulizer tip to the plasma results in a potential problem of damaging the quartz nebulizer tip by the high temperature plasma. To protect the sensitive nebulizer tip from any possible damage, the nebulizer assembly is inserted into a larger quartz tube that is tapered down at the end to a 2-mm i.d. orifice for the Ar makeup gas flow. The addition of the Ar makeup gas served two functions. First, it provides a sheath gas flow around the nebulizer tip, isolating it thermally from the hot plasma to prevent melting. Second, it serves as the makeup gas so that the total gas flow into the axial channel of the plasma could be adjusted independent of the nebulizer gas flow for purposes of signal optimization (see Section 2.2.3.4).

2.2.3 Optimization of the CE-ICP-MS Interface

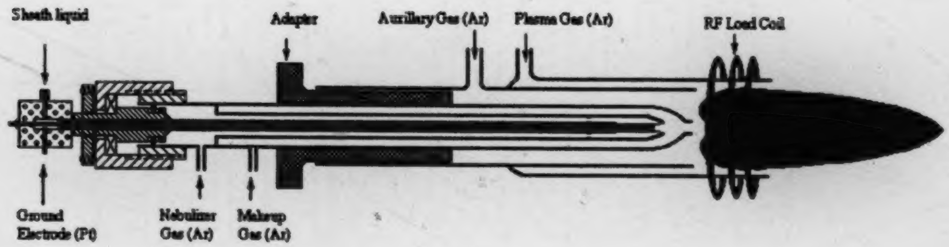
Sheath liquid
Adapter
Auxillary Gas (Ar)
Plasma Gas (Ar)
RF Load Coil
Ground
Electrode (Pt)
Nebulizer
Gas (Ar)
Makeup
Gas (Ar)

Figure 2.03 Schematic diagram showing position of the DIN interface inside the ICP torch

2.2.3.1 Optimization of the Positioning of the Sheath Flow Capillary

The positioning of the sheath flow capillary end relative to the tip orifice of the nebulizer tube should be optimized as it was found to be an important factor affecting the signal intensity. To monitor the nebulization of the DIN, 50 ppb Rh was added into the sheath flow liquid (2% HNO_3). The signal intensity of ^{103}Rh was monitored with time and the capillary position was varied by turning the adjusting nut until a stable and maximum signal intensity of ^{103}Rh was obtained. The position of the adjusting nut was then fixed by tightening a set screw on the nut. The DIN was able to provide stable operation for several months without need for readjustment.

2.2.3.2 Optimization of the Nebulizer Gas Flow

As with any pneumatic nebulizer, the nebulizer gas flow rate of the DIN has significant effects on analytical performance. The DIN is a microconcentric nebulizer. The high velocity nebulizer gas stream that exits through the annular tip of the nebulizer tube draws solution out of the sheath liquid capillary and breaks the liquid into a fine aerosol. As a result, the pressure difference created across the CE capillary, results in a suction flow (laminar flow) inside the CE capillary. Laminar flow is normally considered undesirable in CE since it has a parabolic flow profile, which may contribute to band broadening [3]. However, it can be utilized advantageously in certain cases. For example, suction flow in the direction of the detector can be used to reduce analysis time and to detect both positive and negative ions in a single run, which will be discussed in Chapter 3. It can also be used effectively for quantitative sample injection in CE (Chapters 3-6).

For the DIN interface described above, the suction flow rate was strongly influenced by the nebulizer gas flow rate. Table 2.01 summarizes the suction-induced flow rates at different nebulizer gas flow rates. The suction flow rate was estimated by measuring the time needed for an injected sample plug to flow through the whole capillary when no electric field was applied and by calculating the volume of the whole capillary (from the length and inner diameter). As the nebulizer gas flow rate increases, the negative pressure at the end of the CE capillary increases, and as a result the suction-induced flow rate increases. Generally, electrophoretic resolution degrades with increasing suction-induced flow towards the detector because of a decrease in analysis time. Therefore, it is necessary to control the suction-induced flow rate within an appropriate range for an optimal compromise between analysis time, resolution and sensitivity. The optimum nebulizer gas flow rate for the DIN interface was found to be of the order of 0.55 L/min generating a suction-induced flow rate of ~0.20 µL/min within the CE capillary.

2.2.3.3 Optimization of the Sheath Liquid Flow

For some interfaces reported previously [4-7], the suction-induced flow rate was minimized by increasing the liquid sheath flow rate, which generated a back pressure in the liquid-carrying tube in the nebulizer. For our DIN interface, increasing the sheath flow rate from 20 to 40 µL/min had essentially no effect on the suction-flow rate, as shown in Table 2.02. Further increase in the sheath flow rate beyond 40 µL/min produced unstable signals probably caused by introducing too much solvent into the plasma.

In order to evaluate the effect of sheath flow rate on analyte signal intensities, 5 ppm Y was added into the CE background electrolyte (buffer). Figure 2.04 shows the effect of sheath liquid flow on the signal intensities of Rh (marker for sheath liquid flow) and Y (marker for bulk flow inside CE capillary). Rh intensity increased with increasing the sheath liquid flow rate, as expected. However, the Y intensity as a marker for bulk flow inside the CE capillary decreased with increasing the sheath liquid flow rate. Since the

Table 2.01 Effect of the nebulizer gas flow rate on the suction-induced flow rate[a]

Nebulizer gas flow rate (L/min)	Suction-induced flow rate (μL/min)
0.60	0.22
0.55	0.20
0.50	0.18
0.45	0.15
0.40	0.13

[a] Sheath liquid flow rate: 30 μL/min.

Table 2.02 Effect of the sheath liquid flow rate on the suction-induced flow rate[a]

Sheath liquid flow rate (μL/min)	Suction-induced flow rate (μL/min)
20	0.20
25	0.20
30	0.20
35	0.20
40	0.20

[a] Nebulizer gas flow rate: 0.55 L/min.

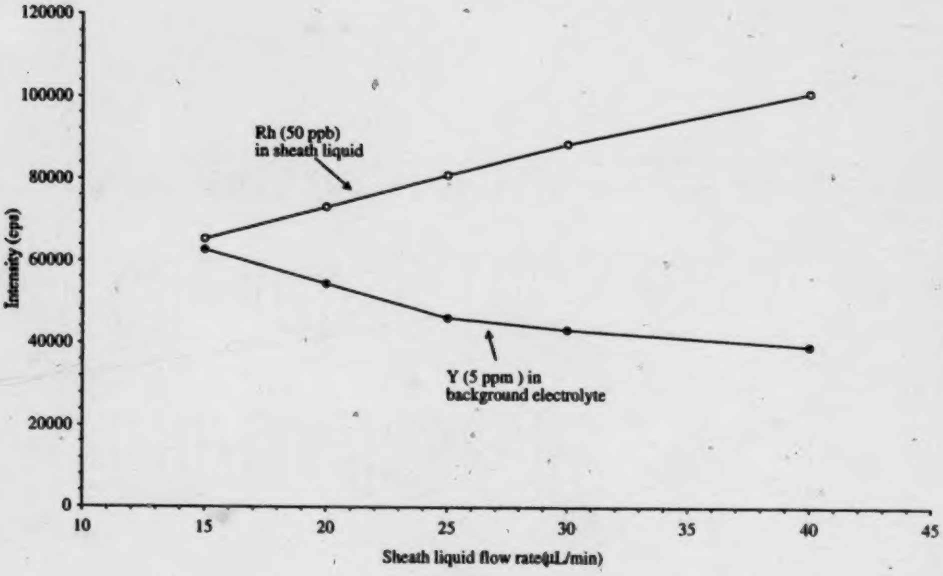

Figure 2.04 Dependence of signal intensities of Rh (in sheath liquid) and Y (in CE background electrolyte) on the sheath liquid flow rate. Nebulizer gas flow rate: 0.55 L/min. Makeup gas flow rate: 0.66 L/min.

suction flow rate did not change with a change in the sheath liquid flow rate, the decreased Y intensity was more likely a result of the decreased sample aerosol transport efficiency owing to the increased liquid flow rate [4] and may also be related to dilution of CE analytes by the sheath liquid flow. In order to get the highest sensitivities for CE analytes, the sheath liquid flow rate should be as small as possible. But too small a sheath low rate may result in unstable operation of the DIN, leading to increased signal fluctuations. As a compromise, a sheath liquid flow rate of 20 μl/min was used in the experiments in this thesis.

2.2.3.4 Optimization of the Makeup Gas Flow

Figure 2.05 illustrates the effect of makeup gas flow rate on the signal intensities of Rh (in sheath liquid flow) and Y (in CE buffer) at a nebulizer gas low rate of 0.55 L/min. The dependence of the signal intensities of Rh and Y on the makeup gas flow rate is similar to that observed in the optimization of the nebulizer gas flow in a conventional ICP-MS experiment. The intensities of Rh and Y maximize at a makeup gas flow rate of 0.70 and 0.65 L/min, respectively. This indicates that the optimal range for the total central gas flow (nebulizer gas plus makeup gas) is around 1.2 L/min. The results demonstrate the necessity of using makeup gas in addition to the nebulizer gas.

2.2.3.5 Stability of the CE-DIN-ICP-MS Coupling

The stability of nebulization in the DIN can be monitored using the signal intensity of Rh added into the sheath liquid. The stability of the CE buffer flow can be monitored using the signal intensity of Y added into the CE buffer. As shown in Figure 2.06, the initial signal of Y is due to the suction-induced flow within the CE capillary. When 10 kV voltage is applied to the CE capillary inlet, the Y signal jumps immediately

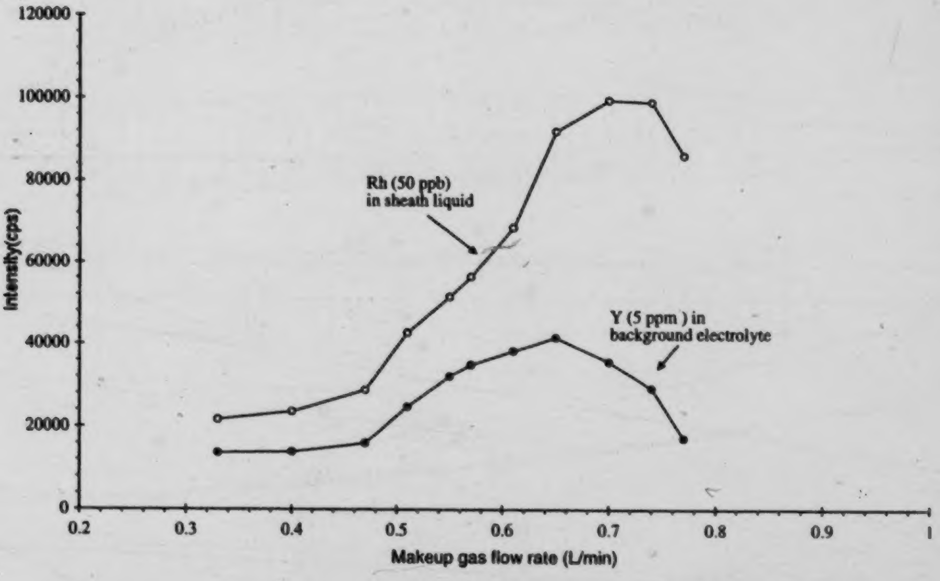

Figure 2.05 Dependence of signal intensities of Rh (in sheath liquid) and Y (in CE background electrolyte) on the makeup gas flow rate. Nebulizer gas flow rate: 0.55 L/min. Sheath liquid flow rate: 30 μL/min.

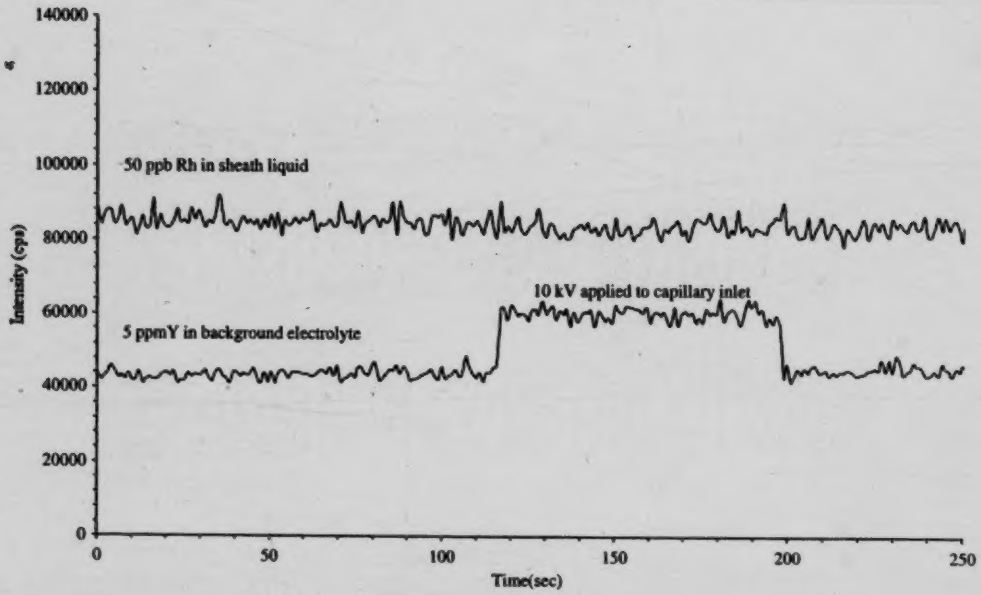

Figure 2.06 Plots of signal intensities of Rh (in sheath liquid) and Y (in CE background electrolyte) vs. time with and without the applied voltage. Nebulizer gas flow rate: 0.55 L/min. Makeup gas flow rate: 0.66 L/min. Sheath liquid flow rate: 30 μL/min.

to a higher level presumably as a result of the increased liquid flow (EOF plus electrophoretic flow of Y^{3+}) toward the detector. The Y signal remains stable at the higher level until the voltage is turned off and the Y signal then drops back to its original value. The Rh signal, however, remains stable regardless of the application of the voltage. These results demonstrate that the CE-DIN-ICP-MS system is capable of providing stable electrophoretic conditions, and that the nebulization of the DIN is independent of the CE process, which ensures reproducible operations of the DIN interface when different CE buffer systems are employed.

2.2.4 ICP-MS

A Perkin-Elmer SCIEX ELAN 5000A ICP-MS instrument (SCIEX, Thornhill, ON, Canada) was used as the element detector throughout this thesis. The instrument consists of an RF generator, an ICP torch, an ICP-MS interface, a vacuum system including turbo pumps and roughing pumps, a mass spectrometer including ion optics and a quadrupole assembly, an electron multiplier detector, and an instrument control and data handling computer. A schematic diagram of the main components of the instrument is shown in Figure 2.07, and a functional description of these components is provided below.

The RF power is provided by a free-running 35 MHz RF generator, which means that the actual frequency output by the generator is automatically varied to maintain tuning. The radio frequency power (600 to 1400 W) is inductively coupled into the flowing argon through the load coil to create and sustain the high temperature plasma.

The ICP torch consists of three concentric quartz tubes. The outer tube is surrounded by a RF load coil near its end. The plasma forms inside the outer tube within the region surrounded by the load coil. The argon gas flowing between the outer and intermediate

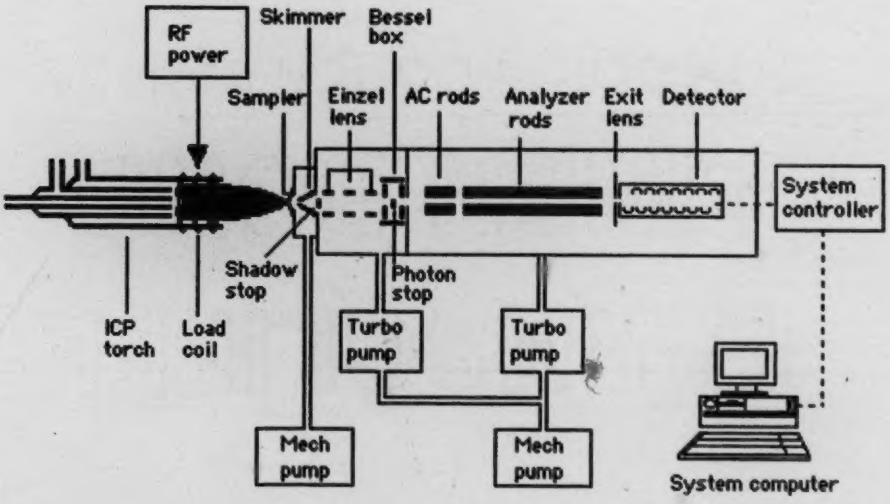
RF power
Skimmer
Bessel box
Sampler
Einzel lens
AC rods
Analyzer rods
Exit lens
Detector
System controller
Shadow stop
Photon stop
ICP torch
Load coil
Turbo pump
Turbo pump
Mech pump
Mech pump
System computer

Figure 2.07 Schematic diagram of the main components of Perkin-Elmer SCIEX ELAN 5000A ICP-MS system used in this thesis

tubes is referred to as the plasma gas with a typical flow rate of 15 L/min. In addition to sustaining the plasma, it also cools the outer quartz tube and prevents it from melting. The argon gas flowing between the intermediate and center tubes is called the auxiliary gas with a typical flow rate about 1 L/min. Its function is to push the plasma away from the center and intermediate tubes to prevent melting. A third argon gas flowing through the center tube is often called the nebulizer gas or carrier gas, which directs the sample aerosol from the nebulizer through the center of the plasma.

The plasma is sampled through two metal cones into the mass spectrometer. The first cone, called the sampler cone, has a central orifice of 1.1-mm diameter. The sampler cone extracts the gases moving through the central portion of the plasma, allowing only the gases that are richest in sample ions to enter the interface region. The second cone, called the skimmer cone, has a central orifice of 0.9-mm diameter. The function of the skimmer is again to sample gases in the central part of the beam initially coming from the plasma, allowing a fraction of the sample and gas species to pass into the vacuum chamber of the mass spectrometer. The interface region between the sampler and skimmer is evacuated by a mechanical pump and is maintained at a pressure of approximately 4 torr during operation. Both the sampler and skimmer are made of nickel and water-cooled.

Passing through the skimmer cone, the plasma stream enters a vacuum chamber that contains the ion optics. The optics include a small disk lens called a shadow stop located at the base of the skimmer cone, a set of three-cylinder lens called an Einzel lens, and a lens set called a Bessel box. The shadow stop is grounded and is used to intercept unvaporized plasma particles and photons. It also protects a photon stop in the center of the Bessel box from being bombarded with too many ions, which has a deleterious effect on the stability of the voltage of the photon stop. The Einzel lens consists of three cylinders: E1, E2 and E3. The E1 and the E3 lens are tied together and have the same voltage. The E2 lens voltage is not normally adjusted and was preset by the manufacture at –130 V. The Einzel lens serves to focus the broadened ion beam coming from the skimmer cone into a narrower beam. The Bessel box consists of the barrel (B lens), the front and back plates tied together (P lens), and a small disk lens located in the center called photon stop (S2 lens). The Bessel box functions as an energy pass filter. Only ions of the selected energies are transmitted through the box while those of higher or lower energies are rejected. The B lens and P lens act to deflect ions around the photon stop, and out of the Bessel box. Most of the neutral atoms and photons are blocked by the photon stop from reaching the detector, therefore reducing background noise. The ion optics chamber is maintained at a pressure of ~ 8×10^{-4} torr by a turbo molecular pump, which is supported by a mechanical pump.

Ions leaving the ion optics chamber are directed into the higher vacuum (~ 1.5×10^{-5} torr) mass analyzer chamber, which contains the quadrupole mass analyzer and the ion detector. The entry AC rods are used to focus the ions into the center the quadrupole mass analyzer. Mass selection is achieved by varying the ac and dc voltages applied on the four rods. The combination of the ac and dc fields causes oscillations in ion trajectories, the magnitude of which depends on the mass to charge (m/z) ratio. For a particular field, ions with a small range of m/z value have stable trajectories that allow them to pass through the filter, all other ions will strike a quadrupole rod and are pumped away by the vacuum system. The ion detector is an ETP Model AF570 Active Film discrete dynode electron multiplier, operated in the pulse counting mode. Ions leaving the quadrupole mass analyzer strike the surface of the first dynode. Electrons are emitted as a result of the impact. These primary electrons are then accelerated toward the next dynode. Upon impact each primary electron induces the emission on average of two further electrons. After sufficient repetitions of this impact process, a large number of electrons will have been produced. The multiplication factor will typically be on the order of 10^8. The last element in the electron multiplier is a collector electrode that collects the electrons. The resulting pulses are counted by the system electronics over a preset period of time to give an ion count rate.

The ELAN 5000 ICP-MS system uses an IBM PS/2 Model 70 computer with an Intel 80386 microprocessor for instrument control and data acquisition. The computer has 5 MB RAM, a 120-MB hard disk drive and a floppy disk drive. Floppy disks were used to transfer the data files to a Power Macintosh G3 computer, where the data processing was performed using commercially available programs such as Microsoft Excel.

Prior to coupling the CE system with the ICP-MS instrument, the optimization and mass calibration of the ICP-MS was performed with a conventional sample introduction system (Scott-type spray chamber and cross flow nebulizer) in place. A standard solution of Rh, Mg, Pb (10 ppb each) was used to optimize the x-y position, the Ar gas flow and the ion lens system for maximum signal intensities. Then the conventional sample introduction system was removed and replaced with the DIN interface, and the instrument was re-optimized using a 50 ppb Rh solution. The lens setting was not re-adjusted. The same settings were used for all the studies in this thesis. The RF power, Ar gas flow rate, and the x-y position were re-optimized. The ICP-MS operating parameters are summarized in Table 2.03.

Table 2.03 ICP-MS operating parameters

RF power	1250 W
Ar gas flow rate:	
Plasma gas (outer)	15 L/min
Auxiliary gas (intermediate)	1.0 L/min
Nebulizer (central)	0.55 L/m
Sampling depth	9.1 mm
Sampler orifice	1.1 mm
Skimmer orifice	0.9 mm
Ion optics	
P lens	-82.0 V
S2 lens	-7.8 V
B lens	14.6 V
E1 lens	5.89 V
Detector	-3.3 kV
Data acquisition:	
Dwell time	200 ms
Point per peak	1

2.3 References

1. Liu, Y., Lopez-Avila, V., Zhu, J. J., Weiderin, D. R., Beckert, W. F., *Anal. Chem.,* 1995, **67**, 2020.
2. Wiederin, D. R., Smith, F. G., and Houk, R. S., *Anal. Chem.,* 1991, **63**, 219.
3. Olesik, J. W., Kinzer, J. A., Grunwald, E. J., Thaxton, K. K., and Olesik, S. V., *Spectrochim. Acta*, 1998, **53B**, 239.
4. Kinezer, J. A., Olesik, J. W., and Olesik, S. V., *Anal. Chem.,* 1996, **68**, 3250.
5. Majidi, V., and Miller-Ihli, N. J., *Analyst*, 1998, **123**, 803.
6. Holderbeke, M. V., Zhao, Y., Vanhaecke, F., Moens, L., Dams, R., and Sandra, P., *J. Anal. At. Spectrom.,* 1999, **14**, 229.

Chapter 3

Quantitative Speciation of Chromium

3.1 Introduction

There is demand for analytical procedures for trace element speciation because the toxicity, bioavailability, transport, and accumulation of an element in the environment depend on the different chemical forms and oxidation states in which the element is present. Chromium is one of many elements that fall into this category. Chromium exists in aqueous solution mainly in two oxidation states, Cr(III) and Cr(VI). They have drastically different toxicological and biological behavior. Cr(III) is non toxic and is reported to be essential for the maintenance of normal carbohydrates and lipid metabolism, while Cr(VI) (as $Cr_2O_7^{2-}$ or CrO_4^{2-}) is highly toxic and carcinogenic to humans [1-3]. Over-exposure to Cr(VI) may cause a number of diseases such as dermatitis, bronchitis, pneumonia, and various forms of cancer. The transport and accumulation of chromium in soils and water systems is also species dependent. Because of its low mobility, landfill disposal of Cr(III) would not pose a pollution problem but where oxidation of Cr(III) to Cr(VI) occurs it can make the total load of metal more toxic [5]. The widespread application of chromium in industry activities, such as tanning, electroplating and pigment production, leads to substantial disposal of waste containing Cr(VI). The release of Cr(VI) into the environment can contaminate soils and waters, and subsequently being taken up by plants and ultimately having a significant impact on human health.

In order to get valid toxicological and risk assessments of chromium contamination and to understand the mechanisms for the inter-conversion between oxidation states and bioavailability of this element, the determination of total chromium concentration is not sufficient. Therefore, quantitative speciation of chromium is necessary.

Numerous methods are available in the literature for the speciation of chromium. One of the traditional methods for determining Cr(VI) uses diphenylcarbazide to form a red-purple complex with Cr(VI) in acidic solution. The complex is measured quantitatively by its visible absorption at 550 nm [5]. To determine Cr(III), the sample is first oxidized by permanganate to convert Cr(III) to Cr(VI), then the total chromium concentration is determined again. The Cr(III) concentration is estimated indirectly as the difference between the total chromium concentration and Cr(VI) concentration. This method is subject to potential interferences from colored species in the sample as well as from other elements that form colored complexes with diphenylcarbazide.

By 1990, a variety of papers had been published for the speciation of chromium, based on selective extraction, co-precipitation, electrochemical separation and ion exchange. Many of these methods have the disadvantage that the conversion from one oxidation state to another is needed, and therefore they are labor and time-consuming and contamination-prone (Sperling et al. [7]). Over the past decade, however, significant advances in chromium speciation have been made using chromatographic techniques coupled to an element-specific detector. Among the various chromatographic techniques, high performance liquid chromatography (HPLC) has been the most widely used. Commonly used detection systems include flame atomic absorption spectrometry (FAAS) [7-10], inductively coupled plasma atomic emission spectrometry (ICP-AES) [11-13] and inductively coupled plasma mass spectrometry (ICP-MS) [14-22]. The high sensitivity and element selectivity of ICP-MS as a detector has made HPLC-ICP-MS one of the most popular methods for chromium speciation [23].

Recently, capillary electrophoresis (CE) coupled to ICP-MS has become an attractive alternative for element speciation [24, 25]. CE-ICP-MS has an important advantage over HPLC-ICP-MS: the lack of a stationary phase minimizes the chemical interactions between analyte and stationary phase. In HPLC, those interactions may shift the equilibrium between analytes resulting in changes in speciation during separation. Other advantages of CE-ICP-MS include: high separation efficiency, small sample and buffer volume requirements and fast analysis time [26-28].

To date, only a few reports have been published on the speciation of chromium using CE with different interfaces and detection systems. Since the chromium species [$Cr(H_2O)_6^{3+}$, CrO_4^{2-}] are oppositely charged, they migrate in opposite directions in an electric field, making it difficult to determine both species in a single run. For the simultaneous determination of Cr(III) and Cr(VI) by CE with UV detection, Timerbaev et al. [29] proposed a method based on conversion of the positively charged Cr(III) into a negatively charged complex with cyclohexane-1,2-diaminetetraacetic acid (CDTA) prior to CE separation. The detection limits achieved were 50 ppb for Cr(III) and 10 ppb for Cr(VI). The same strategy was utilized by Jung et al. [30] and Pozdniakova and Padarauskas [31] for the speciation of chromium. The former used ethylenediaminetetraacetic acid (EDTA), and the latter used EDTA, CDTA, and diethylenetriaminepentaacetic acid (DTPA) as complexing agents with a detection limit about 420 ppb achieved for Cr(VI) using UV detection. In general, CE methods with UV detection lack sufficient sensitivity in terms of concentration, which is a major limitation for their application to element speciation. Besides, pre-capillary complexation is not desirable, especially for Cr(III) because of its kinetic inertness to ligand substitution. At room temperature the complex formation reactions between Cr(III) and EDTA, CDTA or DTPA require several days to run to completion [29-31], therefore heating or boiling the reaction mixtures with excess ligands is necessary to facilitate the chelation with the risk of sample evaporation and changes in speciation distribution due to the oxidation ability of Cr(VI) [29].

Olesik et al. [32] reported the first application of CE with ICP-MS using a conventional concentric nebulizer and a conical spray chamber. The detection limits for chromium (Cr(III) as $Cr(OH)^{2+}$ and Cr(VI) as $Cr_2O_7^{2-}$) were roughly estimated as 9 ppb based on peak height and 2 ppb based on peak area. Mei et al. [33] coupled CE with ICP-AES using a commercial microconcentric nebulizer and a 78 mL spray chamber, resulting in limits of detection of 310 ppb for Cr^{3+} and 85 ppb for $Cr_2O_7^{2-}$ based on peak height and 2.5 ppb for Cr^{3+} and 0.75 ppb for $Cr_2O_7^{2-}$ based on peak area. More recently, Chan and Chan [34] reported on interfacing CE with ICP-AES using a modified Meinhard concentric nebulizer and a locally-constructed spray chamber for the speciation of chromium, and a detection limit of ~ 10 ppb for Cr(III) and Cr(VI) was obtained. All of these sample introduction systems [32-34] were utilized in conjunction with a spray chamber. A major concern of using a spray chamber is its dead volume, which may contribute to peak broadening from convection.

In this study, a method is presented for the quantitative speciation the oxidation states of chromium. A CE- capillary was coupled to an ICP-MS using a laboratory-made direct injection nebulizer interface (Chapter 2) without spray chamber. The sample is first subjected to electrostack in the capillary. This results in the separation and pre-concentration of the chromium species. The effects of carrier electrolyte and the sample pH, the applied voltage and the injection volume on sensitivity, peak shape and separation are discussed. The analytical performance of the method, in terms of linear dynamic range, precision and detection limits, is also described.

In order to provide a guide for optimization of the method and identification of the species, a brief description of the solution chemistry of chromium is necessary. In aqueous solution chromium mainly exists in the III or VI oxidation states. Chromium (III) exists in solution as several possible forms [35], including the mononuclear species Cr^{3+}, $Cr(OH)^{2+}$, $Cr(OH)_2^+$, $Cr(OH)_3$, $Cr(OH)_4^-$, and some polynuclear species $Cr_2(OH)_2^{4+}$, $Cr_3(OH)_4^{5+}$ and $Cr_4(OH)_6^{6+}$. The dominant forms present, however, depend on specific conditions such as pH, temperature and total chromium concentration. The hydrolysis of chromium(III) in aqueous has been studied extensively by Marty and co-workers [36-40] and also Rai et al [41]. There is still controversy over the extent to which polynclear chromium species are present, especially in systems of low total chromium concentration. Under the conditions of the present study (room temperature, total chromium concentration < 1 mM), the amounts of polynuclear species present may be negligible, and therefore can be ignored [41], only the following equilibrium are considered:

$$Cr^{3+} + H_2O \Leftrightarrow Cr(OH)^{2+} + H^+ \qquad K_1 = 1.6 \times 10^{-4} \qquad (3.01)$$

$$Cr(OH)^{2+} + H_2O \Leftrightarrow Cr(OH)_2^+ + H^+ \qquad K_2 = 4.0 \times 10^{-7} \qquad (3.02)$$

$$Cr(OH)_2^+ + H_2O \Leftrightarrow Cr(OH)_3\,(aq) + H^+ \qquad K_3 = 4.0 \times 10^{-7} \qquad (3.03)$$

$$Cr(OH)_3\,(aq) + H_2O \Leftrightarrow Cr(OH)_4^- + H^+ \qquad K_4 = 3.9 \times 10^{-12} \qquad (3.04)$$

Data were taken from reference [41], and the thermodynamic equilibrium constants (K) were calculated and listed above. It should be noted that the data were reported for conditions of 0.01M ionic strength and the solutions were in equilibrium with $Cr(OH)_3(s)$. Assuming the species involved in Equations (3.01-3.04) are the only species present in significant amounts in solution, the following equation can be written:

$$[Cr(total)] = [Cr^{3+}] + [Cr(OH)^{2+}] + [Cr(OH)_2^+] + [Cr(OH)_3] + [Cr(OH)_4^-] \qquad (3.05)$$

Based on this equation and the equilibrium constants from Equations (3.01-3.04), the species distribution can be calculated. Figure 3.01 presents a graphical representation of the species distribution of the above equilibria between the pH ranges of 1 and 14. The pH dependence of the species distribution is evident. It should be noted that the Cr(III) species mentioned above are all hydrated, the aqua ligands were omitted for simplicity. For example, Cr^{3+}, $Cr(OH)^{2+}$ and $Cr(OH)_2^+$ were abbreviated from $Cr(H_2O)_6^{3+}$, $Cr(OH)(H_2O)_5^{2+}$ and $Cr(OH)_2(H_2O)_4^+$, respectively.

Chromium (VI) exists in solution as several different species, such as H_2CrO_4, $HCrO_4^-$, CrO_4^{2-}, $Cr_2O_7^{2-}$, $HCr_2O_7^-$, $Cr_3O_{10}^{2-}$, and $Cr_4O_{13}^{2-}$. The last three ions have been detected only in solution pH < 0 or at [Cr(VI)] > 1 M [35,42], and therefore contributions from these ions can be ignored under the conditions of the present study. Only the equilibria listed below will be considered [42,43]:

$$H_2CrO_4 \Leftrightarrow HCrO_4^- + H^+ \qquad K_1 = 1.6 \qquad (3.06)$$

$$HCrO_4^- \Leftrightarrow CrO_4^{2-} + H^+ \qquad K_2 = 3.1\times 10^{-7} \qquad (3.07)$$

$$2\,HCrO_4^- \Leftrightarrow Cr_2O_7^{2-} + H_2O \qquad K_3 = 34 \qquad (3.08)$$

A mass balance equations can be written as

$$[Cr(total)] = [H_2CrO_4] + [HCrO_4^-] + [CrO_4^{2-}] + 2[\,Cr_2O_7^{2-}] \qquad (3.09)$$

Based on Equation 3.09 and the K values from Equations (3.06-3.08) the species distribution can be calculated. Figure 3.02 shows the calculated species distribution as a function of pH for total Cr(VI) concentrations of 10^{-3} M (50 ppm) and 10^{-5} M (0.5 ppm). It

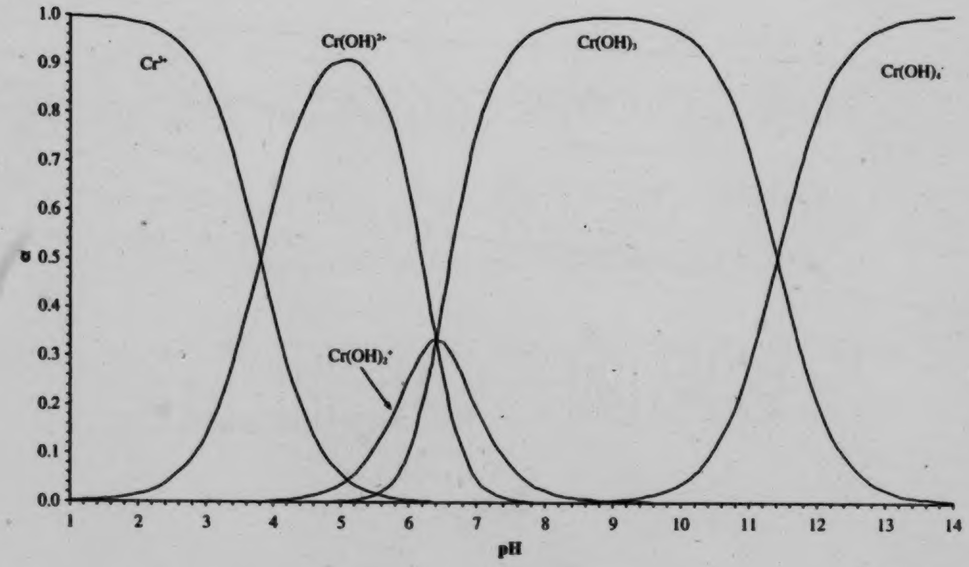

Figure 3.01 Fractional composition diagram for chromium (III) as a function of pH

is obvious from the plots that species distribution depends on the pH and total chromium concentration. It should be noted that the above equilibrium constants were reported for conditions of 0 ionic strength [43] and the effect of ionic strength on equilibrium constants can be quite large. Moreover, there is still some debate over the solution chemistry of Cr(VI) [44,45], therefore these graphs should be viewed with caution.

3.2 Experimental

3.2.1 Chemical Reagents

All chemicals were of analytical reagent grade. De-ionized water (18 MΩ cm) was provided by a Milli-Q water system (Millipore, Bedford, MA). Standard stock solutions (100 ppm) of Cr(III) and Cr(VI) were prepared by dissolving appropriate amounts of $Cr(NO_3)_3 \cdot 9H_2O$ (Bakers & Adamson, Morristown, NJ) and Na_2CrO_4 (BDH, Toronto, ON) in de-ionized water, respectively and stored in a refrigerator at 4°C. Daily working solutions were freshly prepared by diluting the stock solution as needed. Stock solutions of the background electrolyte were prepared by dissolving appropriate amounts of $Ca(NO_3)_2 \cdot 4H_2O$ (BDH) in de-ionized water and adjusting the pH with concentrated HNO_3 (Anachemia, Montreal, QC). The background electrolyte solutions were de-aerated before use.

3.2.2 Instrumentation

A laboratory-built CE system was used. A 76-cm long fused silica capillary (Polymicro Technologies Inc., Phoenix, AZ) with an inner diameter of 50 μm and an outer diameter of 182 μm was used as the separation capillary. The separation voltage was provided by a

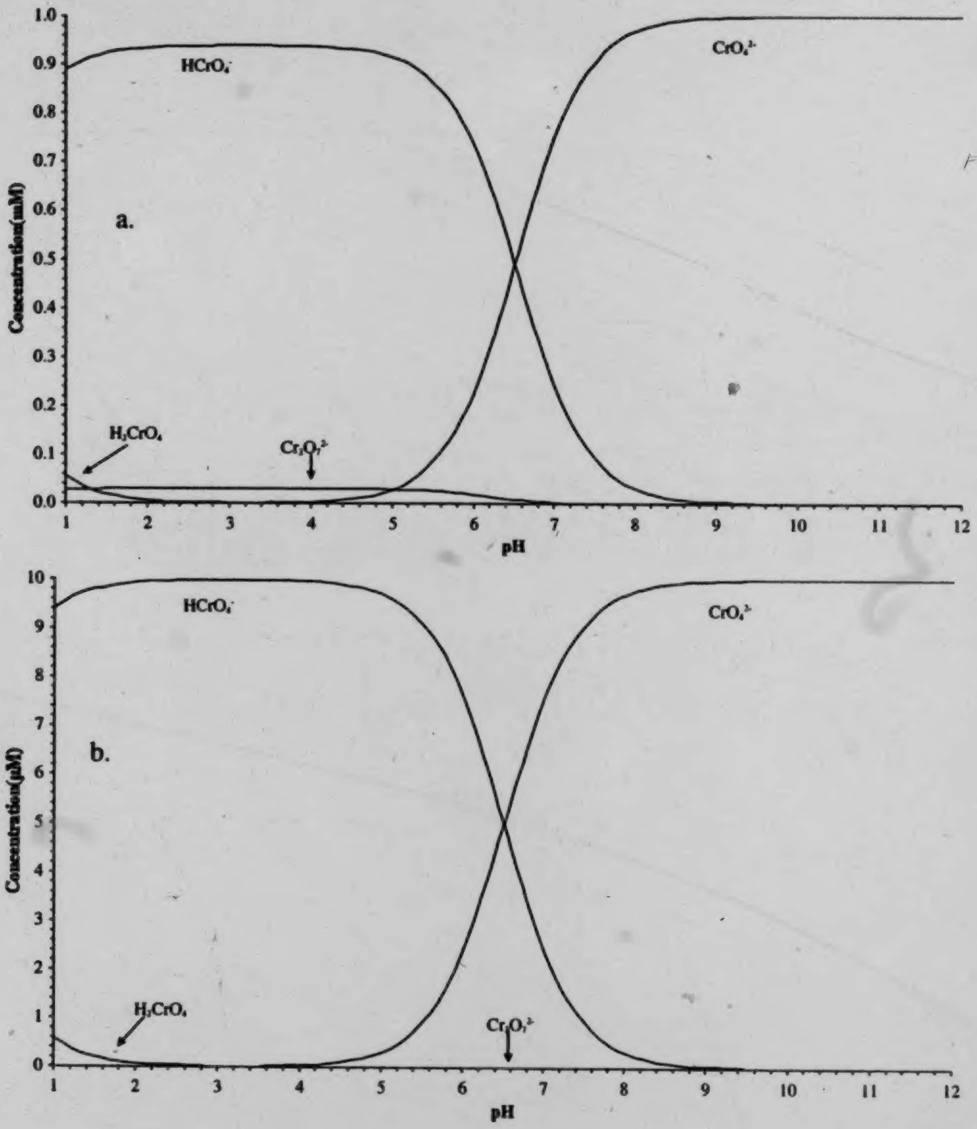

Figure 3.02 Dependence of Cr(VI) species distribution on pH and total chromium concentration of (a) 10^{-3} M and (b) 10^{-5} M

CZE1000R high voltage power supply (Spellman, Hauppauge, NY). A positive potential was applied to the capillary inlet while the outlet was connected to ground by means of a sheath liquid (2% HNO_3). Platinum wires were used as electrodes. A new capillary was conditioned by flushing it with 1M NaOH (15 min), followed by 0.1M NaOH (15 min) and de-ionized water (10 min) by pressure. The capillary was also rinsed with background electrolyte for 5 minutes before each run using nebulizer suction.

The interface coupling CE to ICP-MS was developed in the laboratory. This interface has been described in detail in Chapter 2. A 74900 series syringe pump (Cole-Parmer, Niles, IL) was used to deliver the sheath liquid (2% HNO_3).

A Perkin-Elmer SCIEX ELAN 5000A ICP-MS instrument (Thornhill, ON, Canada) was used for the element detection. The chromium isotope m/z 52 was monitored in the graphic mode of the instrument. Electropherogram data were collected using a 200 ms dwell time. Data analysis was conducted after the data were transferred to a Microsoft Excel spreadsheet. Peak areas were calculated using a program written in Visual Basic. The ICP-MS operating parameters have been summarized in Chapter 2.

pH was measured using an ORION pH Meter Model 420A (Orion Research Inc., Beverly, MA). The pH probe (Orion Triode Combination Electrode) was calibrated with three buffer solutions (pH 4, 7 and 10).

3.2.3 Sample Injection

In order to avoid suction of air into the capillary, the nebulizer gas was first turned off. Then the capillary inlet end was transferred from the electrolyte reservoir to the sample. By turning on the nebulizer gas, sample was hydrodynamically injected into the capillary by nebulizer suction. Sample injection volume was calculated by multiplication of injection time and suction flow rate. Suction flow rate was estimated as the volume of the whole capillary (calculated from the length and inner diameter) divided by the time needed for a sample plug flow through the whole capillary (measured from the migration time of the sample due to suction flow only with no voltage applied).

3.3 Results and Discussion

3.3.1 On-line Concentration Method

From Figures of 3.01 and 3.02, it can be seen that in the acidic pH range of 2-3, Cr(III) exists in solution presumably as cation Cr^{3+} and Cr(VI) exists presumably as anion $HCrO_4^-$. Their opposite polarity presents a major problem in developing a CE method for speciation [29-31]. In this study, we use a simple yet effective method for chromium speciation - on-line concentration by sample stacking. Both positive and negative species can be determined in a single run and sample pre-complexation is not needed.

Sample stacking in CE results from differences between the conductivity of the sample zone and that of the background electrolyte. The lower conductivity of the sample zone results in higher field strength (E) across the zone. Since electrophoretic velocity is directly proportional to the field strength, a higher velocity can be realized in the sample zone. This forms the basis for sample stacking [46-49].

Figure 3.03 illustrates the stacking and separation procedure. First, a long plug of sample dissolved in water or low concentration buffer is hydrodynamically injected into the capillary filled with a background electrolyte of higher concentration (step a). After the capillary is placed back in the electrolyte reservoir (step b), a high voltage (+10 kV) is

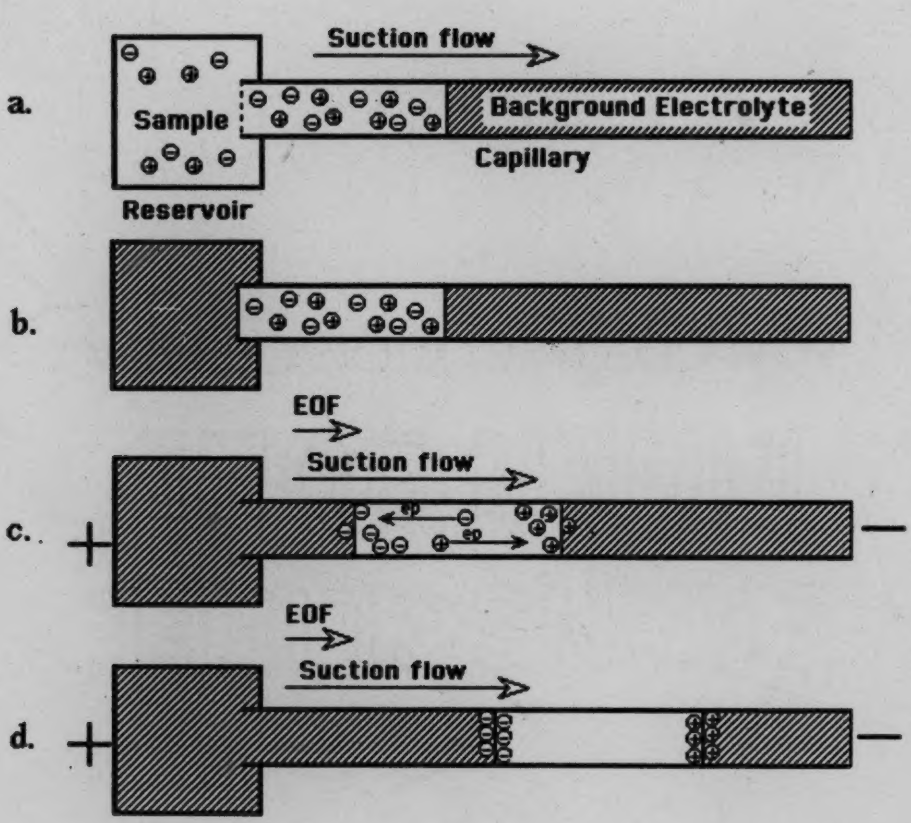
a.
Suction flow
Sample
Background Electrolyte
Capillary
Reservoir
b.
EOF
Suction flow
c.
ep
ep
+
—
EOF
Suction flow
d.
+
—

Figure 3.03 Schematic diagram showing the stacking processes: (a) sample injection by suction, (b) capillary transfer, (c) application of voltage (+10 kV) and suction, (d) analyte stacking

applied across the capillary, causing cations to migrate toward the cathode and anions toward the anode (step c). Because the low concentration sample region has a higher electric resistance, the electric field in the sample zone is much higher than in the background electrolyte. Thus, ions in the sample plug migrate very fast. As the ions reach the boundary between the sample plug and background electrolyte, they slow down because the electric field is lower within the electrolyte. In the mean time, ions in the rest of the sample zone are still exposed to the high field and still migrate toward the boundary at high speed, causing the sample ions to stack into narrow zones. This stacking process continues until most of the positive ions are concentrated at the front edge of the sample plug and most of the negative ions are at the rear of the plug. Since almost all the applied voltage is dropped across the sample plug, there is virtually no field strength across the background electrolyte region. Once an analyte ion diffuses out of the sample plug into the electrolyte, its electrophoretic velocity will approach zero. Consequently, all ions will move at the same velocity of the bulk flow. In this case the bulk flow is mainly the suction-induced flow which drives the sample plug out of the capillary for detection. This method has two advantages. First, sample stacking increases sensitivity and improves detection limits. Second, both positive and negative ions can be detected in a single run using the suction-induced flow.

Figure 3.04 is an electropherogram showing the separation of Cr(III) and Cr(VI) species by sample stacking and verifies the model discussed above. A sample containing 1 ppm Cr(III) and 1 ppm Cr(VI) was prepared in de-ionized water, and the pH was adjusted to 3.0 with HNO_3. A volume of 0.60 μL of the sample was injected into the capillary. Cr(III), which exists presumably as Cr^{3+} was stacked up at the front of the plug and Cr(VI), which exists presumably as $HCrO_4^-$, was focused at the rear of the sample plug. In order to visualize the sample plug, Y^{3+} was added to the background electrolyte and its signal at m/z 89 is monitored as a function of time. The bulk flow of the electrolyte

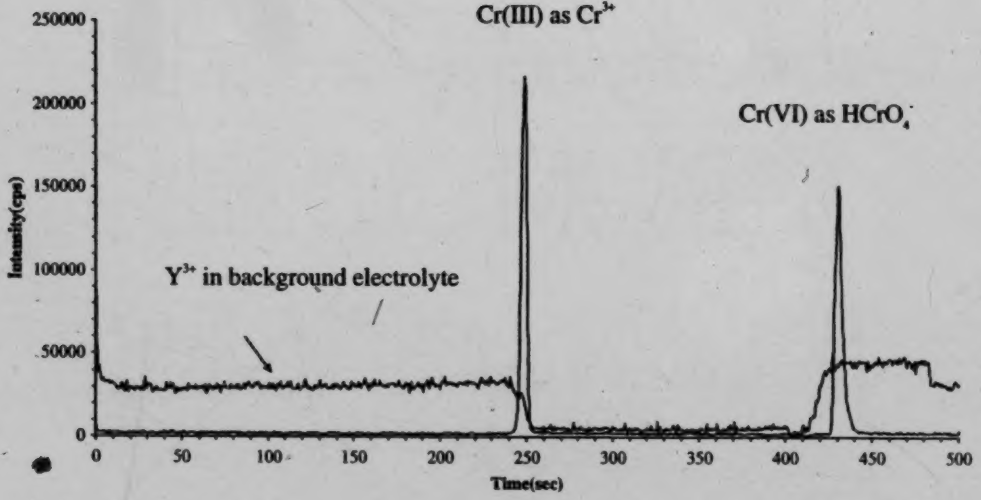

Figure 3.04 Electropherogram for a sample solution containing Cr(III) and Cr(VI) at 1 ppm each. Conditions: background electrolyte, 50 mM $Ca(NO_3)_2$ at pH 2.0; sample pH, 3.0; applied voltage, +10 kV; injection volume, 0.60 μL.

caused by nebulizer suction results in a stable background signal. Once the sample plug replaces the background electrolyte, the Y^{3+} signal drops, showing clearly the location of the sample plug within the capillary. As can be seen from Figure 3.04, Cr^{3+} was focused on the leading boundary, producing a sharp peak, while $HCrO_4^-$ diffused somewhat into the background electrolyte at the trailing boundary, giving rise to a somewhat broadened peak. The latter is probably a result of the fact that $HCrO_4^-$ stays in the capillary longer and that the sample matrix leaves the capillary before $HCrO_4^-$. The signal level of Y^{3+} after the sample plug is higher than before the sample plug, a result of the different contributions from electrophoretic flow. When the sample plug is in the capillary, the field strength over the electrolyte would be very small, as a result the electrophoretic velocity of Y^{3+} would also be near zero. After the sample plug exits the capillary, all the voltage is dropped across the electrolyte, the electrophoretic velocity of Y^{3+} would be much higher leading to a higher signal level.

3.3.2 Identification of Chromium Species

The assignment of species peaks in Figure 3.04 was based on the stacking model and the polarity of the applied voltage and assumptions as to what species will be present. Species identification can be verified experimentally by comparison of CE migration times of unknown peaks with those of standards. Figure 3.05 illustrates the identification of Cr(III) and Cr(VI) species by standard injection. The injections of standard solutions of Cr(III) and Cr(VI) are shown respectively in Figure 3.05a and Figure 3.05b. An electropherogram of a sample containing Cr(III) and Cr(VI) is shown in Figure 3.05c and the peaks can be identified easily by comparison.

3.3.3 Optimization of Electrostacking Parameters

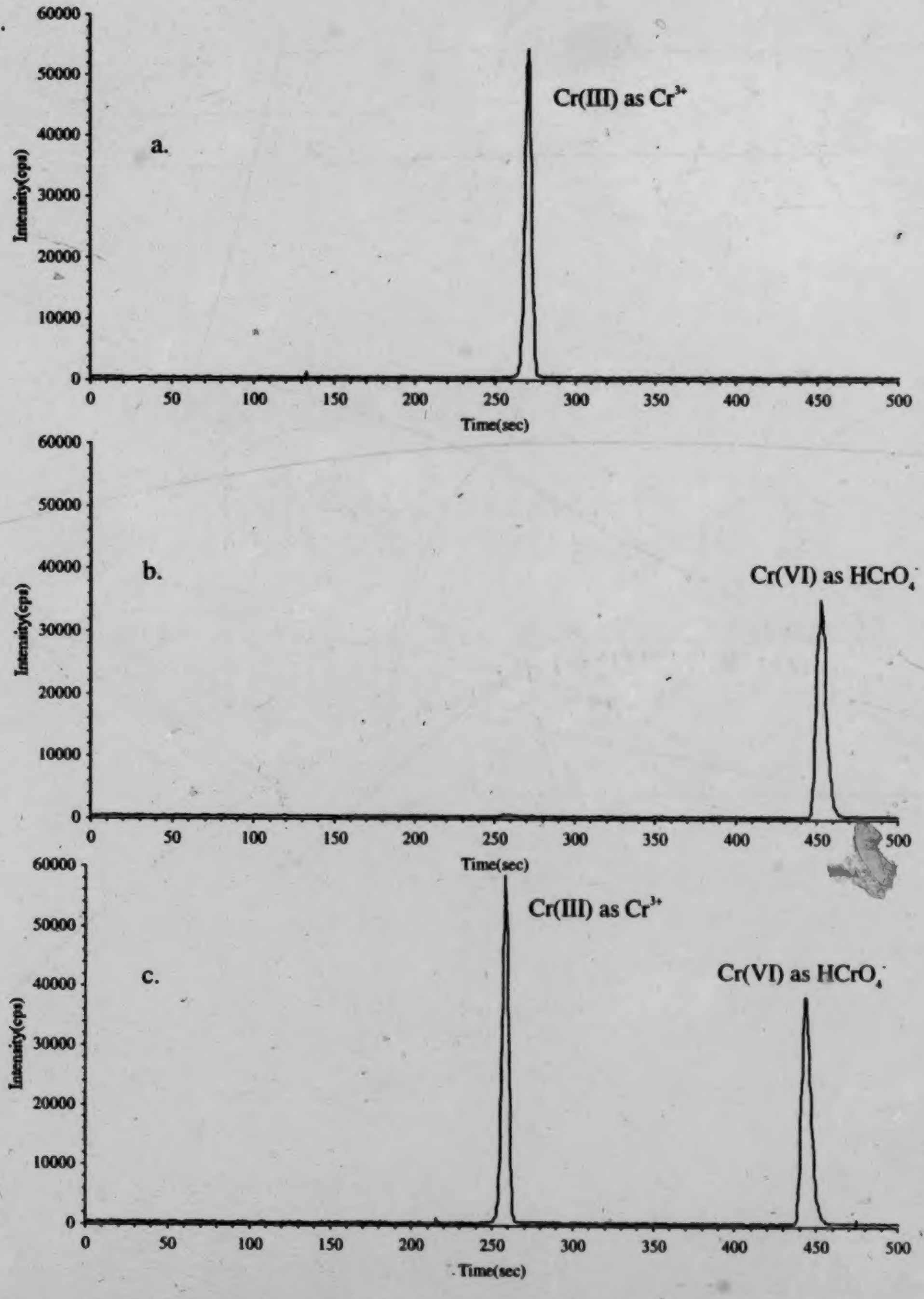

Figure 3.05 Electropherograms for (a) 1 ppm Cr(III), (b) 1 ppm Cr(VI) and (c) sample containing Cr(III) and Cr(VI) at 1 ppm each. Conditions as in Fig. 3.04

In order to establish the optimal working conditions and to achieve the best detection limits, the CE-DIN-ICP-MS system has to be carefully optimized. This includes the optimization of three parts of the system. The optimization of the direct injection nebulizer interface and the ICP-MS has been discussed elsewhere (Chapter 2). In this section, the focus will be on the optimization of electrostacking parameters.

3.3.3.1 Choice of Background Electrolyte

The proper choice of background electrolyte (BGE) is critical for the success of quantitative speciation. An ideal BGE should not chemically interact with the analytes of interest, because such interaction can alter the quantitative speciation information. The BGE should not produce any signals that interfere with the analyte determination. For the speciation of chromium by CE-ICP-MS, BGEs containing carbon, sulfur and chlorine species are not appropriate because they can form molecular species $^{40}Ar^{12}C^+$, $^{36}S^{16}O^+$ and $^{35}Cl^{16}OH^+$ in the plasma that interfere with the determination of $^{52}Cr^+$ - the most abundant isotope of chromium [50]. Organic buffers and chlorides should be avoided. The concentration of the BGE should also be properly chosen. A high BGE concentration decreases the double layer thickness and increases the shielding of negative sites on the capillary surface and therefore decreases the absorption of Cr^{3+} ions on the capillary wall [51]. However, the BGE concentration can not be too high, otherwise excess Joule heating will lead to band broadening. In order to minimize the analyte loss due to the absorption on the capillary wall, a BGE with a polyvalent cation can also be used because it will be more readily absorbed onto the negative sites to reduce Cr^{3+} adsorption [26,32]. Taking the above factors into consideration, 50 mM $Ca(NO_3)_2$ was chosen as the BGE for chromium speciation.

3.3.3.2 Effect of pH of Background Electrolyte on Electrostacking

The pH of background electrolyte is an important factor to consider when optimizing the electrostacking procedure. The pH affects ionization of the silanol groups (Si-OH) on the silica surface, which in turn influences the analyte-wall interaction and the magnitude of EOF. Figure 3.06 is a comparison of electropherograms obtained at different background electrolyte pH values. At electrolyte pH 6.0 (Figure 3.06a), the Cr^{3+} peak shows broadening and tailing. This can be attributed to the strong electrostatic interactions between Cr^{3+} and the negatively charged silica surface at this pH. It is well known that above pH 2-3, the silica surface becomes negatively charged due to silanol ionization ($Si\text{-}OH \rightarrow Si\text{-}O^-$)[52]. Cr^{3+} can be adsorbed onto this negatively charged surface. The slow kinetics of adsorption/desorption leads to a broadened and tailed peak. At electrolyte pH 2.0 the dissociation of all surface silanol groups is suppressed. Consequently, the Cr^{3+} adsorption should also be minimal. As anticipated, a sharper peak for Cr^{3+} was observed at pH 2.0 (Figure 3.06b). Since both analyte adsorption and EOF originate from the silica surface charges, low pH that suppresses adsorption also decreases EOF. The different migration times between the two runs are consistent with this suggestion. At pH 6.0, the contribution to bulk flow from EOF is higher, thus the peaks move faster toward the detector resulting in shorter migration times. At pH 2.0, EOF would be very small because of the surface charge suppression, therefore the migration times are longer. The observed difference in sample plug length is also consistent with this explanation. In order to get a good peak shape for Cr^{3+}, an electrolyte pH 2.0 was chosen for further studies.

3.3.3.3 Effect of pH of Sample on Electrostacking

The pH of the sample is another important parameter that needs careful consideration, because chromium species distribution in solution depends on sample pH. The pH of the

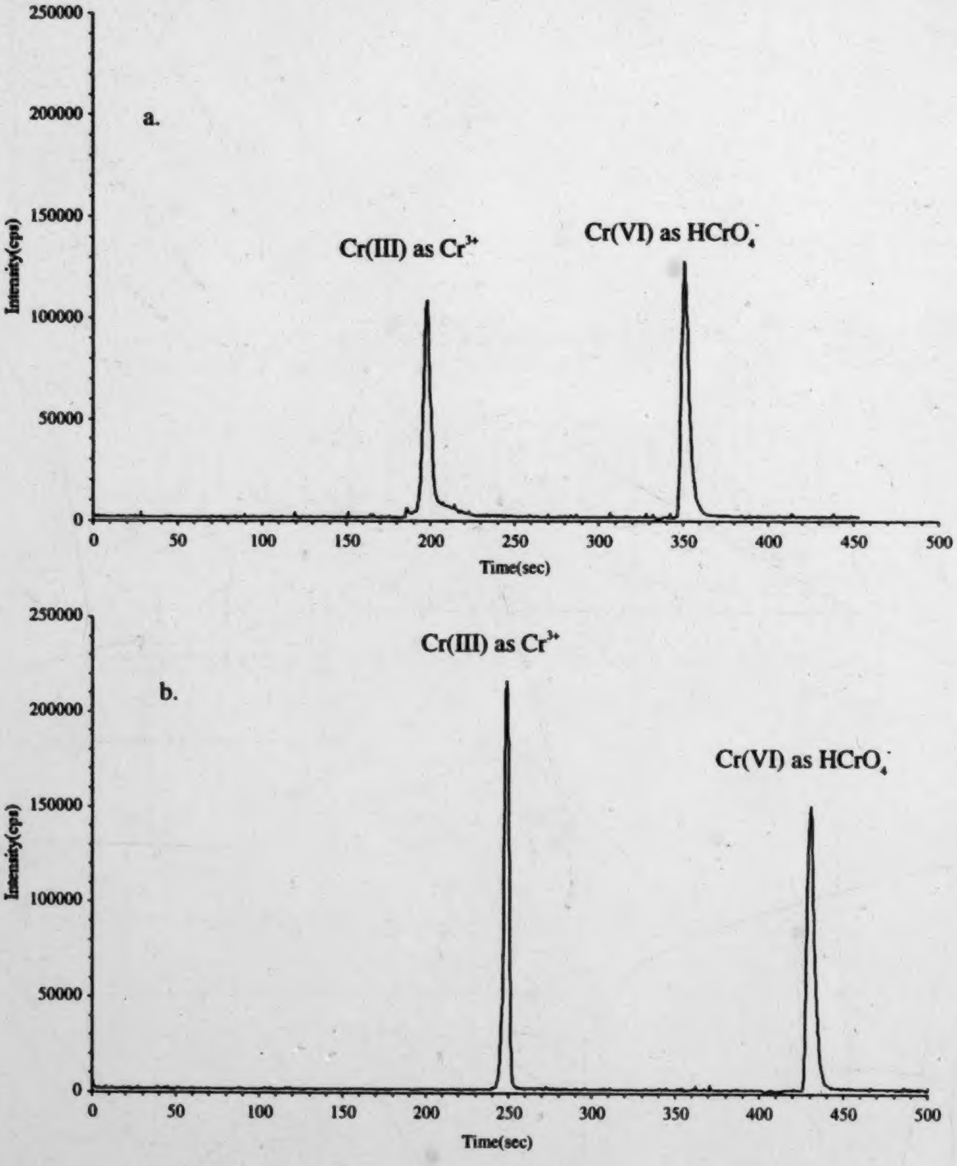

Figure 3.06 Electropherograms of 1 ppm each Cr(III) and Cr(VI) solution with a background electrolyte pH of (a) 6.0 and (b) 2.0. Other conditions as in Fig. 3.04.

sample affects the analyte-wall interaction and EOF as well, because a long plug of sample is injected into the capillary.

Figure 3.07 presents a comparison of electropherograms at different sample pH values. The background electrolyte pH was adjusted to 2.0 for both runs. At a sample pH of 5.0, Cr(III) exists presumably as $Cr(OH)^{2+}$. The broadened tailed peak of $Cr(OH)^{2+}$ is probably indicative of electrostatic interactions with capillary wall. Although the capillary was initially filled with pH 2.0 electrolyte, once the sample at pH 5.0 is injected into the capillary, the silanol groups on the wall within the sample region can dissociate making possible the absorption of $Cr(OH)^{2+}$. In contrast, the dissociation is not significant at a sample pH of 3.0, as the peak shape for Cr^{3+} is sharp. Interestingly, a sharper $HCrO_4^-$ peak was observed at pH 5.0. This is probably due to the fact that sample stacking is better at pH 5.0 than pH 3.0, because the pH 5.0 sample has a lower conductivity. A sample pH of 3.0 was chosen for subsequent studies.

It is interesting to note that if 50 mM HNO_3 (pH 1.3) is used as the background electrolyte the Cr^{3+} adsorption problem is insignificant regardless of sample pH values. This can be seen from Figure 3.08. In this case a sample pH 5.0 is a better choice because of the lower conductivity of the sample and consequently the better sample stacking at this pH.

3.3.3.4 Effect of Applied Voltages on Electrostacking

In CE, the applied voltage affects the ion migration velocity. Generally, a higher voltage results in a shorter migration time, narrower peak width and better resolution (limited by Joule heating). The present study, however, is based on sample stacking. Thus, it is necessary to determine how the applied voltage influences electrostacking.

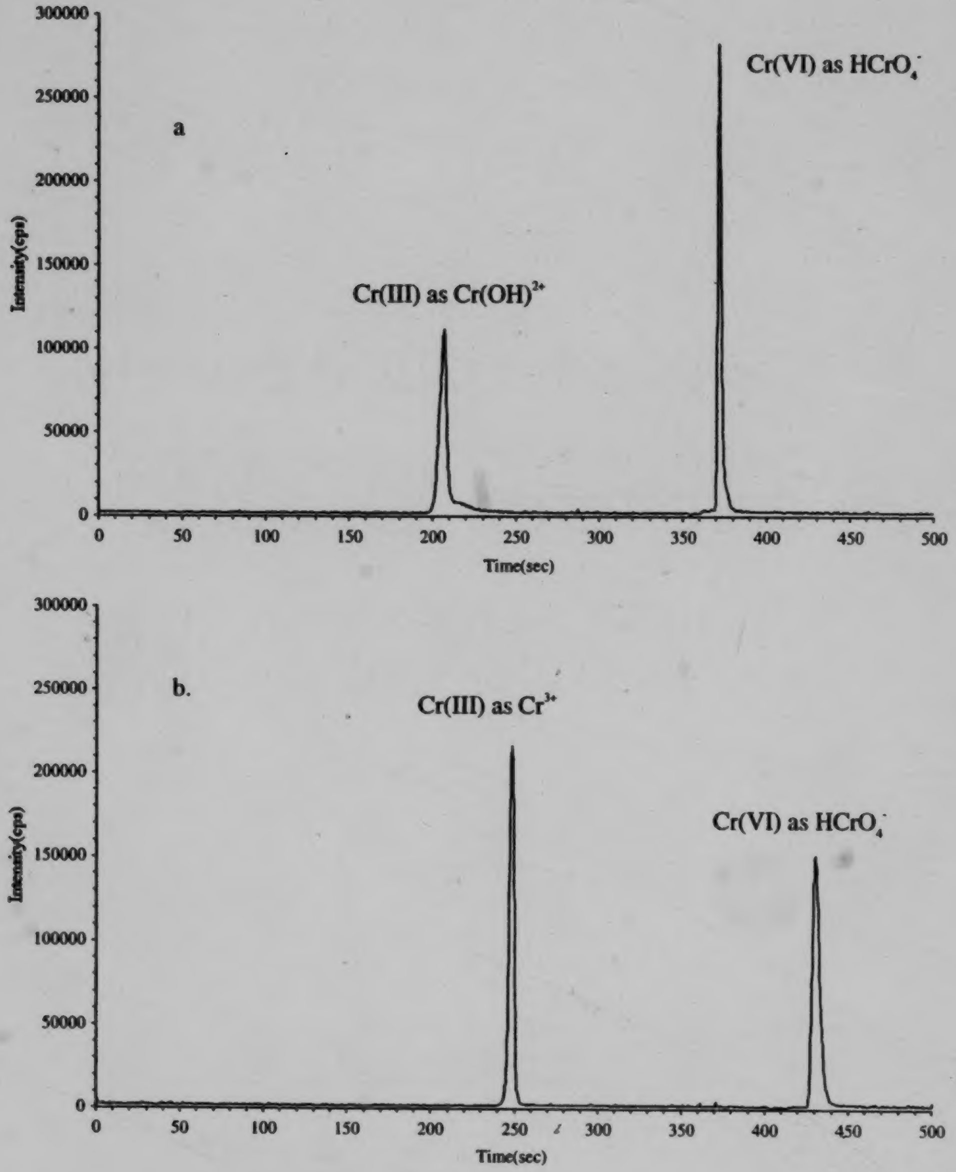

Figure 3.07 Electropherograms of 1 ppm each Cr(III) and Cr(VI) sample solution with pH of (a) 5.0 and (b) 3.0. Other conditions as in Fig. 3.04.

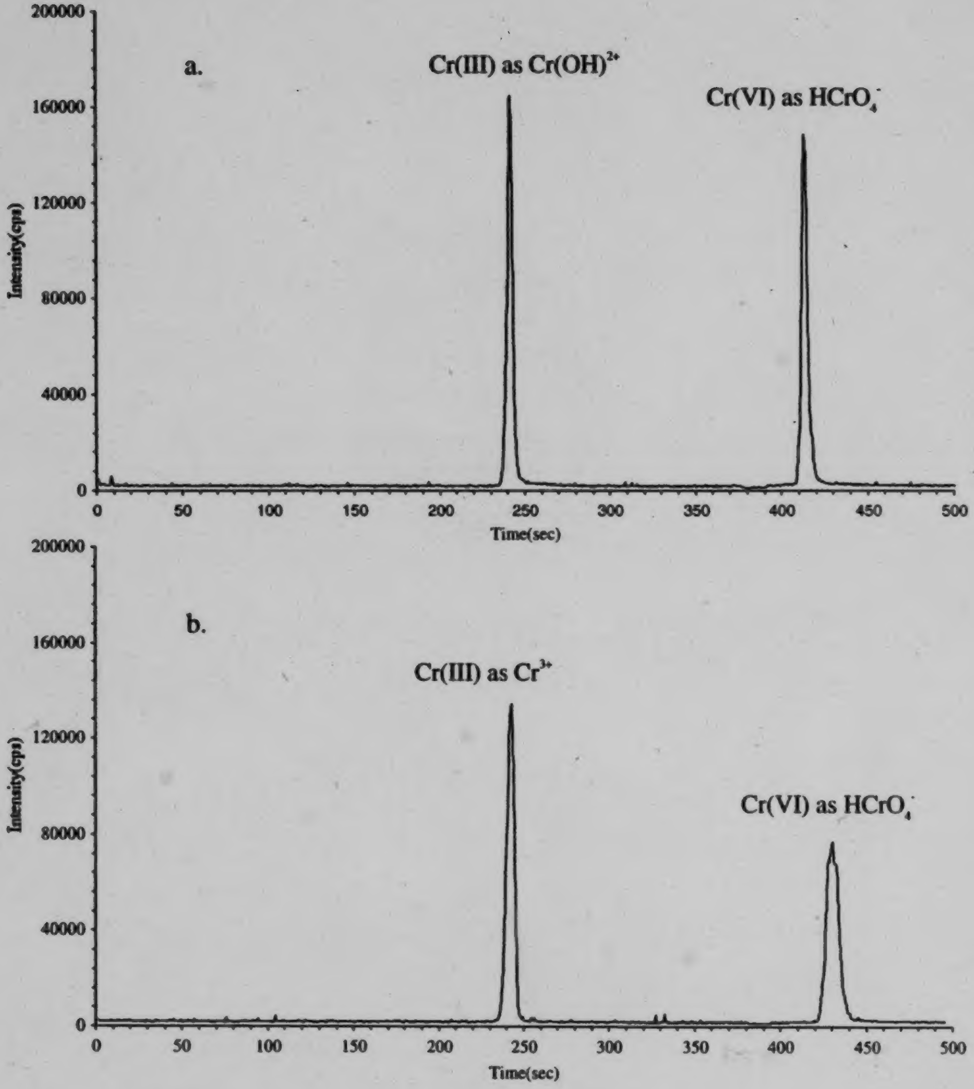

Figure 3.08 Electropherograms of 1 ppm each Cr(III) and Cr(VI) sample solution with pH of (a) 5.0 and (b) 3.0. Conditions as in Fig. 3.04 except 50 mM HNO_3 (pH 1.3) was used as the background electrolyte.

Figure 3.09 shows a comparison of electropherograms of Cr(III) and Cr(VI) with different voltages (6-15 kV) applied across the capillary. Measured values of peak area (arbitrary unit), peak height (cps), peak separation (s) and peak width (s, full width at half maximum) are listed in Table 3.01. Increasing the voltage from 6.0 to 15.0 kV results in no significant changes in peak areas for both Cr(III) and Cr(VI), as might be expected when the adsorption problem is eliminated and the analyte loss due to adsorption is negligible at the pH condition used. Increasing the voltage from 6.0 to 12.0 kV does not have a noticeable influence on the migration time for both Cr(III) and Cr(VI), consistent with the suggestion that the EOF is very small at this low pH and the bulk flow is mainly due to the suction-induced flow which is independent of voltage. However, at a voltage of 15.0 kV, both peaks come out earlier, indicating that bulk flow is faster. This may be related to the problem of Joule heating, which at this high voltage, results in a higher temperature and lower viscosity for the electrolyte solution in the capillary. The suction-induced flow (hydrodynamic flow) is inversely proportional to solution viscosity as predicted by Poiseuille' Law:

$$\upsilon = \frac{\Delta P \pi r^4}{8\eta L}$$

where υ is the volumetric flow rate, ΔP is the pressure difference between the ends of the capillary, r is internal radius of the capillary, η is viscosity of the fluid, and L is the total length of the capillary.

No change in peak width is observed for Cr^{3+} while an increasingly broadened peak is observed for $HCrO_4^-$ with an increase in the voltage (Table 3.01). The effect of peak broadening for $HCrO_4^-$ may be related to its penetration into the background electrolyte (see Fig. 3.04). It can be seen that the sample water plug leaves the capillary before $HCrO_4^-$. Once the water leaves the capillary, the applied voltage is dropped across the

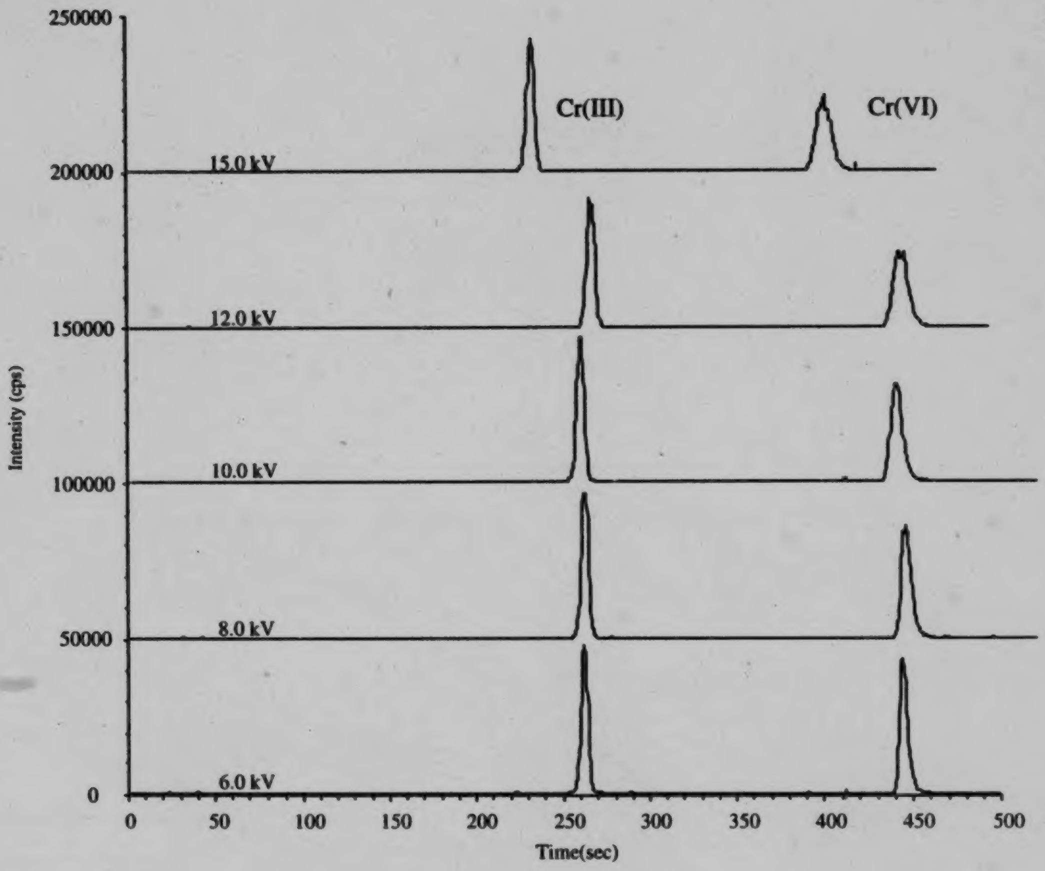

Figure 3.09 Electropherograms of 1ppm each Cr(III) and Cr(VI) solutions with different applied voltages (6-15 kV). Conditions: background electrolyte, 50 mM $Ca(NO_3)_2$ at pH 2.0; sample pH, 3.0; injection volume, 0.60 µL.

Table 3.01 Effect of applied voltages on peak area, peak height, peak width, and peak separation [a]

applied voltage (kV)	peak area($\times10^5$) (a.u.)		Peak height($\times10^4$) (cps)		fwhm (s)		peak separation (s)
	Cr(III)	Cr(VI)	Cr(III)	Cr(VI)	Cr(III)	Cr(VI)	
6.0	5.50	5.79	4.74	4.31	5	5	183
8.0	5.76	5.84	4.62	3.58	5	6	183
10.0	5.85	6.02	4.68	3.09	5	8	180
12.0	5.38	5.74	4.09	2.39	5	9	179
15.0	5.27	5.50	4.24	2.36	5	10	168

[a] Conditions: Cr(III) and Cr(VI) solutions, 1ppm each; carrier electrolyte, 50 mM $Ca(NO_3)_2$; injection time, 180 s; injection volume, 0.60 µL.

background electrolyte region. The concentrated $HCrO_4^-$ band migrating in this region will now experience an anti-stacking leading to band broadening.

In all, the effect of voltage on sample stacking is different from that in conventional CE separation. Higher voltage may not be beneficial to sample stacking. A voltage of 10 kV was used for subsequent studies.

3.3.3.5 Effect of Injection Volume on Electrostacking

In conventional CE separation, the injection volume is an important factor that affects efficiency and band broadening. For generating a maximum 10% broadening, the total length of the sample plug should be less than 1% of the capillary length [46,49]. In the present study, species separation is based on sample stacking and a long plug of sample is injected in capillary, it is therefore necessary to investigate the effect of injection volume on sample stacking.

Figure 3.10 shows a comparison between five different injection volumes. All the electropherograms are plotted on the same scale in order to visualize the influence of injection volumes. Injection volumes are estimated by calculation from the suction flow rate and injection time. The five injection volumes 0.20, 0.40, 0.60, 0.80, and 1.0 μL correspond to 13%, 27%, 40%, 54%, and 67% of the total capillary volume, respectively. Listed in Table 3.02 are the measured values of peak area, peak height, peak width, and peak separation as well as the injection time and volumes. As seen in the figure and table, both peak area and peak height for Cr(III) and Cr(VI) increase with increasing injection volume up to 54% of the total capillary volume. This clearly demonstrates the concentration effect of this technique. However, at an injection volume of 1.0 μL, the Cr(III) peak is seriously broadened, indicating that sample loading exceeds the stacking

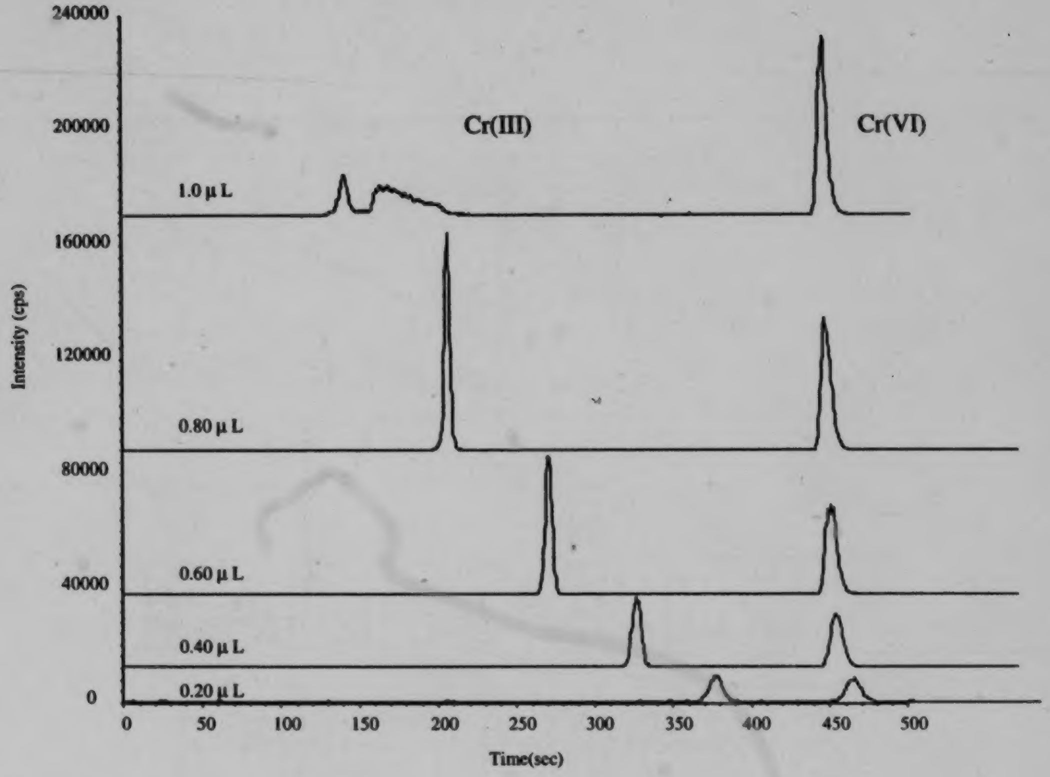

Figure 3.10 Electropherograms of 1 ppm each Cr(III) and Cr(VI) solution with different injection volume (0.20-1.0 µL). Conditions: background electrolyte, 50 mM $Ca(NO_3)_2$ at pH 2.0; sample pH, 3.0; applied voltage, +10 kV.

Table 3.02 Effect of injection volume on peak area, peak height, peak width, and peak separation [a]

injection time (sec)	injection volume (µL)	peak area($\times10^5$) (a.u.)		peak height($\times10^4$) (cps)		fwhm (s)		peak separation (s)
		Cr(III)	Cr(VI)	Cr(III)	Cr(VI)	Cr(III)	Cr(VI)	
60	0.20	2.05	2.04	0.905	0.84	10	11	87
120	0.40	4.02	4.17	2.45	1.87	7	8	138
180	0.60	6.01	6.20	4.80	3.06	6	8	180
240	0.80	7.94	8.17	7.58	4.46	4	7	242
300	1.0	10.2	10.4		6.23		6	

[a] Conditions: Cr(III) and Cr(VI) solutions, 1 ppm each; carrier electrolyte, 50 mM $Ca(NO_3)_2$ at pH 2.0; sample pH, 3.0; applied voltage, +10 kV.

capacity, i.e., the migration time for Cr(III) is too short to complete the stacking before it exits the capillary. So the concentration technique has its limit. A linear relationship has been observed between peak area and injection volume, but the relationship between peak height and injection volume is non-linear (Figure 3.11). This is expected, since peak area is only affected by analyte adsorption, while the peak height is affected by additional variables such as sample stacking, band broadening as well as adsorption. For quantitative work, peak area is a better choice than peak height. In this study, peak areas were used for quantitation.

The peak width for Cr(III) decreases slightly with increasing the injection volume (up to 0.80 μL), while the peak width for Cr(VI) remains essentially constant with changing the injection volume. This probably results from the band broadening due to longitudinal diffusion. The longer the sample plug the less time the Cr(III) stays in the capillary, and therefore less band broadening due to diffusion. Since Cr(VI) has about the same migration time for each run, the band broadening remains essentially constant. Of course, the peak separation between Cr(III) and Cr(VI) increases with an increase in the injection volume, consistent with the model prediction that they are focused at opposite ends of the sample plug.

3.3.4 Quantitative Speciation

3.3.4.1 Calibration Curves

Calibration curves for Cr(III) and Cr(VI), linear over 3 orders of magnitude, are shown in Figure 3.12 . The slope of log-log plot is 1.00 for Cr(III) and 0.99 for Cr(VI). The two curves almost overlap, indicating both Cr(III) and Cr(VI) species are efficiently converted to Cr^+ in the ICP, and they have the same sensitivity.

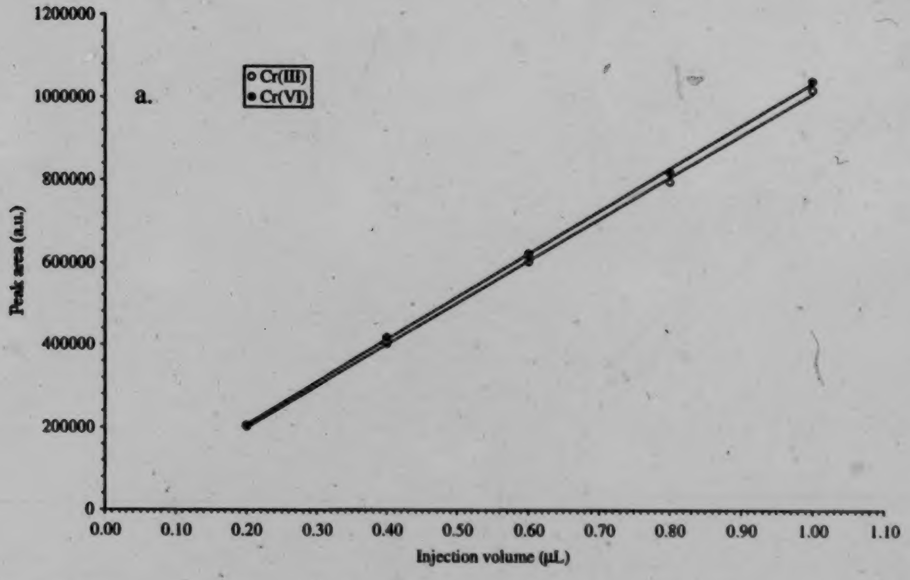

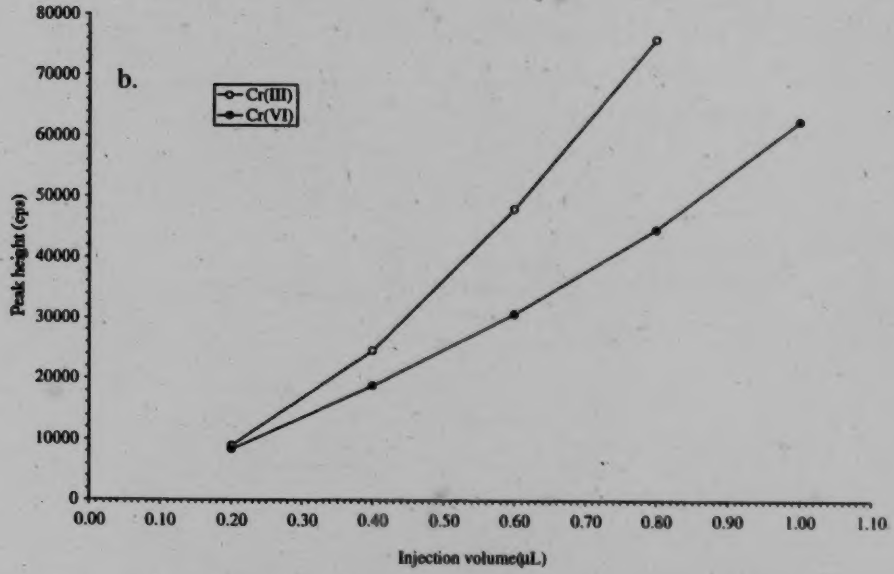

Figure 3.11 Plots of peak area (a) and peak height (b) versus injection volume. Conditions as in Table 3.02.

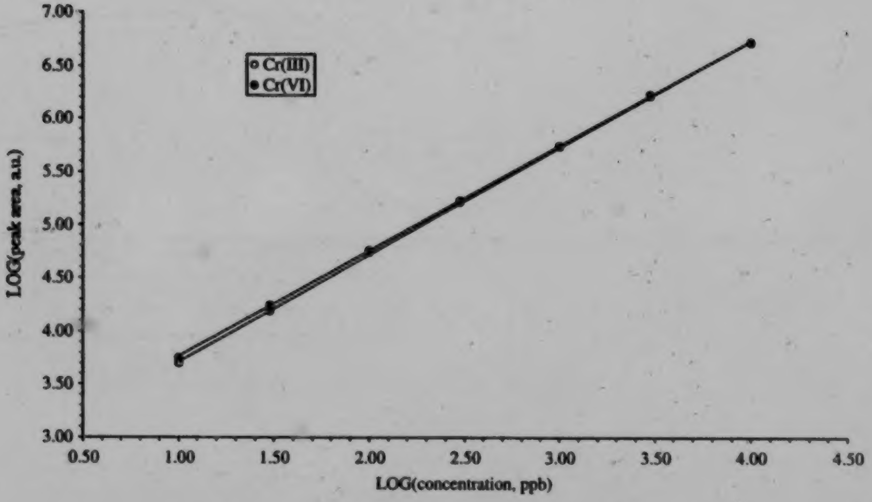

Figure 3.12 Calibration curves for Cr(III) and Cr(VI). Conditions: background electrolyte, 50 mM $Ca(NO_3)_2$ at pH 2.0; sample pH, 3.0; applied voltage, +10 kV; injection volume,0.60 μL.

3.3.4.2 Limits of Detection

Detection limits were defined as the concentration that produces a net signal equivalent to three times the standard deviation of the blank signal. The detection limit was based on peak area. Peak areas were obtained by summation of the intensities of the data points across the peak and were background subtracted. To obtain the standard deviation of the background for peak area, five to seven electropherograms of the background were acquired. The intensities of the data points (equal in number to the points across the peak) from the baseline were added up for each electropherogram, and the standard deviation of the added baseline points was calculated. The detection limit was calculated as three times the standard deviation of the peak area of the background divided by the slope of the calibration curve (peak area vs. concentration). The detection limits (concentration and absolute), along with slopes of log-log plot, linear dynamic range and repeatability are listed in Table 3.03. The detection limits are lower than those of CE method using UV detection [29-31], but comparable to the results of CE-ICP-MS using conventional concentric nebulizer [32].

3.3.4.3 Matrix Effects

Matrix effects may be present in both the ICP-MS system and the CE system. The sample matrix effects in the ICP-MS would probably be small, because the ratio of sample flow to sheath flow is very small. The sheath liquid flow rate used is around 20-30 μL/min, while the suction flow rate is about 0.20 μL/min. Therefore, the sheath liquid is the major matrix that the ICP-MS detects which is constant over time and from sample to sample [26]. On the other hand, sample matrix effects from the CE part may be large. Particularly, sample stacking depends on the relative conductivity of the sample and background electrolyte. Efficient sample stacking requires a lower conductivity for the

Table 3.03 Analytical figures of merit for the speciation of chromium by CE-DIN-ICP-MS[a]

Analyte	Linear dynamic Range (ppm)	Slope of log-log plot	Correlation coefficient	Detection limit		Repeatability (RSD%)[b]
				Concentration (ppb)	Absolute (pg)	
Cr(III)[c]	0.01 - 10	1.00	0.999	1.4	0.8	1.7
Cr(VI)[c]	0.01 - 10	0.99	0.999	3.4	2.0	2.2
Cr(III)[d]	0.1 - 100	1.07	0.999	4.4	0.9	2.1
Cr(VI)[d]	0.1 - 100	1.02	0.999	5.0	1.0	3.0

[a] Detection limits based on peak area.

[b] Repeatability based on 1 ppm solution.

[c] Conditions: background electrolyte, 50 mM $Ca(NO_3)_2$ at pH 2.0; sample pH, 3.0; applied voltage, +10 kV; injection volume, 0.60 μL.

[d] Conditions: background electrolyte, 50 mM HNO_3 at pH 1.3; sample pH, 5.0; applied voltage, +10 kV; injection volume, 0.20 μL.

sample compared to that of the electrolyte. If the sample conductivity is high, the field strength over the sample plug will be low and the analyte peak will be broadened. Figure 3.13 shows the effects of changing sample matrix on the peak width. Changing the sample matrix from 1 mM HNO_3 to 10 mM HNO_3 and $NaNO_3$ results in broadened peaks. The major limitation of the stacking method is the difficulty to analyze samples where the matrix components are concentrated. Nevertheless, there may be ways to reduce the matrix effects. For example, Ding et al. [51] reported that samples containing 0.5 M salt (e.g. sea water) can be analyzed directly by CE by making the BGE salt content even higher (1.5 M) to obtain electrostacking. Gil et al. [53] reported that modification of the sample matrix with methanol is an effective way to reduce the conductivity of aqueous samples, making them suitable for sample stacking. Other methods such as isotachophoresis, and solid-phase extraction may also be used to overcome the matrix effects [54].

3.4 Conclusions

An effective method for the quantitative speciation of chromium using CE-DIN-ICP-MS has been presented. The coupling of CE to ICP-MS using a laboratory-constructed DIN has been demonstrated to be successful. On-line sample stacking not only allows for enhancement of sensitivity but also results in separation of Cr(III) and Cr(VI). The presence of suction-induced flow toward the detector did not cause any significant band broadening, and the simultaneous separation of both species in a single run was achieved in less than 8 min, without the need for sample pre-complexation or conversion. Good repeatability and linearity were observed. Concentration detection limits were obtained at the ppb level and absolute detection limits at the pg level. Linear dynamic range extended over at least four orders of magnitude. It has also been demonstrated that it is necessary to control the pH of the background electrolyte and sample (i.e. make sure it is acidic) to

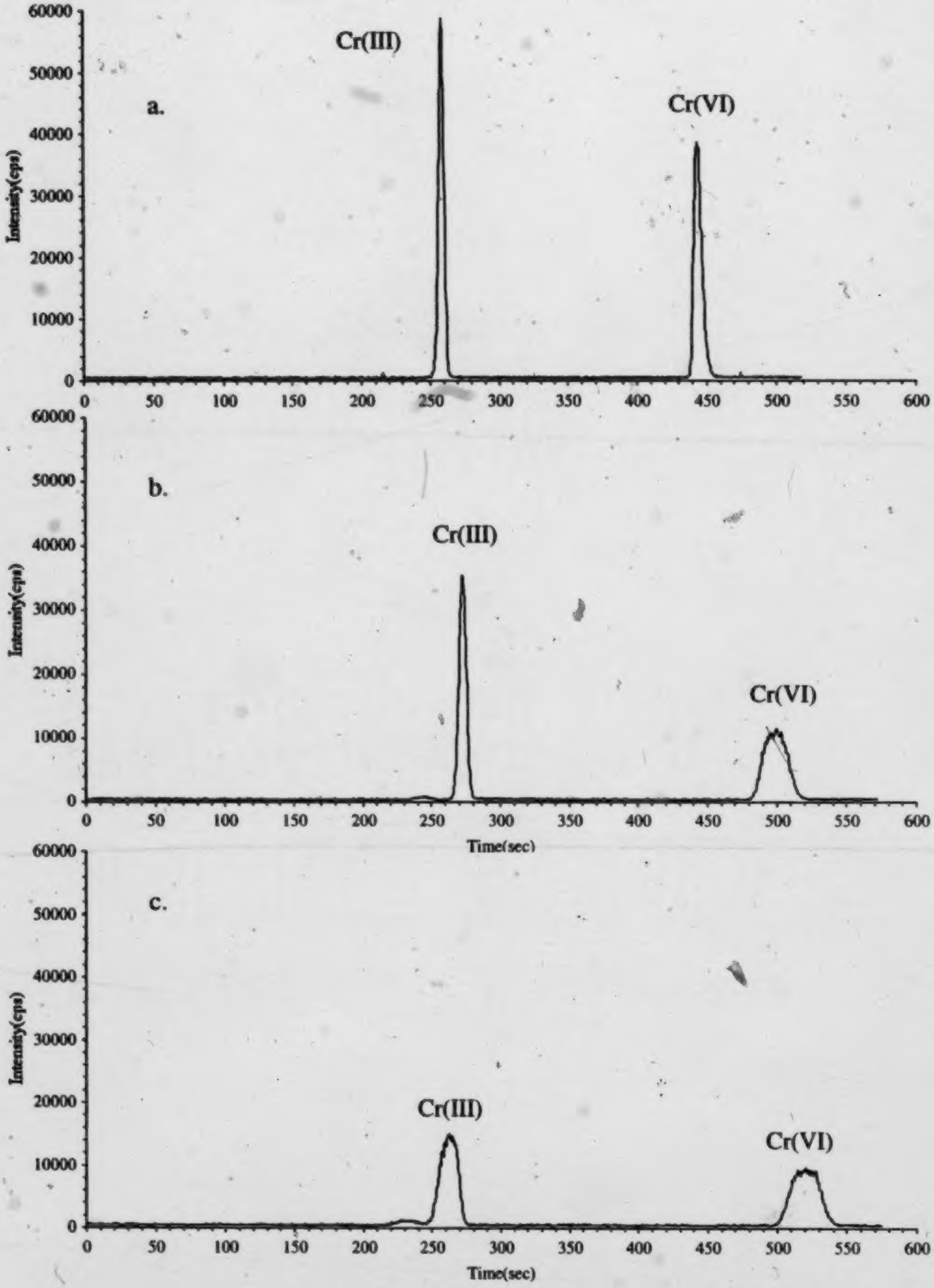

Figure 3.13 Electropherograms of 1ppm each Cr(III) and Cr(VI) solutions with sample matrix of (a) 1mM HNO_3, (b) 10 mM HNO_3 and (c) 10 mM $NaNO_3$. Conditions: background electrolyte, 50 mM $Ca(NO_3)_2$ at pH 2.0; applied voltage, +10 kV; injection volume, 0.60 μL.

minimize the adsorption of Cr(III). A sample volume up to 54% of total capillary volume can be injected into the capillary without significant band broadening and the longer sample plug results in better resolution of the Cr(III) and Cr(VI) peaks.

3.5 References

1. Nriagu, J. O. and Nieboer, E., *Chromium in the Natural and Human Environments*, John Wiley and Sons, New York, 1988.
2. Katz, S. A. and Salem, H., *The Biological and Environmental Chemistry of Chromium*, VCH, New York, 1994.
3. Stoecker, B. J., *J. Trace Elem. Exp. Med.*, 1999, **12**, 163 and references therein.
4. Connet, P. H. and Wetterhahn, K. E., *Structure and Bonding*, 1983, **54**, 93.
5. Campanella, L., in *Element Speciation in Bioinorganic Chemistry*, Caroli, S., ed., John Wiley and Sons, New York, 1996, Ch. 12, pp. 419-443.
6. Cheng, K. L., Ueno, K., and Imamura, T., eds, *Handbook of Organic Analytical Reagents*, CRC Press, 1982, pp. 277-283.
7. Sperling, M., Xu, S., and Welz, B., *Anal. Chem.*, 1992, **64**, 3101.
8. Posta, J., Berndt, H., Luo, S., and Schaldach, G., *Anal. Chem.*, 1993, **65**, 2590.
9. Gaspar, A., Posta, J., and Toth, R., *J. Anal. At. Spectrom.*, 1996, **11**, 1067.
10. Gaspar, A., Sogor, C., and Posta, J., *Fresenius' J. Anal. Chem.*, 1999, **363**, 480.
11. Cox, A. G., and Mcleod, C. W., *Microchim. Acta*, 1992, **109**, 161.
12. Byrdy, F. A., Olson, L. K., Vela, N. P., and Caruso, J. A., *J. Chromatogr. A*, 1995, **712**, 311.
13. Posta, J., Alimonti, A., Petrucci, F., and Caroli, S., *Anal. Chim. Acta*, 1996, **318**, 185.
14. Pantsar-Kallio, M., and Manninen, P. K. G., *Anal. Chim. Acta*, 1996, **325**, 335.
15. Tomlinson, M. J., Wang, J., and Caruso, J. A., *J. Anal. At. Spectrom.*, 1994, **9**, 957.
16. Zoorob, G., Tomlinson, M. J., Wang, J., and Caruso, J. A., *J. Anal. At. Spectrom.*, 1995, **10**, 853.
17. Tomlinson, M. J., and Caruso, J. A., *Anal. Chim. Acta*, 1996, **322**, 1.

18. Powell, M.J., Boomer, D. W. and Wiederin, D. R., *Anal. Chem.*, 1995, **67**, 2774.

19. Lintschinger, J., Kalcher, K., Gossler, W., and Kolbl, G. and Novic, M., *Fresenius' J. Anal. Chem.*, 1995, **351**, 604.

20. Andrle, C. M., Jukubowski, N., and Broekaert, J. A. C., *Spectrochim. Acta Part B*, 1997, **52B**, 189.

21. Barnowski, C., Jakubowski, N., Stuewer, D., and Broekaert, J. A. C., *J. Anal. At. Spectrom.*, 1997, **12**, 1115.

22. Saverwyns, S., Hecke, K. V.,Vanhaecke, F., Moens, L., and Dams, R., *Fresenius' J. Anal. Chem.*, 1999, **363**, 490.

23. Welz, B., *J. Anal. At. Spectrom.*, 1998, **13**, 413.

24. Dabek-Zlotorzynska, E., Lai, E. P. C., and Timerbaev, A. R., *Anal. Chim. Acta*, 1998, **359**, 1.

25. Timerbaev, A. R., Dabek-Zlotorzynska, E., and van den Hoop, M. A. G. T., *Analyst*, 1999, **124**, 811.

26. Olesik, J. W., Kiner, J. A., Grunwald, E. J., Thaxton, K. K. and S.V. Olesik., *Spectrochim. Acta*, 1998, **53B**, 239.

27. Majidi, V., and Miller-Ihli, N., *Analyst*, 1998, **123**, 809.

28. Taylor, K. A., Sharp, B. L., Lewis, D. J., and Crews, H. M., *J. Anal. At. Spectrom.*, 1998, **13**, 1095.

29. Timerbaev, A. R., Semenova, O. P., Buchberger, W., and Bonn, G. K., *Fresenius' J. Anal. Chem.*, 1996, **354**, 414.

30. Jung, G. Y., Kim, Y. S., and Lim, H. B., *Anal. Sci.*, 1997, **13**, 463.

31. Pozdniakova, S., and Padarauskas, A., *Analyst*, 1998, **123**, 1497.

32. Olesik, J. W., Kinzer, J. A., and Olesik, S. V., *Anal. Chem.*, 1995, **67**, 1.

33. Mei, E., Ichihashi, H., Gu, W., and Yamasaki, S., *Anal. Chem.*, 1997, **69**, 2187.

34. Chan, Y. Y., and Chan, W. T., *J. Chromatogr. A*, 1999, **853**, 141.

35. Baes, C. F., and Mesmer, R. E., *The Hydrolysis of Cations*, John Wiley and Sons, New York, 1976, pp.211-219.

36. Stunzi, H., and Marty, W., *Inorg. Chem.*, 1983, **22**, 2145.

37. Rotzinger, F. P., Stunzi, H., and Marty, W., *Inorg. Chem.*, 1986, **25**, 489.

38. Spiccia, L. and Marty, W., *Inorg. Chem.*, 1986, **25**, 266.

39. Speccia, L., Stoeckli-Evans, H., Marty, W., and Giovanoli, R., *Inorg. Chem.*, 1987, **26**, 474.

40. Stunzi, H., Speccia, L., Rotzinger, F. P., and Marty, W., *Inorg. Chem.*, 1989, **28**, 66.

41. Rai, D., Sass, B. M., and Moore, D. A., *Inorg. Chem.*, 1987, **26**, 345.

42. Tandon, R. K., Crisp, P.T., Ellis, J., and Baker, R. S., *Talanta*, 1984, **31**, 227.

43. Tong, S., and K., Li, *Talanta*, 1986, **33**, 775.

44. Michel, G., and Machiroux, R., *J. Raman Spectrosc.*, 1983, **14**, 22.

45. Michel, G., and Cahay, R., *J. Raman Spectrosc.*, 1986, **17**, 79.

46. Burgi, D. S., and Chien, R. L., *Anal. Chem.*, 1991, **63**, 2042.

47. Chien, R. L., and Burgi, D.S., *Anal. Chem.*, 1992, **64**, 1046.

48. Chien, R. L., and Burgi, D.S., *Anal. Chem.*, 1992, **64**, 489A.

49. Albin, M., Grossman, P. D., and Moring, S. E., *Anal. Chem.*, 1993, **65**, 489A

50. Tan, S. H., and Horlick, G, *Appl. Spectrosc.*, 1986, **40**, 445.

51. Ding, W., Thornton, M. J. and Fritz, J. S., *Electrophoresis*, 1998, **19**, 2133.

52. Jandik, P., and Bonn, G., *Capillary Electrophoresis of Small Molecules and Ions*, VCH, New York, 1993.

53. Gil, E. P., Ostapczuk, P., and Emons, H., *Anal. Chim. Acta*, 1999, **389**, 9.

54. Timerbaev, A. R., and Buchberger, W., *J. Chromatogr. A*, 1999, **834**, 117.

Chapter 4

Quantitative Speciation of Vanadium

4.1 Introduction

Vanadium occurs in biological systems and in the environment in a number of oxidation states, two of which, V(IV) and V(V) are the most commonly occurring states. Biological studies involving V(IV) and V(V) have increased over the past 15 years due to discovery of the biological activities of this element, especially with respect to phosphate metabolism and insulin-mimetic properties [1-3]. Vanadium has stimulatory, regulatory and inhibitory effects on many phosphate-metabolizing enzymes [4,5]. Vanadium (IV) is the more stimulatory form of the element, while V(V) is the more inhibitory form [5]. Several vanadium compounds have been developed for the treatment of diabetes [6-8]. Although vanadium is known to be essential for chickens and rats, conclusive evidence is still lacking that it is an essential element for humans [9,10]. There is little doubt that vanadium can be toxic at higher concentrations for both animals and humans [11-14]. The toxicity of vanadium depends on its oxidation state. It is recognized that V(V) as vanadate is more toxic than V(IV) as vanadyl ion [15]. When V(V) enters a cell, it can be reduced in vivo by cellular components to V(IV) causing DNA damage, protein synthesis blocking, as well as lipid peroxidation, a primary step in the development of cardiovascular disease [16].

Vanadium is also of environmental interest because of its widespread industrial applications and large releases into the environment. Vanadium is extensively used in the production of special vanadium steels, in the manufacture of pigments, printing inks and paints, in petrochemical, glass and nuclear industries [17]. The combustion of fossil fuels, including crude oil, gasoline, and coal, releases large quantities of vanadium into the atmosphere [18]. Over-exposure to vanadium can cause lung irritation, nausea, nervous depression and kidney damage. Since toxicity, biological activity and transport of vanadium are species dependent, it is essential to develop methods for accurate determination of vanadium in its different forms or oxidation states in environmental and biological samples.

Numerous methods for determination of vanadium (total content or one oxidation state) are available in the literature, but little work on the speciation of vanadium has been reported [19-29]. These are briefly summarized in Table 4.01. A majority of the methods are based on ion exchange and liquid chromatography (LC). Most of the methods are far from ideal and have one or more limitations. These include the need for pre-complexation or derivatization, relatively large sample and reagent requirements, time consumption, limited sensitivities and complicated procedures.

Capillary electrophoresis (CE) as a separation technique has unique capabilities including highly efficient separation, small sample and buffer volume requirements and fast analysis time. Compared with LC methods, CE has another important advantage, the lack of a stationary phase, which minimizes the chemical interactions between analyte and stationary phase. These unique properties make CE an attractive technique for trace element speciation [30,31]. In spite of this, the application of CE to the speciation of vanadium has been reported only in three recent studies [32-34]. Jen et al. [32] used a method based on chelation of V(IV) and V(V) with ethylenediaminetetraacetic acid (EDTA) to form anionic V(IV)-EDTA and V(V)-EDTA complexes prior to CE separation. The separated species were measured spectrophotometrically at 280 nm. The detection limits achieved were 400 ppb for V(IV) and 100 ppb for V(V). Thornton and Fritz [33] separated V(IV) as vanadyl ion (VO^{2+}) and V(V) as vanadate ion (VO_2^+) at pH

Table 4.01 Summary of methods for vanadium speciation

Separation method	Detection system	Detection limits		Ref.
		V(IV)(ppb)	V(V)(ppb)	
Solvent extraction of V(IV) and (V) with 2-hydroxyacetophenone oxime at different pH values	UV-VIS 350 nm for V(IV) 400 nm for V(V)	~1000	~1000	[19]
Ion chromatography of V(IV) and V(V) as EDTA complexes	Conductivity	200	100	[20]
Pre-concentration of V(IV) on EDTA-bonded silica gel and of V(V) on ethylenediamine-bonded silica gel	ICP-AES	2.4	2.4	[21]
Ion chromatography of V(IV) as CDTA complex and V(V) as vanadate	UV-VIS(282 nm)	145	70	[22]
Liquid chromatography of V(IV) and V(V) as EDTA complexes	UV(245 nm)	50	50	[23]
Liquid chromatography of V(IV) and V(V) using 4-(2-pyridylazo)resorcinol as the chelating reagent	UV-VIS(540 nm)	1	2	[24]
Liquid chromatography of V(IV) and V(V) using 2,6 pyridinedicarboxylic acid as chelating reagent	ICP-MS	2.3	0.48	[25]
Separation of V(IV) and V(V) by sorption on an iminodiacetic chelating resin	GF-AAS	10	10	[26]
Liquid chromatography of V(IV) and V(V) as EDTA complexes	USN-ICP-MS	0.025	0.041	[27]
Selective preconcentration of V(IV) and V(V) on an anion exchanger using Eriochrome Cyanine R as chelating reagent	Solid phase spectrophotometry 563 nm for V(IV) 585 nm for V(V)	1.6	1.4	[28]
Liquid chromatography of V(IV) and V(V) using KH-phthalate as a reagent	FAAS	150	180	[29]

2.3 in aqueous $HClO_4$ electrolyte by CE using direct UV detection at 185 nm. Although no pre-capillary complexation was needed, the detection limits were poor (1.0 ppm for VO^{2+} and 5.0 ppm for VO_2^+). More over, the migration times were long, being ~12 min for VO^{2+} and ~21 min for VO_2^+. Pozdniakova and Padarauskas [34] used a method similar to that of Jen et al. [32] for the speciation of vanadium. EDTA, cyclohexane-1,2-diaminetetraacetic acid (CDTA) and diethylenetriaminepentaacetic acid (DTPA) were compared as complexing agents for vanadium. They found that for vanadium speciation the best chelating agent was EDTA, and the use of an electrolyte containing EDTA and pre-capillary complexation of sample was required. The detection limits were not reported but were probably in the range from 60 to 420 ppb using direct UV detection at 214 nm.

In view of above, it is evident that CE methods with UV detection lack sufficient sensitivity in terms of concentration, which is a major limitation for their application to vanadium speciation. Pre-capillary derivatization may not be desirable, as it may cause contamination and is also time consuming.

ICP-MS is a highly sensitive and element-specific detection system [35]. Coupling CE to ICP-MS is becoming an attractive technique for element speciation [30,31,36-38]. To our knowledge, there has been no reports so far dealing with vanadium speciation using CE - ICP-MS.

In this study, the quantitative speciation of vanadium by CE-ICP-MS using a laboratory-constructed direct injection nebulizer interface is presented. The sample is first subjected to an electrostacking step in the CE capillary. This results in the separation of the vanadium (IV) and vanadium (V), which is followed by ICP-MS detection. The optimization of the sample stacking procedure by choice of carrier electrolyte and adjustment of sample pH is examined. The analytical performance of the method, in terms of linear dynamic range, detection limits and repeatability, is described.

Vanadium exists in aqueous solution mainly as two oxidation states, IV and V. Vanadium(IV) has a d^1 electron configuration, and therefore can be studied using electron paramagnetic resonance (EPR) spectroscopy [39]. In acidic aqueous solution and in the absence of strongly complexing ligands, V(IV) exists as the hydrated cation $VO(H_2O)_5^{2+}$, commonly abbreviated as VO^{2+} and called vanadyl ion. This species is stable to air oxidation only at pH < 2.4, and the rate of oxidation increases rapidly at higher pHs [22,40]. Therefore, the standard solution of V(IV) should be kept at acidic conditions and under low temperature and speciation studies of V(IV) in the alkaline solution must consider the stabilization of V(IV) (e.g. using stabilizing ligands to complex it). Increasing the pH leads to the formation of various hydrolysis products [41,42]. These species are likely involved in following equilibria:

$$VO^{2+} + H_2O \Leftrightarrow VOOH^+ + H^+ \qquad K_{11} = 4.4 \times 10^{-6} \qquad (4.01)$$

$$2VOOH^+ + 2H_2O \Leftrightarrow (VOOH)_2^{2+} + 2H^+ \qquad K_{22} = 1.5 \times 10^{-7} \qquad (4.02)$$

$$VO^{2+} + 2OH^- \Leftrightarrow VO(OH)_2\,(s) \qquad K_{sp} = 1.8 \times 10^{-22} \qquad (4.03)$$

$$VO(OH)_2\,(s) + 2OH^- \Leftrightarrow VO(OH)_3^- \qquad (4.04)$$

The equilibrium between $VO(OH)_2(s)$ and $VO(OH)_3^-$ (Equation.4.04) is only slowly established, because of the slow reversibility of the reaction or incomplete dissolution of $VO(OH)_2(s)$ [39]. An anionic polynuclear V(IV) species, $V_{18}O_{42}^{12-}$ has been reported at pH around 5, but this ion is unstable in solutions at V(IV) concentration less than 2 mM giving an uncharacterized monomeric species [43]. Not all of the hydrolysis species in the pH 7-11 range are known, because some species are present below detection limits of currently available methods and some species polymerize to give electron-paired species that are EPR silent. Despite this limited knowledge, a reasonable speciation diagram has been given for the above equilibria [39], and this is illustrated in Figure 4.01. Although the distribution diagram is incomplete, it nevertheless shows the speciation distribution below pH 6, the range of interest in this study. From Figure 4.01, it can be seen that the species distribution is both pH and total vanadium concentration dependent because of the formation of the dimer (Equation 4.02) and the precipitation of $VO(OH)_2$ (s) (Equation 4.03). Below pH 4, the predominant species is VO^{2+}. In the pH range 4 - 6.5, the predominant species is $VOOH^+$ with a minor amount of the dimer $(VOOH)_2^{2+}$ also present. As the pH is raised into the range between 7 and 11, The precipitate $VO(OH)_2$ forms. Owing to its low solubility, the concentration of the soluble species in this range is limited and cannot be detected by EPR. Above pH 11, the dominant species is $VO(OH)_3^-$.

The chemistry of vanadium (V) in aqueous solution is complex owing to the formation of the various polyoxoanions. Such species include monomer, dimer, tetramer and other oligermers. The protonation and condensation equilibria are dependent on pH, total vanadium concentration, temperature, and ionic strength of the medium. Despite this complexity, such systems have been extensively studied by ^{51}V NMR spectroscopy, potentiometry and spectrophotometry [44-56]. The major vanadium (V) species present in aqueous solution along with the values of the formation constants are listed in Table 4.02 [57]. The complex speciation of vanadium (V) in aqueous solution is evident.

Although the existence of the species listed in Table 4.02 in aqueous solution is fairly well accepted, there have been some disagreements over the existence of the uncharged species H_3VO_4 in solution [45,49,54,56]. Figure 4.02 displays a graphical representation of the predominant vanadium (V) species as a function of total vanadium concentration and pH. Figure 4.02a given by Pope [45] shows a small predominant region for the

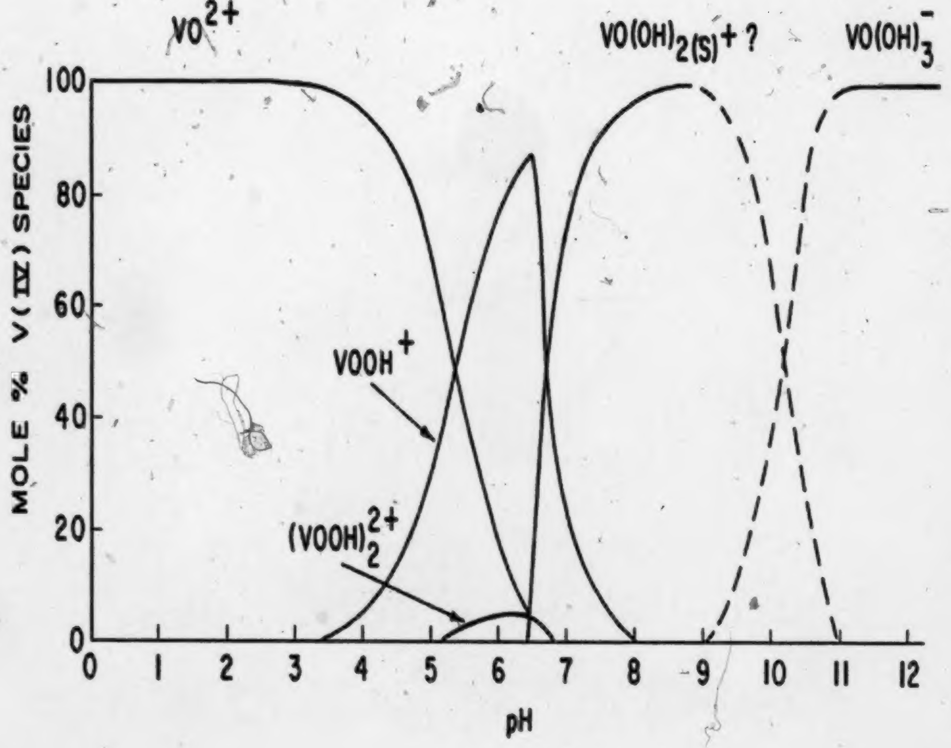

Figure 4.01 Species distribution of vanadium (IV) as a function of pH for a total vanadium concentration of 10^{-5} M. Dashed lines were estimated where reliable equilibrium data are not available [39].

Table 4.02 Vanadium (V) species and formation constants (β) in aqueous solution [a]

V(V) species	(p,q)	Logβ [b]
VO_4^{3-}	(-2,1)	-21.31
HVO_4^{2-}	(-1,1)	-7.946
$H_2VO_4^-$	(0,1)	
VO_2^+	(2,1)	6.919
$V_2O_7^{4-}$	(-2,2)	-15.23
$HV_2O_7^{3-}$	(-1,2)	-5.44
$H_2V_2O_7^{2-}$	(0,2)	2.79
$V_4O_{13}^{6-}$	(-2,4)	-8.60
$HV_4O_{13}^{5-}$	(-1,4)	0.13
$V_4O_{12}^{4-}$	(0,4)	7.89
$V_5O_{15}^{5-}$	(0,5)	12.16
$V_6O_{18}^{6-}$	(0,6)	13.9
$V_{10}O_{28}^{6-}$	(4,10)	51.76
$HV_{10}O_{28}^{5-}$	(5,10)	57.83
$H_2V_{10}O_{28}^{4-}$	(6,10)	61.43
$H_3V_{10}O_{28}^{3-}$	(7,10)	62.64

[a] In 0.6 M Na(Cl) medium at 25°C. Data taken from Ref.[57]

[b] Logβ for the general equation $p\,H^+ + q\,H_2VO_4^- \Leftrightarrow (H^+)_p\,(H_2VO_4^-)_q$

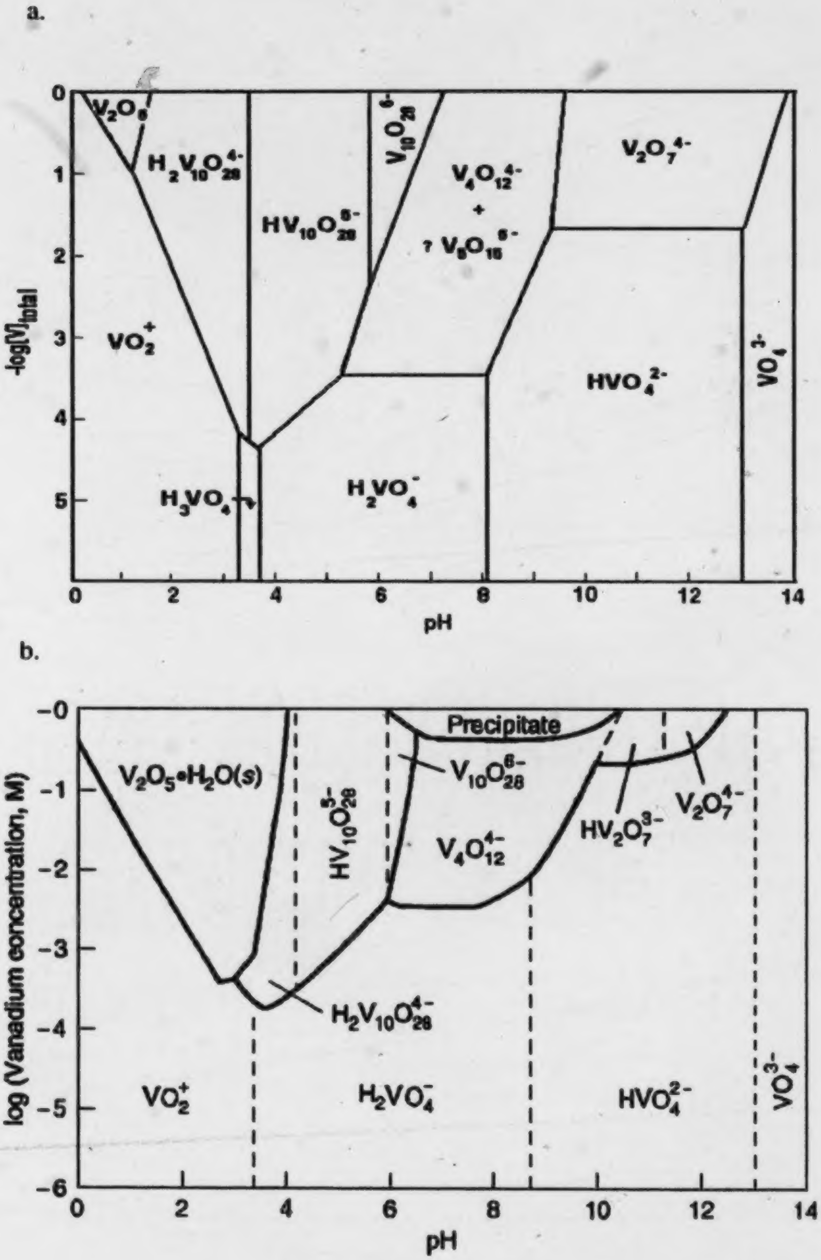

Figure 4.02 Predominant vanadium (V) species as a function of total vanadium concentration and pH. (a) From Ref. [45] (b)From Ref. [54].

H_3VO_4 over the pH range 3.3-3.7 at vanadium (V) concentration lower than 10^{-4} M, while Figure 4.02b given by Larson [54] shows no area of existence for H_3VO_4. Pettersson et al. [49] studied the vanadium (V) speciation using combined potentiometric and ^{51}V NMR technique, covering the pH range 2.5-4.5 at two vanadium concentration 0.3125 and 1.25 mM. They concluded that the uncharged monomer H_3VO_4 is not present in solution in the pH range 2.5-4.5 at total vanadium concentration > 0.3 mM, and H_3VO_4, should it really exist, would only be a minor species at very low total concentrations of vanadium. Cruywagen et al. [56] studied the protonation equilibria of mononuclear vanadate at vanadium concentration 5 × 10^{-5} M with spectrophotometric titration. They found that the percentage concentration of H_3VO_4 present in their system is so low that the protonation of $H_2VO_4^{2-}$ to form VO_2^+ occurs virtually in a single step.

The present study is aimed at quantitative speciation of vanadium at ppb level. Given the very low concentration of vanadium (V) involved, it would be reasonable to assume that the predominant species present in solution are only the monomeric species, namely, VO_4^{3-}, HVO_4^{2-}, $H_2VO_4^-$, H_3VO_4, VO_2^+ and that the polynuclear species present are negligible (see Figure 4.02a). The following four equilibria will be considered:

$$VO_4^{3-} + H^+ \Leftrightarrow HVO_4^{2-} \qquad K_1 = 10^{13.27} \qquad (4.05)$$

$$HVO_4^{2-} + H^+ \Leftrightarrow H_2VO_4^- \qquad K_2 = 10^{7.92} \qquad (4.06)$$

$$H_2VO_4^- + H^+ \Leftrightarrow H_3VO_4 \qquad K_3 = 10^{2.6} \qquad (4.07)$$

$$H_3VO_4 + H^+ \Leftrightarrow VO_2^+ + 2H_2O \qquad K_4 = 10^{4.2} \qquad (4.08)$$

The equilibrium constants (K) were taken from Ref. [56] and the data were reported in 1.0 M $NaClO_4$ medium at 25 °C with vanadium (V) concentration 5×10^{-5} M. A mass balance equation can be written as

$$[V(total)] = [VO_4^{3-}] + [HVO_4^{2-}] + [H_2VO_4^{-},] + [H_3VO_4] + [VO_2^{+}] \qquad (4.09)$$

Based on Equation (4.09) and the equilibria [Equations (4.05) - (4.08)], the species distribution of V(V) in solution can be calculated and the results are shown graphically in Figure 4.03. From the graph the pH dependence of species can be easily seen, and the maximum value of percentage concentration of the H_3VO_4 is about 6%. This low value makes the accurate instrumental determination of the value of K_3 unlikely, the values of K_3 and K_4 in Equations (4.07) and (4.08) were estimates [56]. Since the K values affect the distribution curves, the graph should be viewed with caution.

4.2 Experimental

4.2.1 Chemical Reagents

All chemicals were of analytical reagent grade and were used as received. De-ionized water (18 MΩ cm) was produced by a Milli-Q water purification system (Millipore, Bedford, MA). Stock solutions (100 ppm) of vanadium (IV) and vanadium (V) were prepared by dissolving appropriate amounts of $VOSO_4 \cdot 2H_2O$ (Fisher, Fair Lawn, NJ) and NH_4VO_3 (Fisher, Fair Lawn, NJ) respectively in de-ionized water, and stored under refrigeration. Stock solution of V(IV) was kept at pH 2.0 and at a temperature of 5°C in order to prevent air oxidation. Daily working solutions were prepared immediately by

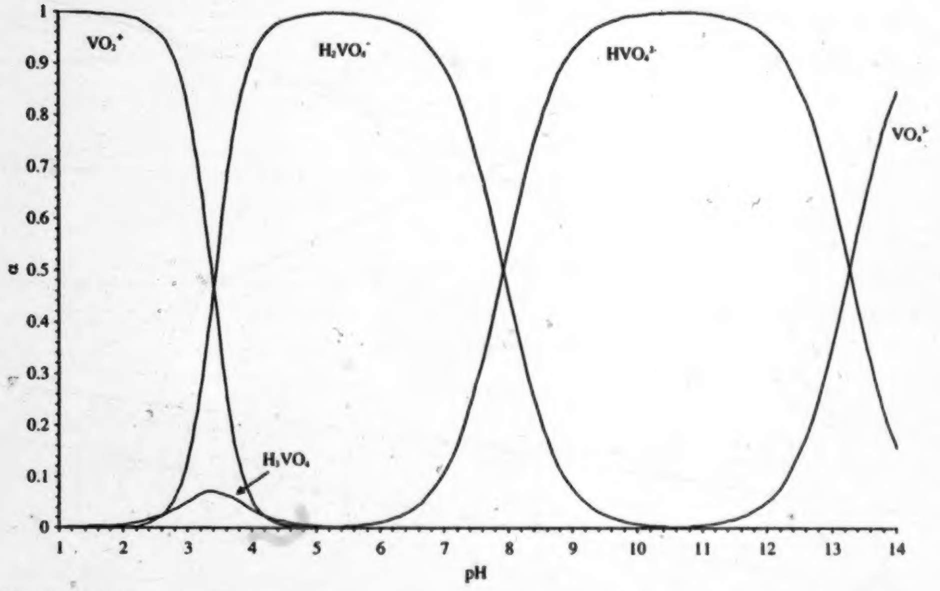

Figure 4.03 Fractional composition diagram for vanadium (V) as a function of pH in very dilute aqueous solution.

diluting the stock solution as needed. The background electrolyte was prepared by dissolving $Ca(NO_3)_2 \cdot 4H_2O$ (BDH, Toronto, ON) in de-ionized water and adjusting to the proper pH with concentrated HNO_3 (Anachemia, Montreal, QC).

4.2.2 Instrumentation

The instrumentation was the same as described in Chapter 3. A lab-built CE system was used. A lab-constructed direct injection nebulizer was used as the interface to connect CE to ICP-MS. The design and optimization of this interface has been described in Chapter 2.

A Perkin-Elmer SCIEX ELAN 5000A ICP-MS instrument (Thornhill, ON, Canada) was used for the detector. The vanadium isotope m/z 51 was monitored in the graphic mode of the instrument. Electropherogram data were collected using a 200 ms dwell time and one point per peak. Data analysis was performed after the data were transferred to a Microsoft Excel spreadsheet. Peak areas were calculated using a program written in Visual Basic. The ICP-MS operating parameters and optimization have been described in Chapter 2.

An ORION pH Meter Model 420A (Orion Research Inc., Beverly, MA) was used to measure pH. The pH probe (Orion Triode Combination Electrode) was calibrated just before use using three buffer solutions (Fisher, Nepean, ON) with pH 4, 7 and 10.

4.2.3 Sample Injection

Sample injections were done hydrodynamically by nebulizer suction. In order to avoid introduction of air into the capillary, the nebulizer gas had to be turned off before transferring the capillary between electrolyte and sample reservoirs. Sample injection volume was estimated by multiplication of the injection time and suction flow rate. The suction flow rate was determined by the method as described previously in Chapter 3.

4.3 Results and Discussion

4.3.1 Optimization of Sample Stacking Parameters

In this study a method of on-line concentration by sample stacking was used for the speciation of vanadium. This method has already been described in detail in Chapter 3. Emphasis in this section will be on the optimization of the stacking parameters.

4.3.1.1 Choice of Background Electrolyte

The proper choice of background electrolyte is important for the success of CE separation. The criteria for an ideal background electrolyte have been outlined in Chapter 3. The background electrolyte should not contain any strong complexing ligands, because V(IV) as hydrated vanadyl cation (VO^{2+}) is known to form complexes with a large number of inorganic and organic ligands such as carbonates, phosphates, halides, and EDTA [58]. V(V) as vanadate cation (VO_2^+) also forms complexes with carbonate, phosphate and EDTA. Using background electrolyte containing complexing ligands could alter the speciation and complicate the study. The background electrolyte should not contribute any signals that interfere with the determination of the analyte. For the speciation of vanadium by CE-ICP-MS, the background electrolyte should not contain chlorine species because it can form the molecular species $^{35}Cl^{16}O^+$ that seriously interfere with the $^{51}V^+$ signal. This vanadium isotope has an abundance of 99.75% and the second isotope, ^{50}V, which is only 0.25% abundant, suffers from interference from

$^{35}Cl^{15}N^+$. The concentration of the buffer should also be chosen appropriately that it is high enough to achieve sufficient sample stacking but not too high to cause excess Joule heating that leads to band broadening. The pH of the buffer should also be carefully considered as experience (Chapter 3) shows that acidic pH minimizes the absorption of positive ions onto the capillary wall. Taking all those factors into consideration, 50 mM $Ca(NO_3)_2$ at pH 2.0 was chosen as the background electrolyte for vanadium speciation.

4.3.1.2 Choice of Applied Voltage and Injection Volume

The effect of applied voltage on sample stacking has been discussed in Chapter 3. Similar effects were observed for vanadium speciation. In short, a voltage of +10 kV was applied to CE operation.

The effect of injection volume on sample stacking was discussed in Chapter 3 for chromium speciation. Similar effects are also observed for vanadium speciation. Increasing the injection volume increases signal intensity and no significant band broadening was observed with a large injection volume. A sample volume of 0.60 μL was used for injection.

4.3.1.3 Effect of pH of Sample on Vanadium Speciation

Our objective is the simultaneous speciation of V(IV) and V(V) by CE-ICP-MS without using pre-complexation or derivatization. However, in the absence of strongly complexing ligands, V(IV) as the VO^{2+} ion is not air stable in the alkaline pH range (Section 4.1). In the neutral pH range, precipitation of $VO(OH)_2$ may occur (Figure 4.01). Therefore it seems that the proper pH range for V(IV) speciation is under pH 3 where the predominant species is VO^{2+}. From Figure 4.03 it can be seen that under pH 3, V(V) mainly exists as the VO_2^+ cation. Thus, they both will electrophoretically migrate toward the cathode when the voltage is applied. However, the difference in their electrophoretic mobilities is not large enough and the migration time might be long for VO_2^+ because of its unit charge. Although Thornton and Fritz [33] were able to separate VO^{2+} and VO_2^+ at pH 2.3 by CE with aqueous $HClO_4$ as electrolyte carrier, the migration times were long (~ 12 min for VO^{2+} and ~21 min for VO_2^+). In our CE-ICP-MS system, the presence of suction-induced flow to detector would shorten the analysis time. Figure 4.04a and Figure 4.04b show the electropherogram of 1 ppm V(IV) and 1 ppm V(V) at pH 1.7, respectively. The background electrolyte pH was adjusted to 2.0 and 0.60 µL of sample was injected for both runs. As can be seen from the graph, the migration times for VO^{2+} and VO_2^+ are shorter (~3.8 min). However, they cannot be separated from each other because they have the same migration time. This might be expected since they both were stacked at the front edge of the sample plug, and so migration time would be identical as long as the water plug stays in the capillary. Also, at pH 1.7, the conductivity of the sample plug is so high that sample stacking was not efficient, resulting in a broad peak for VO_2^+. The peak broadening for VO_2^+ may be due to its smaller electrophoretic mobility.

An attempt was therefore made to lower the sample conductivity by increasing the sample pH to 2.2, and the resulting electopherograms are shown in Figure 4.05. As can be seen from Figure 4.05a, a sharp peak was observed for V(IV). Surprisingly, three peaks were found for V(V) at this pH, as seen from Figure 4.05b. The small peak at 225 sec was presumably assigned to the cation, VO_2^+. The larger peak at ~ 400 sec was presumably assigned to the anion, $H_2VO_4^-$, which may also be represented by VO_3^-. In between those cation and anion peaks, a very broad peak from 250 sec to 360 sec

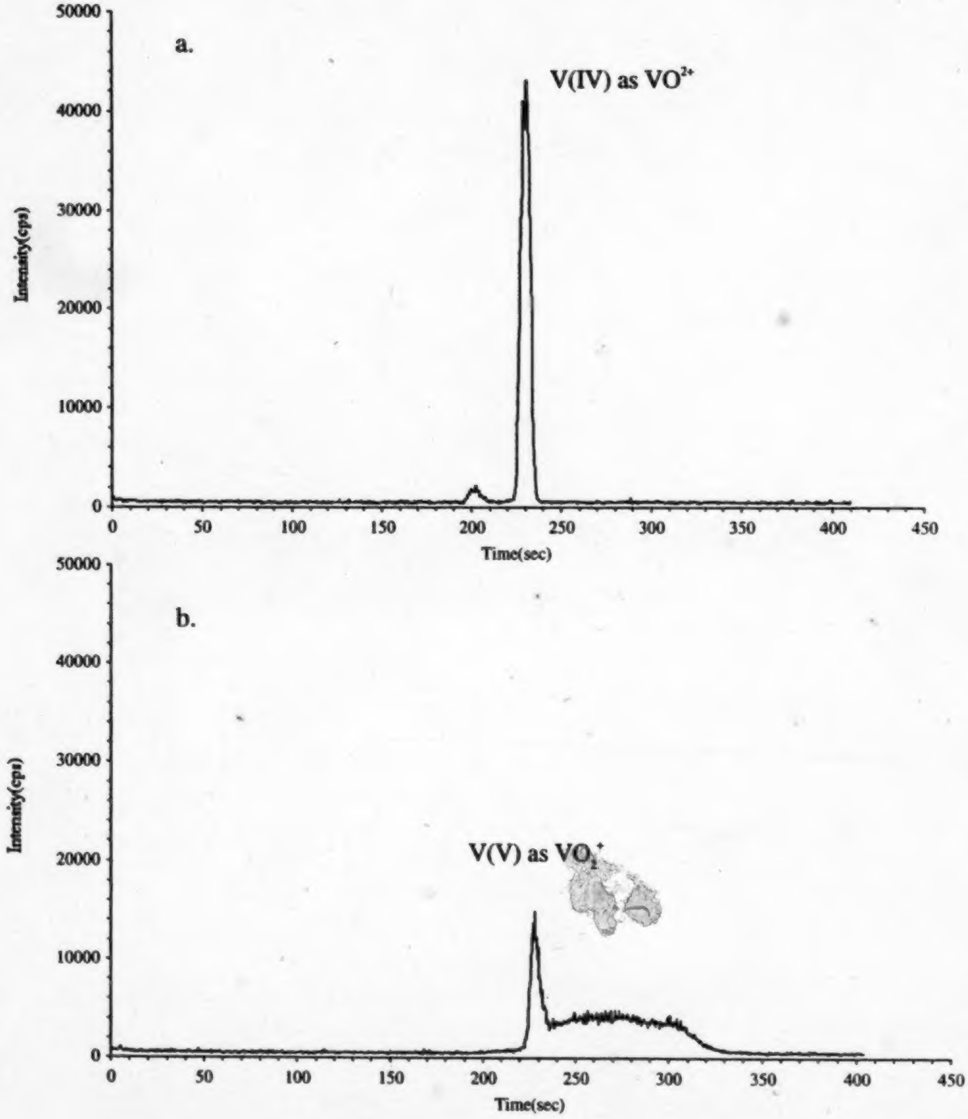

Figure 4.04 Electropherograms of (a) 1 ppm V(IV) and (b) 1 ppm V(V) at sample pH 1.7. Conditions: background electrolyte, 50 mM $Ca(NO_3)_2$ at pH 2.0; injection volume, 0.60 µL; applied voltage, +10 kV.

was observed. Its identity might be the uncharged species H_3VO_4. The broad feature of the peak is in agreement with its neutral character, because there is no electrostacking for an uncharged species. So it migrates in between the positive and negative ions. The detection of the otherwise difficult-to-detect species, H_3VO_4, demonstrates the utility of the CE-ICP-MS method for vanadium speciation. It should be pointed out that according to Figure 4.03, at pH 2.2, neither H_3VO_4 nor $H_2VO_4^-$ is supposed to be present in solution at a significant amount. This discrepancy might be due to two reasons. First, the species distribution of V(V) in Figure 4.03 was calculated based on estimated K_3 and K_4 values and disagreements exist for K_3 values in the literature [56]. Second, the ionic strength in our system is quite different from that used in Ref. [56], and it is well known that equilibrium constants depend on ionic strength [53]. Finally, Thornton and Fritz [33] reported that at pH 2.3, an anionic peak of VO_3^- was observed for V(V) as well as VO_2^+. This partially confirms our observation. Figure 4.05c shows an electropherogram of a 1 ppm sample solution containing V(IV) and V(V) at pH 2.2. It is basically the sum of the electropherograms of Figure 4.05a and 4.05b except for a little change in migration times, most likely a result of changes in sample matrix or flow rate variations. Although the above observations are interesting, they do not fulfill our purpose. Our objective is the quantitative speciation of V(IV) and V(V). To this end, the peak integrity of V(V) should be kept as much as possible, that is, as one peak. The sample pH was thus increased to 3.1. Figure 4.06 illustrates the result of this change in pH. At pH 3.1, V(IV) as VO^{2+} shows a sharp peak (Figure 4.06a), and V(V) as $H_2VO_4^-$ (Figure 4.06b) shows a somewhat broad peak most likely caused by its longer residence time in the capillary and its unit charge. Figure 4.06c shows an electropherogram of a 1 ppm sample solution containing V(IV) and V(V). Compared with Figure 4.06a and 4.06b, the peaks can be easily identified. When the pH of the sample is raised to 4.0, The VO^{2+} peak starts to show significant tailing indicating adsorption on the capillary wall or change in

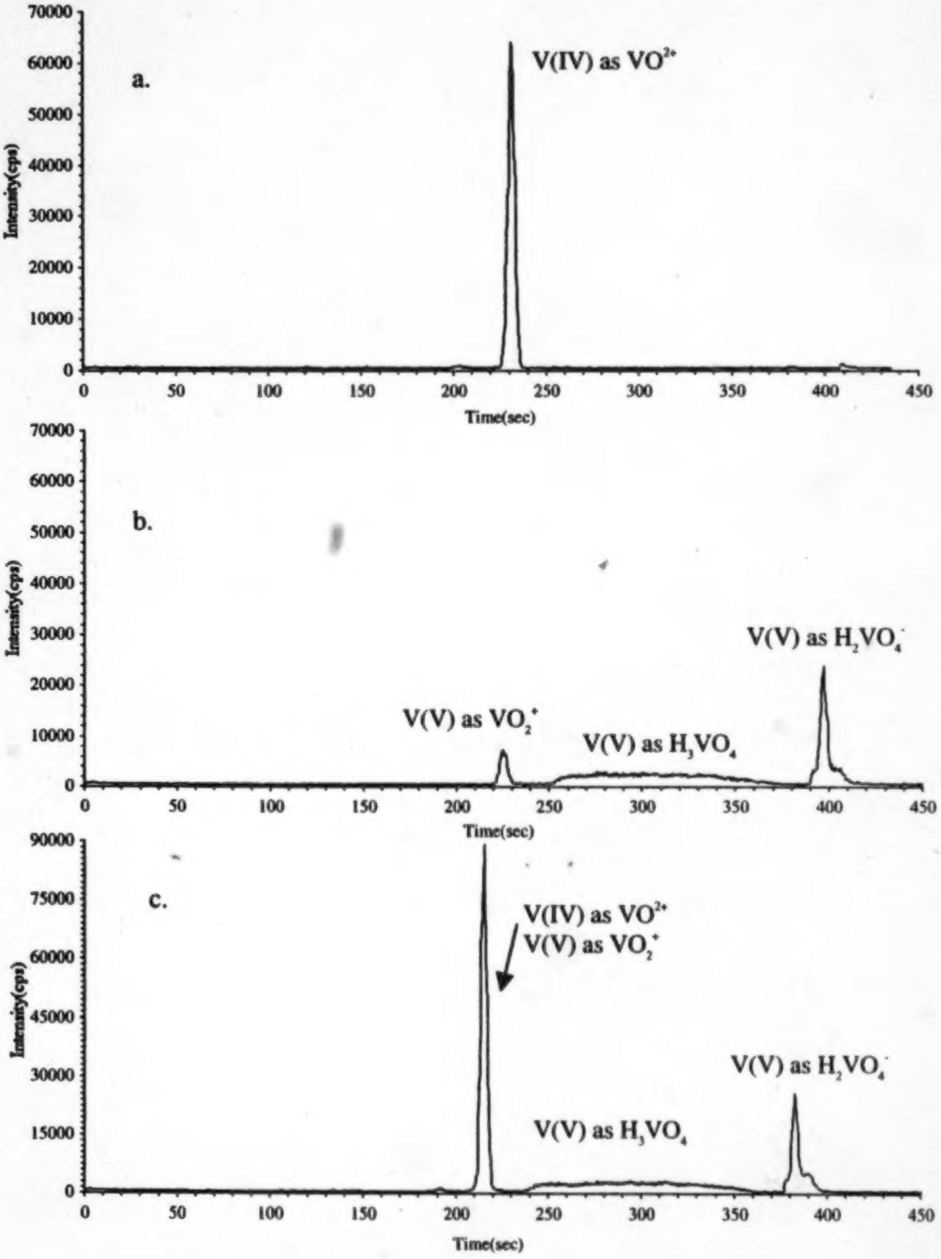

Figure 4.05 Electropherograms of (a) 1 ppm V(IV) and (b) 1 ppm V(V) and (c) 1 ppm V(IV)/V(V) at sample pH 2.2. Conditions as in Figure 4.04.

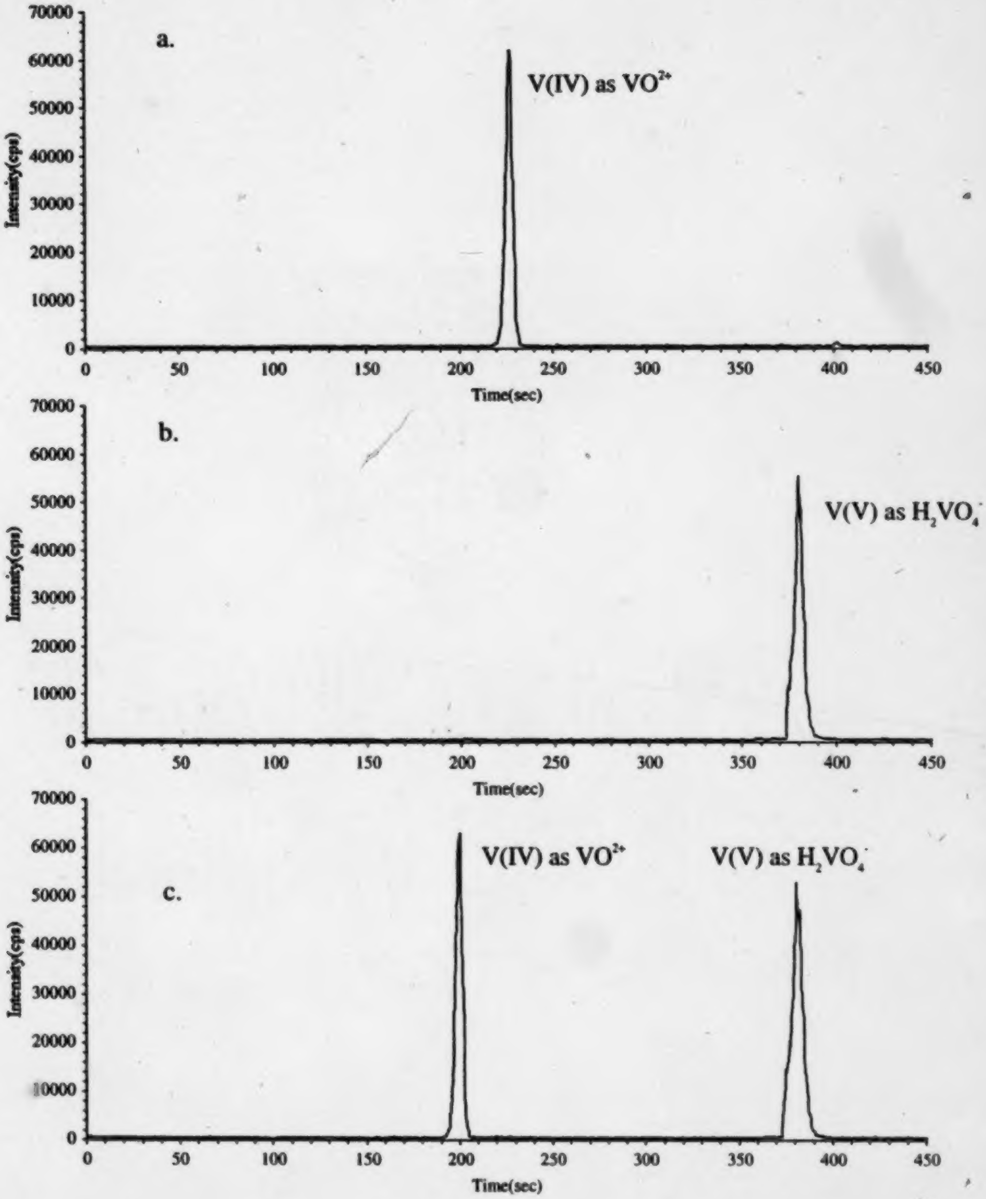

Figure 4.06 Electropherograms of (a) 1 ppm V(IV) and (b) 1 ppm V(V) and (c) 1 ppm V(IV)/V(V) at sample pH 3.1. Conditions as in Figure 4.04.

speciation from VO^{2+} to $VOOH^{+}$ (electropherogram not shown here). Therefore, the sample pH value for speciation of vanadium was selected to be 3.1.

Figure 4.07 is an electropherogram showing the separation of V(IV) and V(V) species by sample stacking and demonstrates the sample stacking process for vanadium speciation. The sample containing 1 ppm V(IV) and 1 ppm V(V) was prepared in de-ionized water, and the pH was adjusted to 3.1 with HNO_3. A volume of 0.60 µL of the sample was injected into the capillary. V(IV), which exists as VO^{2+} was stacked up at the front of the plug and V(V) , which exists as $H_2VO_4^-$, was focused at the rear of the sample plug. In order to visualize the sample plug, Y^{3+} was added to the background electrolyte and its signal at m/z 89 was monitored as a function of time. The bulk flow of the electrolyte caused by nebulizer suction results in a stable background signal. Once the sample plug replaces the background electrolyte, the Y^{3+} signal drops, showing clearly the location of the sample plug within the capillary. As we can see from Figure 4.07, both VO^{2+} and $H_2VO_4^-$ was focused right on the plug boundaries. The signal level of Y^{3+} after the sample plug is higher than before the sample plug, a result of the different contributions from electrophoretic velocity of Y^{3+}. When the sample plug is in the capillary, the field strength over the electrolyte would be small, as a result the electrophoretic velocity of Y^{3+} would also be near zero. After the sample plug exits the capillary, all the voltage is dropped across the electrolyte, the electrophoretic velocity of Y^{3+} would be higher leading to a higher signal level.

4.3.2 Quantitative Speciation

4.3.2.1 Calibration Curves

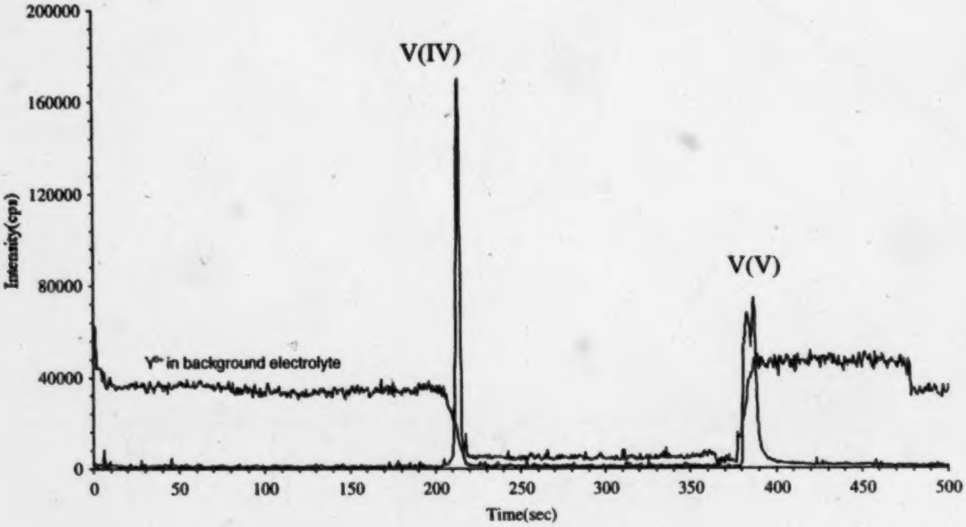

Figure 4.07 Electropherogram for a sample solution containing V(IV) and V(V) at 1 ppm each. Conditions: background electrolyte, 50 mM $Ca(NO_3)_2$ at pH 2.0; sample pH, 3.1; applied voltage, +10kV; injection volume, 0.60 μL

Calibration curves for V(IV) and V(V) were established under the selected conditions and are shown in Figure 4.08. Both V(IV) and V(V) species yield a linear relationship between peak area and concentration over 3 orders of magnitude. The slope of the log-log plot is 0.99 for V(IV) and 1.01 for V(V). The two curves almost overlap, indicating both V(IV) and V(V) species are efficiently converted to V^+ in the ICP and they have essentially the same sensitivity, which is expected for such a high temperature ion source as the ICP.

4.3.3.2 Limits of Detection

Detection limits were defined as the concentration that produces a net signal equivalent to three times the standard deviation of the blank signal. In this study, the detection limits were calculated based on peak area. Peak areas were obtained by adding the intensities of the data points across the peak after background correction. To obtain the standard deviation of the background for peak area, five to seven electropherograms of the background were acquired. The intensities of the data points (equal in number to the points across the peak) from the baseline were added up for each electropherogram, and the standard deviation of the added baseline points was calculated. The detection limit was calculated as three times the standard deviation of the peak area of the background divided by the slope of the calibration curve (peak area vs. concentration). The repeatability was determined by making five consecutive injections of a standard solution containing 1 ppm each of V(IV) and V(V). The relative standard deviations (RSDs) of the peak areas and migration times were calculated. The detection limits (concentration and absolute), along with slopes of the log-log plots, linear dynamic range and repeatability are listed in Table 4.03. Compared with the speciation methods using CE-UV detection [32-34], the present method has concentration detection limits that are better by 2 or 3 orders of magnitude. Compared with other chromatographic

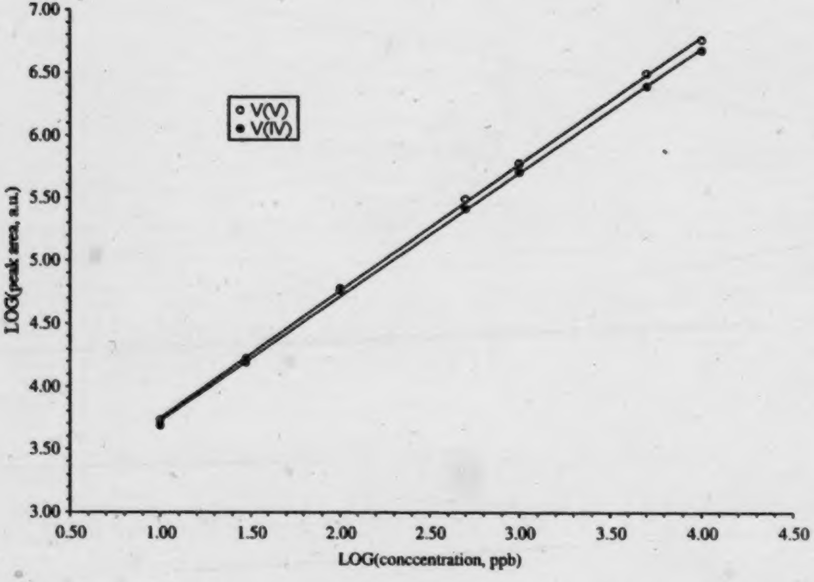

Figure 4.08 Calibration curves V(IV) and V(V). Conditions: background electrolyte, 50 mM $Ca(NO_3)_2$ at pH 2.0; sample pH, 3.1; applied voltage, +10 kV; injection volume, 0.60 µL.

Table 4.03 Analytical figures of merit for the speciation of vanadium by CE-DIN-ICP-MS[a]

Analyte	V(IV)	V(V)
Linear dynamic range (ppb)	10-10000	10-10000
Slope of log-log plot	0.99	1.01
Correlation coefficient	0.999	0.999
Detection limit[b] concentration (ppb)	3.1	3.6
Detection limit[b] absolute (pg)	1.8	2.1
Repeatability (RSD%)[c] peak area	3.5	3.5
Repeatability (RSD%)[c] migration time	1.0	0.4

[a] Conditions: background electrolyte, 50 mM $Ca(NO_3)_2$ at pH 2.0; sample pH, 3.1; applied voltage, +10 kV; injection volume, 0.60 µL.

[b] Detection limits based on peak area.

[c] Repeatability based on 1ppm solution.

or solvent extraction methods (Table 4.01), the concentration detection limits of this method are either similar or better depending on the detection system. But the absolute detection limits are generally better than these methods because of the smaller sample requirement in CE.

4.3.3 Multi-element (Chromium and Vanadium) Speciation

The method is also capable of multi-element speciation because of the element specific multi-element detector (ICP-MS). To test this capability, a sample solution was made by adding 1 ppm each of V(IV), V(V), Cr(III) and Cr(VI) species to de-ionized water. The pH was adjusted to pH 3.0. The background electrolyte was 50 mM $Ca(NO_3)_2$ at pH 2.0. Figure 4.09 shows the electropherograms obtained from this solution. As expected, the two cations (VO^{2+} and Cr^{3+}) were stacked up in the front of the sample plug, while the two anions ($H_2VO_4^-$ and $HCrO_4^-$) were stacked up at the back of the sample plug. Although their migration times overlapped, the element selective detector, ICP-MS, was still be able to differentiate Cr and V species. This demonstrated the unique advantage of CE-ICP-MS. There is no need to separate ions containing different elements from each other, and only ions that contain the same element need to be separated by CE.

It should be noted that the VO^{2+} peak in Figure 4.09 is unexpectedly small. It is suspected that a redox reaction occurred in the solution and VO^{2+} was oxidized by $HCrO_4^-$.
The standard potentials [59] of the following half reactions supports this idea:

$$HCrO_4^- + 7H^+ + 3e \Leftrightarrow Cr^{3+} + 4H_2O \qquad E° = 1.350\ V \qquad (4.10)$$

$$VO^{2+} + H_2O \Leftrightarrow VO_2^+ + 2H^+ + e \qquad E° = -\ 0.991\ V \qquad (4.11)$$

$$HCrO_4^- + 3VO^{2+} + H^+ \Leftrightarrow Cr^{3+} + 3VO_2^+ + H_2O \qquad E° = 0.359\ V \qquad (4.12)$$

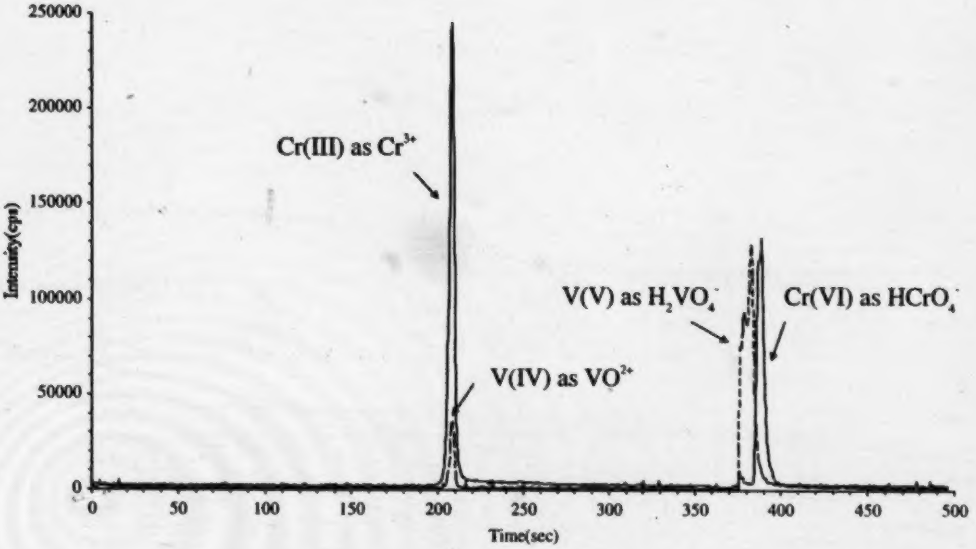

Figure 4.09 Electropherograms for a sample solution containing V(IV), V(V), Cr(III) and Cr(VI) at 1 ppm each. Conditions: background electrolyte, 50 mM $Ca(NO_3)_2$ at pH 2.0; sample pH, 3.0; applied voltage, +10kV; injection volume, 0.60 μL

But under the experimental conditions of this study, V(V) exists as $H_2VO_4^-$ instead of VO_2^+, the following equilibrium should also be considered:

$$VO_2^+ + 2H_2O \Leftrightarrow H_2VO_4^- + 2H^+ \qquad \log K = -6.76 \qquad (4.13)$$

The including of this equilibrium castes some doubt on the presence of the redox reaction in solution because of its negative log K value. So another experiment was done to confirm the redox reaction. A solution was made by adding 1 ppm (20 μM) $HCrO_4^-$ and 1 ppm (20 μM) VO^{2+} to de-ionized water. Figure 4.10 shows the electropherogram for this solution. As seen from the graph, the peak for VO^{2+} was not observed, but instead the peaks for Cr^{3+} and $H_2VO_4^-$ were seen. This clearly demonstrates that the following reaction indeed occurred in the solution:

$$\underset{20\ \mu L}{HCrO_4^-} + \underset{20\ \mu L}{3VO^{2+}} + 5H_2O \rightarrow Cr^{3+} + 3H_2VO_4^- + 5H^+ \qquad (4.14)$$

$HCrO_4^-$ was also observed because it was in excess. According to Equation(4.14) the limiting reagent would be VO^{2+}.

4.4 Conclusions

A method for the quantitative speciation of vanadium by CE-DIN-ICP-MS has been presented. The sample pH was adjusted to pH 3.1. It was found that at this pH vanadium (IV) exists presumably as the cation (VO^{2+}) and vanadium (V) exists mainly as the anion ($H_2VO_4^-$). Their opposite polarity allows for their separation by on-line sample stacking. A large sample volume was used to increase the signal intensity and to improve the

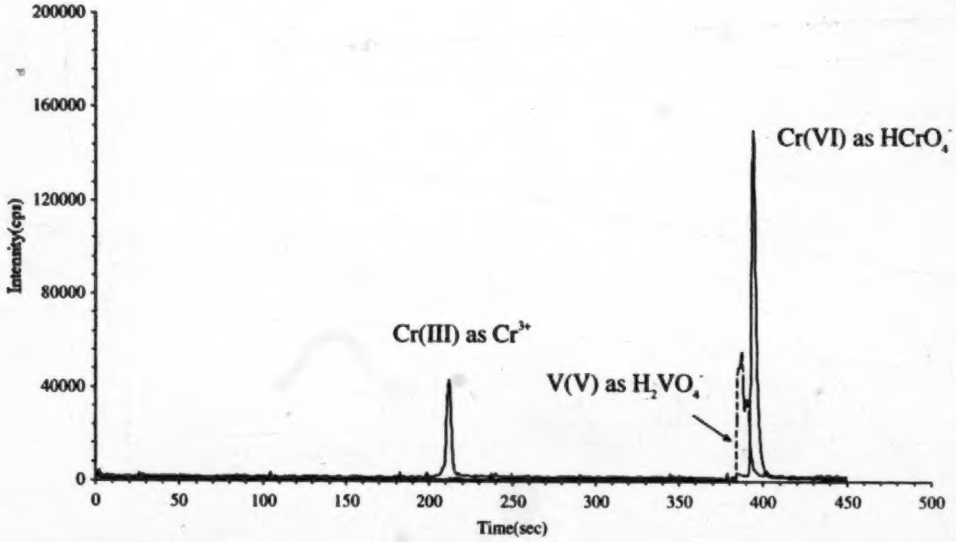

Figure 4.10 Electropherograms for a sample solution containing V(IV) and Cr(VI) at 1 ppm (20 μM) each. Conditions as in Figure 4.09

detection limits. Good repeatability and linearity were observed. Linear dynamic ranges were over three orders of magnitude. Concentration detection limits were obtained at the ppb level and absolute detection limits were at the pg level. Compared with literature methods for vanadium speciation using CE–UV system, the present method has a concentration detection limit two to three orders of magnitude lower. Compared with other chromatographic or extraction methods, the present method has concentration detection limits that are comparable or better, and absolute detection limits are generally better than other methods. Besides, no sample pre-complexation or conversion is necessary, and the analysis time is short. It has also been demonstrated to be effective for multi-elements speciation.

4.5 References

1. Nriagu, J.O., Ed., *Vanadium in the Environment*, In *Advances in Environmental Science and Technology*, John Wiley and Sons, New York, 1998, Vol. **30** and **31**.
2. Cran, D.C., Tracy, A. S., Eds, *Vanadium Compounds: Chemistry, Biochemistry, and Therapeutic Applications,* ACS Symposium Series, American Chemical Society, Washington, DC, 1998.
3. Sigel, H.; Sigel, A., Eds., *Vanadium and Its Role for Life, Metal Ions in Biological Systems*, Marcel Dekker Inc., New York, 1995, Vol. **31**.
4. Zaporowska, H., and Scibior, A., In *Vanadium in the Environment*, In *Advances in Environmental Science and Technology*, Nriagu, J.O., Ed., John Wiley and Sons, New York, 1998, Vol. **31**, pp.121-133.
5. Chasteen, N.D., Ed., *Vanadium in Biological Systems*, Kluwar Academic Pulishers, Boston, 1990.
6. Thomson, K. H., Yuen, V. G., McNeill, J. H., and Orvig, C., In *Vanadium Compounds: Chemistry, Biochemistry, and Therapeutic Applications,* Cran, D.C., Tracy, A. S., Eds, ACS Symposium Series, American Chemical Society, Washington, DC, 1998, pp. 329-343.
7. Shechter,Y., Li, J., Meyerovitch, J., Gefel, D., Bruck, R., Elberg, G., Miller, D. S., Shisheva, A., *Mol. Cell., Biochem.*, 1995,**153**, 39.
8. Brichard., S. M., Henquin, J.C., *Trends Pharmacol. Sci.*, 1995, **16**, 265.
9. Nielsen, F. H., In *Vanadium Compounds: Chemistry, Biochemistry, and Therapeutic Applications,* Cran, D.C., Tracy, A. S., Eds, ACS Symposium Series, American Chemical Society, Washington, DC, 1998, pp. 297-307.
10. French, R. J., and Jones, P. J. H., *Life Sci.*, 1993, **52**, 339.

11. Altamirano-Lozano, M. A., and Roldan-Reyes, M. E., In *Vanadium in the Environment*, In *Advances in Environmental Science and Technology*, Nriagu, J.O., Ed., John Wiley and Sons, New York, 1998, Vol. **31**, pp. 159-179.

12. Willsky, G. R., Goldfine, A. B., and Kostyniak, P. J., In *Vanadium Compounds: Chemistry, Biochemistry, and Therapeutic Applications*, Cran, D.C., Tracy, A. S., Eds., ACS Symposium Series, American Chemical Society, Washington, DC, 1998, pp.278-296.

13. Baran, E. J., In *Vanadium in the Environment*, In *Advances in Environmental Science and Technology*, Nriagu, J.O., Ed., John Wiley and Sons, New York, 1998, Vol. **31**, pp. 317-345.

14. Sabbioni, E., Pozzi, G., Devos, S., Pintar, A., Casella, L., and Fischbach, M., *Carcinogenisis*, 1993,**14**, 2565.

15. Bertini, I., Gray, H. B., Lippard, S. J., and Valentine, J.S., Ed., *Bioinorganic Chemistry*, University Science Books, Mill Valley, CA, 1994.

16. Sreedhara, A., Susa, N., and Rao, C. P., *Inorg. Chim. Acta*, 1997, **263**, 189.

17. Nriagu, J.O., In *Vanadium in the Environment*, In *Advances in Environmental Science and Technology*, Nriagu, J.O., Ed., John Wiley and Sons, New York, 1998, Vol. **30**, pp. 1-36.

18. Mamane, Y., and Pirrone, N., In *Vanadium in the Environment*, In *Advances in Environmental Science and Technology*, Nriagu, J.O., Ed., John Wiley and Sons, New York, 1998, Vol. **30**, pp. 37-68.

19. Murthy, G. V. R., Reddy, T. S., and Rao, S. B., *Analyst*, 1989, **114**, 493.

20. Komarova, T. V., Obrezkov, O. N., and Sphigun, O. A., *Anal. Chim. Acta*, 1991, **254**, 61.

21. Hirayama, K., Kageyama, S., and Unohara, N., *Analyst*, 1992, **117**, 13.

22. de Beer, H., and Coetzee, P.P., *Fresenius', J. Anal. Chem.*, 1994, **348**, 806.

23. Jen, J. F. and Yang, S. M., *Anal. Chim. Acta* ,1994, **289**, 97.

24. Tsai, S. J. J., and Hsu, S. J., *Analyst,* 1994, **119**, 403.

25. Tomlison, M.J., Wang, J., and Caruso, J. A., *J. Anal. At. Spectrom.*, 1994, **9**, 957.

26. Soldi, T., Pesavento, M., and Alberti, G., *Anal. Chim. Acta*, 1996, **323**, 27.

27. Wann, C.C., and Jiang, S. J., *Anal. Chim. Acta*, 1997, **357**, 211.

28. Bosque-Sendra, J. M., Valencia, C., and Boudra, S., *Fresenius', J. Anal. Chem.*, 1998, **360**, 31.

29. Gaspar, Attila, and Posta, J., *Fresenius', J. Anal. Chem.*, 1998, **360**, 179.

30. Dabek-Zlotorzynska, E., Lai, E. P. C., and Timerbaev, A. R., *Anal. Chim. Acta*, 1998, **359**, 1.

31. Timerbaev, A. R., Dabek-Zlotorzynska, E., and van den Hoop, M. A. G. T., *Analyst*, 1999, **124**, 811.

32. Jen, J. F., Wu, M. H., and Yang, T. C., *Anal. Chim. Acta* ,1997, **339**, 251.

33. Thornton, M. J., and Fritz, J. S., J.High Resol.Chromatogr.,1997, **20**, 653.

34. Pozdniakova, S., and Padarauskas, A., *Analyst*, 1998, **123**, 1497.

35. Montaser, A., Ed., *Inductively Coupled Plasma Mass Spectrometry*, Wiley-VCH, New York, 1998.

36. Majidi, V., and Miller-Ihli, N., *Analyst*, 1998, **123**, 809.

37. Olesik, J. W., Kinzer, J. A., and Olesik, S. V., *Anal. Chem.*, 1995, **67**, 1.

38. Tomlison, M. J., Lin, L., and Caruso, J. A., *Analyst*, 1995, **120**, 583.

39. Chasten, N. D., in *Biological Magnetic Resonance*, Berliner, L., Reuben, J., Eds., Plenum Press, New York, 1981, Vol. **3**, pp. 53-119.

40. Musafi, D., and Makinen, M.W., *Inorg. Chem.*, 1988, **27**, 3360.

41. Francavilla, J., and Chasteen, N. D., *Inorg. Chem.*, 1975, **14**, 2860.

42. Iannuzzi, M. M., and Rieger, P. H., *Inorg. Chem.*, 1975, **14**, 2895.

43. Johnson, G. K., and Schlemper, E. O., *J. Am. Chem. Soc.*, 1978, **100**, 3645.

44. Baes, C. F., and Mesmer, R. E., *The Hydrolysis of Cations*, John Wiley and Sons, New York, 1976, pp. 197-210.

45. Pope, M. T., *Heteropoly and Isopoly Oxometallates*, Springer-Verlag, New York, 1983, pp. 34-40.

46. Heath, E., and Howarth, O. W., *J. Chem. Soc. Dalton Trans*, 1981, 1105.

47. Pettersson, L., Hedman, B., Andersson, I., and Ingri, N., *Chem. Script.*, 1983, **22**, 254.

48. Pettersson, L., Anderson, I., and Hedman, B., *Chem. Script.*, 1985, **25**, 309.

49. Pettersson, L., Hedman, B., Nenner, A. M., and Anderson, I., *Acta Chim. Scand.* 1985, **39**, 499.

50. Cruywagen, J. J., Heyns, J. B. B., and Visagie, J. L., *Polyhedron*, 1989, **8**, 1800.

51. Cruywagen, J. J., and Heyns, J. B. B., *Polyhedron*, 1991,**10**, 249.

52. Elvingson, K., Fritzsche, M., Rehder, D., and Pettersson, L., *Acta Chim. Scand.* 1994, **48**, 878

53. Tracey, A. S., Jaswal, J.S., and Angus-Dunne, S. J., *Inorg. Chem.*, 1995, **34**, 5680.

54. Larson, J.W., *J. Chem. Eng. Data*, 1995, **40**, 1276.

55. Andersson, I., Pettersson, L., Hastings, J. J., and Howarth, O. W., *J. Chem. Soc. Dalton Trans*, 1996, 3357.

56. Cruywagen, J.J., Heyns, J. B. B., and Westa, A. N., *Inorg. Chem.*, 1996, **35**, 1556.

57. Pettersson, L., and Elvingson, K., In *Vanadium Compounds: Chemistry, Biochemistry, and Therapeutic Applications,* Cran, D.C., Tracy, A. S., Eds., ACS Symposium Series, American Chemical Society, Washington, DC, 1998, pp. 30-50.

58. Crans, D. C., and Tracey, A. S., In *Vanadium Compounds: Chemistry, Biochemistry, and Therapeutic Applications,* Cran, D.C., Tracy, A. S., Eds., ACS Symposium Series, American Chemical Society, Washington, DC, 1998, pp. 2-30.

59. Lide, D. R., Ed., *Handbook of Chemistry and Physics*, 78th Edition, CRC Press, New York, 1997-1998.

Chapter 5

Quantitative Speciation of Antimony

5.1 Introduction

Antimony (Sb) has long been recognized as a non-essential and toxic element. Exposure to Sb at high levels can result in a variety of adverse health effects. Inhalation exposure to antimony compounds has been reported to produce pneumonitis, fibrosis, bone marrow damage and carcinomas and high cancer risk [1]. Lung cancer has been observed in a study of rats that breathed high levels of antimony [2]. The US Environment Protection Agency (EPA) has listed antimony as one of the priority pollutants and has set the Maximum Contaminant Level (MCL) for drinking water at 6 ppb.

Antimony in the human environment arises from natural sources such as rock weathering and soil runoff, and from widespread industrial applications (e.g. manufacturing batteries, paints, ceramics, glasses, flame retardants, and semiconductors, mining and smelting) [3]. The increasing release of this toxic element into the environment has lead to growing concerns regarding its toxicity and the potential health risks. Antimony in the environment exists as two oxidation states, III and V, with various inorganic and organic forms. The toxicity of antimony is species dependent. Inorganic species of antimony are more toxic than organic ones and Sb(III) is ten times more toxic than Sb(V) [4]. Therefore, the determination of total antimony concentration alone is not adequate for estimating its toxicity and environmental impact. It is necessary to develop analytical methods for the accurate determination of antimony in its different forms or oxidation states in a given sample.

In the past two decades, various analytical methods have been described for the determination and speciation of Sb(III) and Sb(V). Recently, methods and techniques for the determination of antimony species in waters have been reviewed [5]. These methods are based on liquid-liquid extraction [6-11], liquid-solid extraction [12-16], electrochemical determination [17-19], selective hydride generation [20-28], and chromatographic separation [4, 29-34]. Selective hydride generation (HG) coupled with atomic spectrometry detection has been so far the most commonly used method for inorganic antimony speciation. With this technique, differentiation between Sb(III) and Sb(V) is achieved by selective reduction to stibine using sodium borohydride under controlled pH conditions. Most of the procedures are based on the determination of total antimony [Sb(III) and Sb(V)] and Sb(III) separately, with Sb(V) content calculated as the difference. However, the method has several drawbacks. The speciation of Sb(III) and Sb(V) is not simultaneous, and Sb(V) content is obtained indirectly, which may introduce errors. The choice of the best method for selective antimony hydride generation may be difficult, because the stibine generation efficiency depends on not only the experimental conditions but also the hydride generation system used. The method may also be time-consuming. Recently a few papers have been published on the coupling of high performance liquid chromatography (HPLC) with atomic spectrometry detection for the speciation of antimony. These are briefly summarized in Table 5.01. Compared with other methods mentioned above, methods listed in the table have the advantage that they allow for the simultaneous separation and determination of Sb(III) and Sb(V) in a single run. As seen from the table, most methods use ICP-MS as the detection system to achieve highly sensitive and element selective detection. For the most part, the detection limits are at the ppb level.

Capillary electrophoresis (CE) as a separation technique has unique capabilities: highly efficient separation, small sample and buffer volume requirements and fast analysis time.

Table 5.01 Summary of methods for antimony speciation

Separation method	Detection system	Detection limits		References
		Sb(III)(ppb)	Sb(V) (ppb)	
Anion Exchange HPLC	HG-AAS ICP-MS HG-ICP-MS	50 7.5 0.4	6 0.9 0.08	Smichowski et al., 1995 [4]
Anion Exchange HPLC	FAAS ICP-MS	~ 1000 0.8	~ 1000 0.5 ppb	Lintschinger et al., 1997 [29]
Anion Exchange HPLC	HG-AAS	1.0	2.0	Zhang et al., 1998 [30]
Anion Exchange HPLC	ICP-AES ICP-MS	400 3	100 0.5	Ulrich, 1998 [31]
Anion Exchange HPLC	ICP-MS	0.005	0.005	Lintschinger et al., 1998 [33]
Anion Exchange HPLC	ICP-MS	< 4.5	< 0.5	Lindemann et al., 1999 [34]

Compared with HPLC methods, CE has another important advantage: lack of a stationary phase, which minimizes the disturbances on the existing equilibrium between different species. These unique properties make CE an attractive technique for trace element speciation [35,36]. In spite of this, there has been no CE method reported for antimony speciation until recently [37,38]. Casiot et al.[37] proposed a method for speciation of Sb(III) and Sb(V) by CE with indirect UV detection using sodium chromate as the carrier electrolyte. The detection limits achieved were quite high, being 104ppb for Sb(III) and 116 ppb for Sb(V) with hydrodynamic injection and 64 ppb for Sb(III) and 147 ppb for Sb(V) with electrokinetic injection. Michalke and Schramel [38] studied antimony speciation by interfacing CE to ICP-MS using phosphate buffer. The detection limits obtained were 0.1 ppb for Sb(V) and 0.7 ppb for $Sb(OH)_3$. However, the resolution of Sb(V) from Sb(III) as tartrate species was unsatisfactory because of the broad peak shape of Sb(III)-tartrate.

In this study, the quantitative speciation of Sb(III) and Sb(V) by CE-ICP-MS using a laboratory-constructed direct injection nebulizer interface is presented. A method of on-line concentration by sample stacking with sample matrix removal was used to increase the sensitivity and resolution. Several experimental parameters are examined and discussed. These include choice of buffer composition and concentration, choice of sample and buffer pH, effect of applied voltage and effect of injection volume. The analytical performance of the method, in terms of linear dynamic range, detection limits and repeatability, is described. The quantitative speciation of synthetic mixtures of Sb(III) and Sb(V) is also demonstrated.

In acidic aqueous solution, Sb(III) exists as SbO^+ derivatives, the species present vary markedly with the acid concentration and the anion present [40]. In aqueous sulfuric acid solution, the cations SbO^+ and $Sb(OH)_2^+$ exist when the sulfuric acid concentration is below 1.5 M. The anionic sulfato complexes $SbOSO_4^-$ and $Sb(SO_4)_2^-$ are present when the acid concentration is ~1.0 – 18 M.

Sb(III) is stable in concentrated hydrochloric acid due to the high acidity of the medium and the formation of chlorinated complex probably as $SbCl_4^-$. On dilution the solution hydrolyzes, and a precipitate of SbOCl is formed. If more water is added, the hydrolysis continues and a precipitate of Sb_2O_3 and a certain amount of the soluble uncharged species $Sb(OH)_3$ are formed. At pH near 12, the Sb_2O_3 dissolves and the antimonite ion $Sb(OH)_4^-$ is formed. The hydrolysis equilibria involving $Sb(OH)_3$ are expressed as follows [41]:

$$Sb(OH)_3(aq) + H^+ \Leftrightarrow Sb(OH)_2^+ + H_2O \qquad \log K_1 = 1.42 \qquad (5.01)$$

$$Sb(OH)_3(aq) + H_2O \Leftrightarrow Sb(OH)_4^- + H^+ \qquad \log K_2 = -11.82 \qquad (5.02)$$

The uncharged monomeric species $Sb(OH)_3$ is the predominant species over a wide range of pH from 2 to11. No polymeric species of Sb(III) appear in significant amounts at Sb(III) concentration below 0.1 M.

In aqueous Sb(III) solution, the presence of the complexing agent tartrate results in the formation of a stable complexes $[Sb_2(C_4H_2O_6)_2]^{2-}$. This complex has been frequently used as a standard for Sb(III) in speciation studies in the literature because of its solubility and stability in aqueous solution. It was thus used for the preparation of Sb(III) standard solutions in this study.

In acidic aqueous solution, Sb(V) seems to form a series of dodecanuclear species $Sb_{12}(OH)_{64}^{4-}$, $Sb_{12}(OH)_{65}^{5-}$, $Sb_{12}(OH)_{66}^{6-}$, $Sb_{12}(OH)_{67}^{7-}$ as well as $Sb(OH)_5$ and $Sb(OH)_6^-$ at concentrations of Sb(V) greater than 1 mM [41]. The species occurring in basic solution have not been established. At lower Sb(V) concentration, the predominant species in aqueous solution are probably the monomeric uncharged species $Sb(OH)_5$ (often written as $H[Sb(OH)_6]$)and $Sb(OH)_6^-$ ion. The pKa of antimonic acid $H[Sb(OH)_6]$ was given as 2.47 [41]. A pH dependent composition diagram for Sb(V) is shown in Figure 5.01.

5.2 Experimental

5.2.1 Chemical Reagents

All chemicals were of analytical reagent grade and were used as received. De-ionized water (18 MΩ cm) was produced by a Milli-Q water purification system (Millipore, Bedford, MA). Standard stock solutions (1000 ppm) of antimony (III) were prepared by dissolving appropriate amounts of potassium antimonyl tartrate (BDH, Poole, UK) in de-ionized water. Standard stock solutions (1000 ppm) of antimony (V) were prepared by dissolving appropriate amounts of potassium hexahydroxyantimonate (Aldrich, Milwaukee, WI) in de-ionized water. Both standard stock solutions of antimony were stored in polyethylene bottles in a fridge at 4°C. In this way, the stability of the antimony species can be maintained for at least 12 months [39]. Daily working solutions were prepared immediately by diluting the stock solution as needed. Stock solutions of Ethylenediaminetetraacetic acid (BDH, Toronto, ON), potassium hydrogen phthalate (BDH), disodium ethylenediamine tetraacetate (Fisher, Fair Lawn, NJ), ammonium dihydrogen orthophosphate (BDH) and potassium hydroxide (ACP, Montreal, QC) were prepared by dissolving appropriate amounts of each in de-ionized water.

5.2.2 Instrumentation

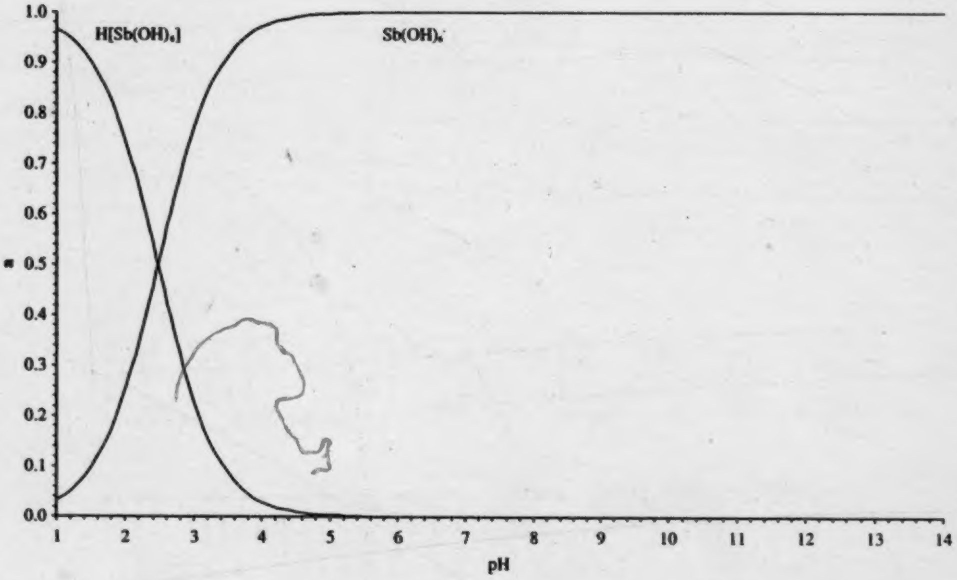

Figure 5.01 Fractional composition diagram for antimony (V) as a function of pH in very dilute aqueous solution.

The CE system was laboratory-constructed. A 76-cm long fused silica capillary (PolymicroTechnologies Inc., Phoenix, AZ) with an inner diameter of 50 µm and an outer diameter of 182 µm was used as the separation capillary. A Model CZE1000R high voltage power supply (Spellman, Hauppauge, NY) was used to provide the stacking and separation voltage. With this power source, polarity switching can be completed within 1.5 seconds at the 20 kV level. The capillary exit end was grounded by pumping a sheath liquid (2% HNO_3) through another capillary that co-axially surround the CE capillary. The conditioning procedure for a new capillary was as described in Chapter 3.

A laboratory-constructed direct injection nebulizer was used as the interface to connect the CE to ICP-MS. The design and optimization of this interface has been described in detail in Chapter 2.

A Perkin-Elmer SCIEX ELAN 5000A ICP-MS instrument (Thornhill, ON, Canada) was used as the detector. The isotope m/z 121 was monitored as a function of time in the graphic mode of the instrument. Electropherogram data were collected using a 200 ms dwell time and one point per peak. Data analysis was performed after the data were transferred to a Microsoft Excel spreadsheet. Peak areas were calculated using a program written in Visual Basic. The ICP-MS operating parameters and optimization have been described in Chapter 2.

An ORION pH Meter Model 420A (Orion Research Inc., Beverly, MA) was used to measure pH. The pH probe (Orion Triode Combination Electrode) was calibrated just before use using three buffer solutions (Fisher, Nepean, ON) with pH 4, 7 and 10.

5.2.3 Sample Injection

Hydrodynamic injections by nebulizer suction were used for the introduction of sample. In order to avoid introduction of air into the capillary, the nebulizer gas had to be turned off before transferring the capillary between electrolyte and sample reservoir. Sample injection volume was estimated by multiplication of the injection time and suction flow rate. The suction flow rate was determined by the method as described previously (Chapter 3).

5.3 Results and Discussion

5.3.1 Development of CE Procedure

5.3.1.1 Sample Stacking without Sample Matrix Removal

As seen from Figure 5.01, in dilute aqueous solutions of pH higher than about 4.6, Sb(V) exists mainly as the singly charged anionic species $Sb(OH)_6^-$. Sb(III), as the tartrate complex, in this pH range exists probably as the doubly charged anionic complex $[Sb_2(C_4H_2O_6)_2]^{2-}$. Their different electrophoretic mobility should allow for their separation by CE. Figures 5.02a and 5.02b show the electropherograms for 1 ppm Sb(V) and 1 ppm Sb(III) solution, respectively. The buffer was 20 mM $(NH_4)H_2PO_4$ at pH 4.6. The sample solutions were adjusted to pH 5.2. A sample injection volume of 0.63 μL of was used and +20 kV was applied to the injection side. As seen from the figures, Sb(V) as $Sb(OH)_6^-$ gave a sharp peak, while Sb(III) as $[Sb_2(C_4H_2O_6)_2]^{2-}$ gave a very broad peak that lasted over 100 seconds of migration time, which causes serious problems for the CE separation. A similar peak broadening for the Sb(III)-tartrate was observed by Michalke and Schramel in their speciation study [38]. The problem might be related to the molecular structure of this Sb(III)-tartrate complex. The structure of the anion $[Sb_2(C_4H_2O_6)_2]^{2-}$ is shown in Figure 5.03 [42]. The binuclear structure results in rather

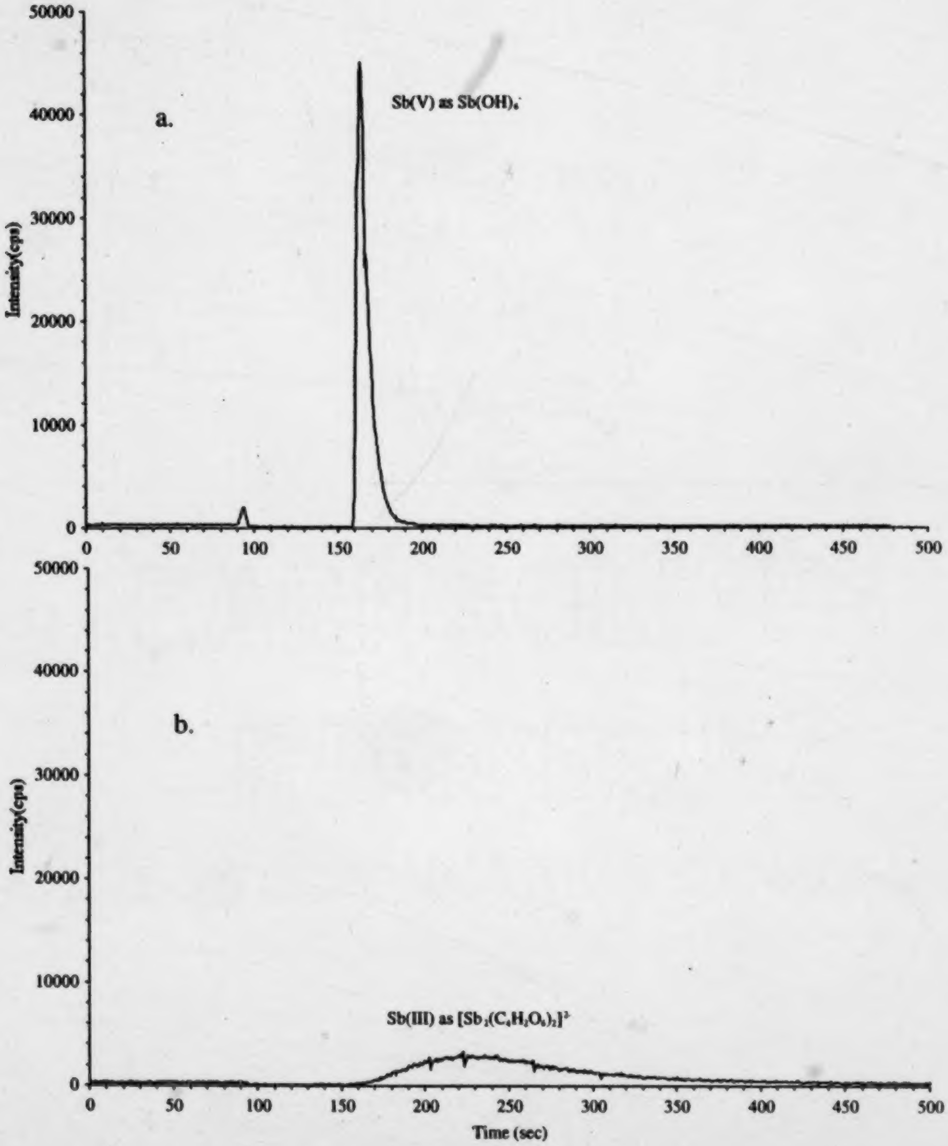

Figure 5.02 Electropherograms for solutions containing (a) 1 ppm Sb(V) and (b) 1 ppm Sb(III). Conditions: buffer, 20 mM $(NH_4)H_2PO_4$ at pH 4.6; sample pH, 5.2; injection volume, 0.63 µL; applied voltage, +20 kV.

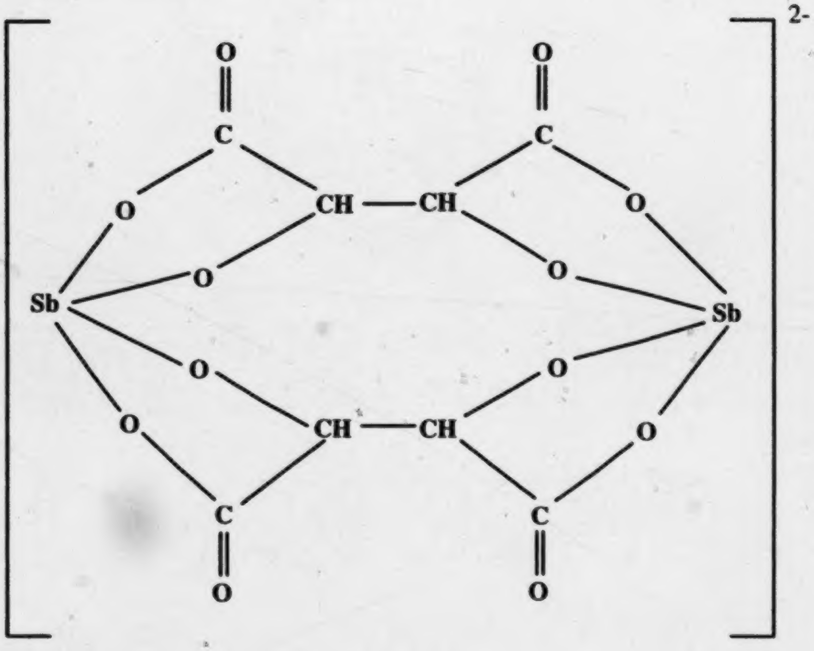

Figure 5.03 Structure of the Sb(III)-tartrate complex anion

large size for this ion, which may adversely affect electrostacking, causing peak broadening and tailing. So attempts were made to convert this binuclear anion into a smaller sized complex by using oxalate and phthalate ligands, but were unsuccessful. Apparently the anion $[Sb_2(C_4H_2O_6)_2]^{2-}$ is a stronger complex than either Sb(III)-oxalate or Sb(III)-phthalate complex. EDTA is a well-known chelating ligand that forms strong 1:1 complex with most metal ions. So EDTA was used to transform $[Sb_2(C_4H_2O_6)_2]^{2-}$ into a Sb(III)-EDTA complex, and the result was successful. Figure 5.04 is a comparison of electropherograms of antimony samples containing Sb(III) and Sb(V) (1 ppm each) with and without EDTA added. Without EDTA added, Figure 5.04a shows a severely broadened and tailing peak for Sb(III). When adding 0.40 mM Na_2H_2EDTA to the sample, the broadened peak for Sb(III) disappears, and the peaks for Sb(III) and Sb(V) coalesce, suggesting the formation of the anion $Sb(EDTA)^-$. The transformation can be described by the following equilibria:

$$[Sb_2(C_4H_2O_6)_2]^{2-} + 4H_2O \Leftrightarrow 2Sb^{3+} + 2C_4H_4O_6^{2-} + 4OH^- \qquad (5.03)$$

$$Sb^{3+} + H_2EDTA^{2-} \Leftrightarrow Sb(EDTA)^- + 2H^+ \qquad (5.04)$$

Since $Sb(EDTA)^-$ is a stronger complex than $[Sb_2(C_4H_2O_6)_2]^{2-}$, and the presence of H_2EDTA^{2-} shifts Equation (5.04) to the right and so does Equation (5.03). The transformation proceeds quickly under room temperature.

5.3.1.2 Sample Stacking with Sample Matrix Removal

Although this conversion solves the peak broadening problem of the Sb(III), the resulting peak for Sb(III) overlaps that of Sb(V). The reason may be attributed to sample stacking without removal of sample matrix. When a long sample plug with low conductivity is

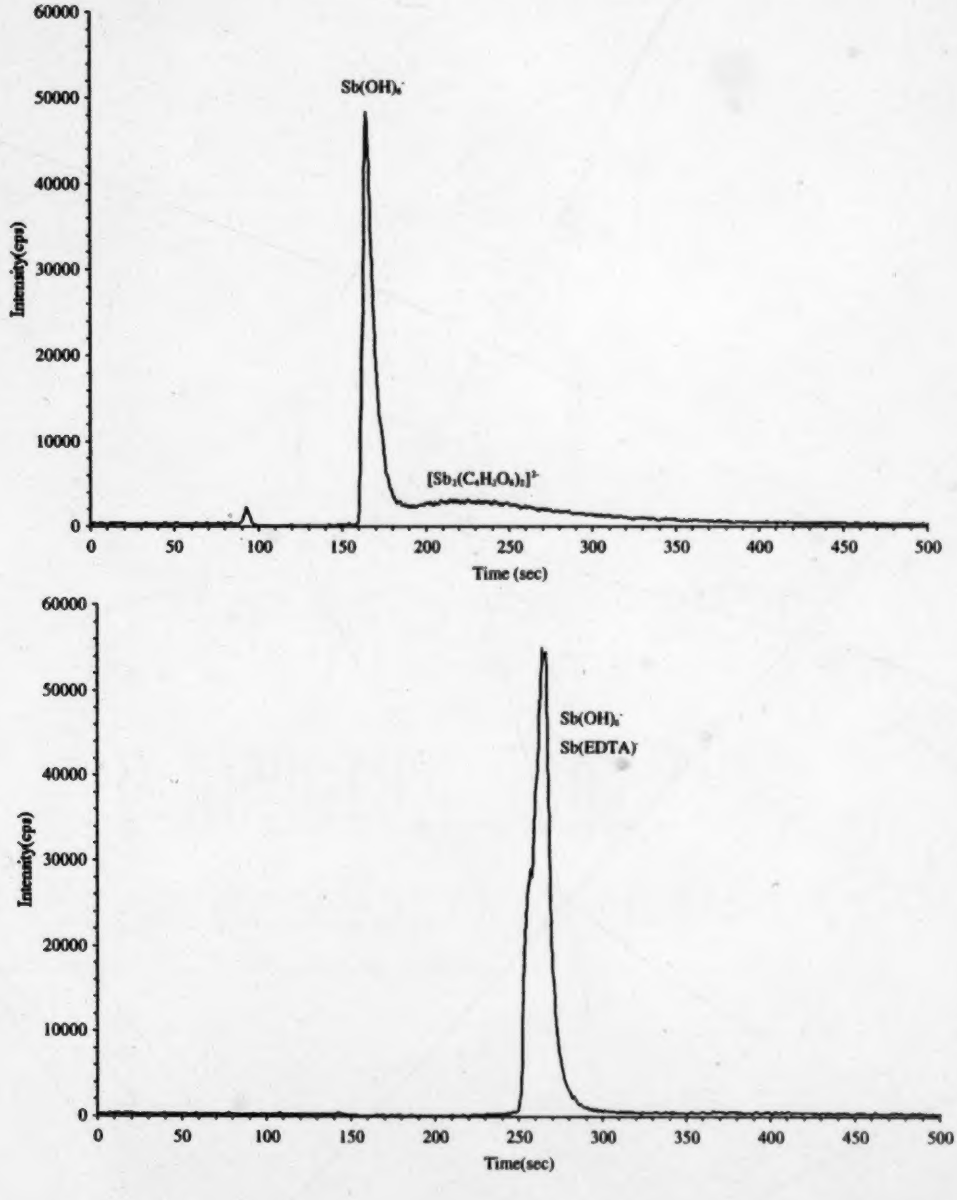

Figure 5.04 Electropherograms for solutions containing (a) 1 ppm Sb(V)/Sb(III) and (b) 1 ppm Sb(V) /Sb(III) and 0.4 mM Na_2H_2EDTA. Conditions as in Fig.5.02.

injected into the capillary filled with a high conductivity buffer, the electric field in the sample zone is higher, therefore the velocities of the analyte ions in the sample region are faster than those in the running buffer region. The analyte ions will move quickly to the concentration boundary between the sample zone and the running buffer zone and stack into a narrow band [43-46]. Since the electric field outside the sample zone is so low that all ions in the stacking band will only move with the bulk flow and no further separation can occur (see Chapters 3 and 4). To improve the resolution, the sample matrix must be removed once the stacking process is completed. This can be done by pumping the sample matrix out of the capillary using the EOF while the sample stacking is in progress [44,45]. This technique is illustrated in Figure 5.05.

As seen in Fig. 5.05, first, a long plug of sample dissolved in water or low concentration buffer is hydrodynamically injected into the capillary filled buffer of higher concentration (step a). After the capillary is placed back in the running buffer reservoir, a negative voltage (-20 kV) is applied at the injection side, causing the positive ions to migrate toward the injection side and the negative ions to migrate toward the detector (step b). Since the direction of the EOF is toward the injection side, the sample matrix along with the positive ions is pushed out of the capillary. In the mean time, the negative ions in the low conductivity of the sample plug experience a high local electric field strength and consequently move at high velocity toward the sample-buffer interface and stack up at the boundary (step c). When most of the sample plug has been removed from the capillary, most of the negative ions are focused at the boundary and the sample plug is now a narrow band of concentrate species. At this moment, the polarity of the applied voltage is switched to a positive value (-20 kV→ +20 kV), and the EOF now is toward the detector (step d). The nebulizer gas is then turned on, and the anion separation occurs under normal CE conditions (step e). With this technique, a 10 to 100-fold sensitivity enhancement can be achieved without loss of resolution [44].

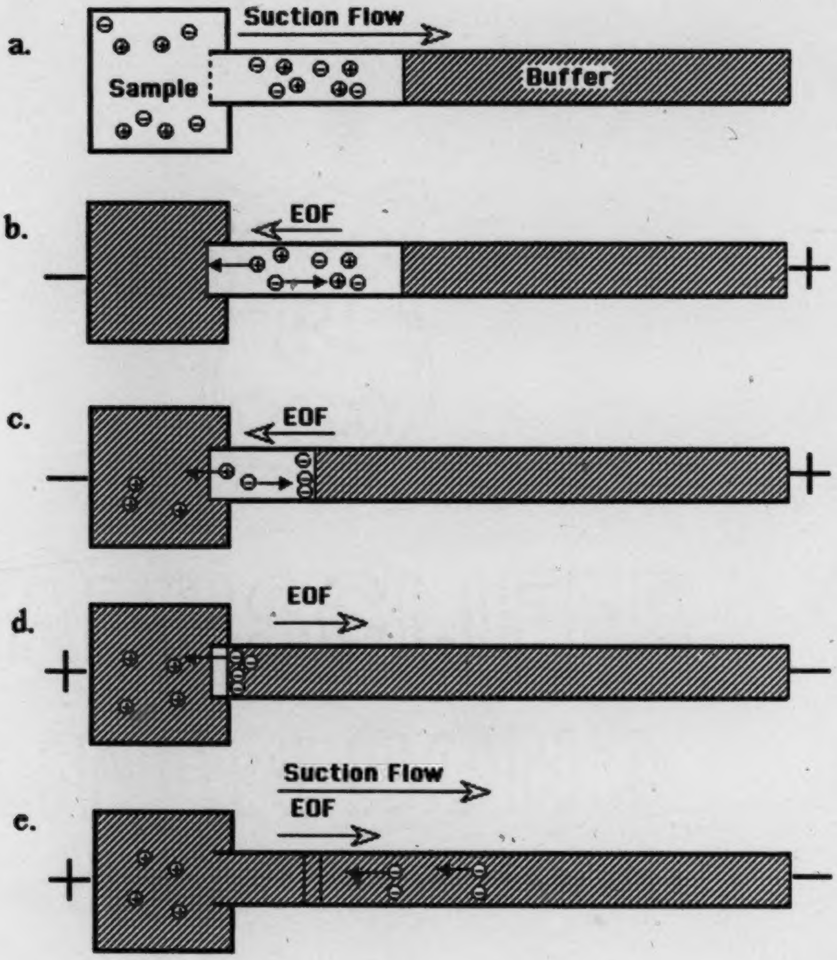
a.
Suction Flow
Sample
Buffer
b.
EOF
c.
EOF
d.
EOF
e.
Suction Flow
EOF

Figure 5.05 Schematic diagram showing the electrostacking with sample matrix removal: (a) sample injection by suction, (b) application of voltage (-20 kV) and no suction, (c) pumping sample matrix out of capillary by EOF while the anions stack up at the boundary, (d) voltage polarity switching (-20 kV→+20 kV), (e) normal CE separation with suction flow.

Figure 5.06 is a demonstration of the CE separation of Sb(III) and Sb(V) species using the above mentioned technique. Figure 5.06a shows the electropherogram for a sample solution containing 1 ppm Sb(III), 1 ppm Sb(V) and 0.4 mM EDTA at pH 5.6. The buffer was 20 mM EDTA at pH 4.6. A volume of 0.63 μL of the sample was injected into the capillary. A value of –20 kV was applied to stack the anions while removing the sample matrix with EOF. The gradual increase in electrophoresis current was carefully monitored. When the current reached 95% of the original value, which had been measured previously when the capillary was filled only the buffer, the polarity of the voltage was switched to +20 kV to start the normal CE separation. As seen in Figure 5.06a, the peaks of Sb(III) and Sb(V) were baseline resolved. Compared with the individual standard injections under the same experimental conditions shown in Figure 5.06b and c, the peaks in Figure 5.06a can be easily identified. The reason that $Sb(EDTA)^-$ came out earlier than $Sb(OH)_6^-$ can be attributed to the larger size of the former and thus slower electrophoretic velocity toward the injection side.

5.3.2 Optimization of the CE Parameters

5.3.2.1 Choice of CE Buffer

Antimony was monitored at isotope m/z 121, and no spectral interference in an Ar ICP-MS is found at mass 121 [47]. However, when using $(NH_4)H_2PO_4$ as the running buffer, a relatively high Sb baseline signal was observed (Figure 5.04). The problem may be due to Sb impurities present in the phosphate buffer. So potassium hydrogen phthalate was tested as the running buffer, and a much lower background signal level was observed. Although the formation of $Sb(EDTA)^-$ complex is fast, the complex formed before injection is unstable in the phthalate buffer system and can partially or completely dissociate in the capillary during the CE process unless a sufficient amount of EDTA was

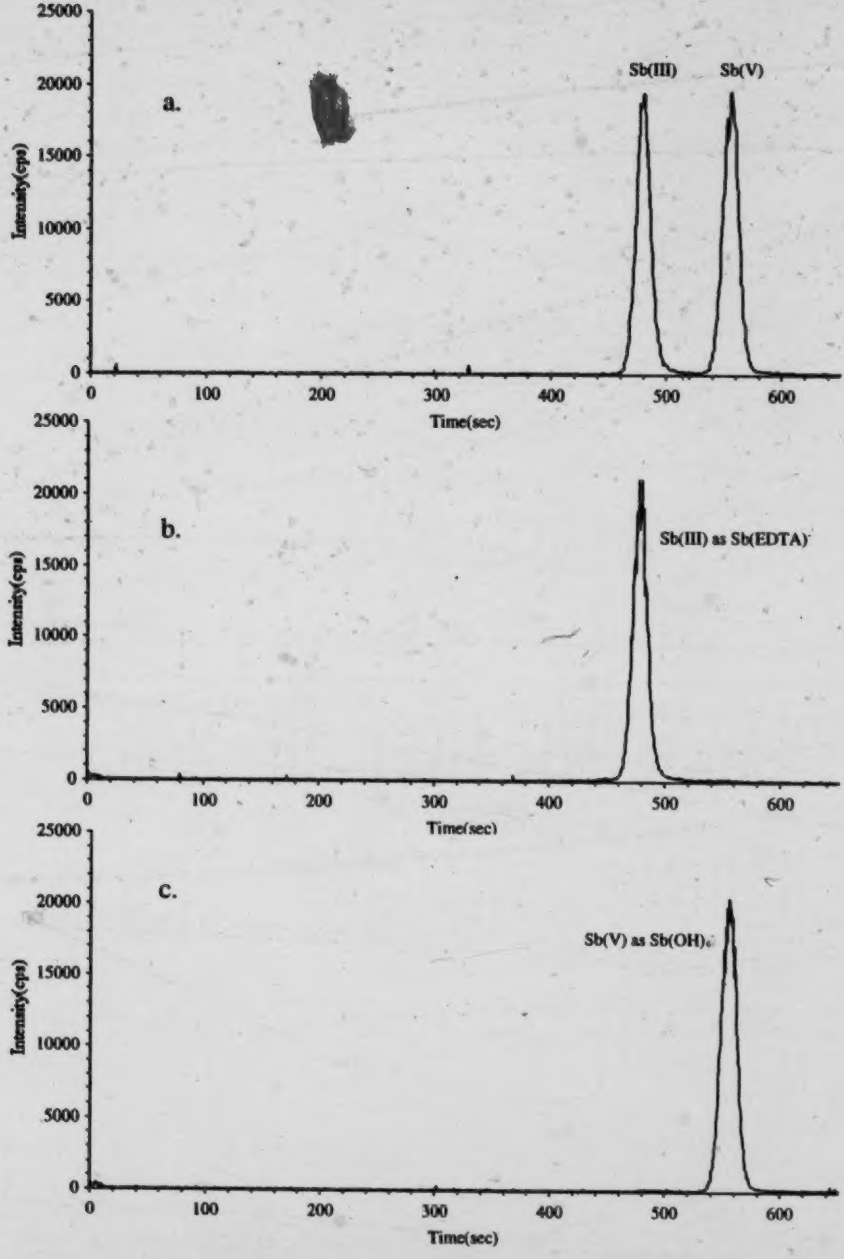

Figure 5.06 Electropherograms for solutions containing (a) 1 ppm each Sb(III)/Sb(V), (b) 1 ppm Sb(III) and (c) 1 ppm Sb(V). Conditions: buffer, 20 mM EDTA at pH 4.6; sample, 0.4 mM EDTA at pH 5.6; injection volume, 0.63 μL; stacking voltage, -20 kV; separation voltage, +20 kV.

introduced in the running buffer. Figure 5.07 shows the effect of EDTA in the running buffer on the separation of Sb(III) and Sb(V). With no EDTA added in the running buffer, a broad and poorly shaped peak was observed for Sb(III) (Figure 5.07a). When 5 mM EDTA was added to the running buffer, the peak area for Sb(III) increased (Figure 5.07b). The peak area for Sb(III) continued to increase with increasing EDTA concentration until the EDTA concentration reached 15 mM. Further increase in EDTA concentration resulted in no change in peak area for Sb(III), suggesting 15 mM EDTA is sufficient to suppress the dissociation and to maintain the stability of $Sb(EDTA)^-$ in the running buffer. The peak area for Sb(V) showed no significant change with increasing EDTA concentration, indicating that $Sb(OH)_6^-$ is stable in the running buffer and no significant interaction between $Sb(OH)_6^-$ and EDTA. In general, increasing the EDTA concentration in the running buffer favors the stability of the EDTA complex, but too high a concentration may lead to excess Joule heating. Considering all those factors, 20 mM EDTA was chosen as the CE running buffer solution. Initially the disodium salt of EDTA, Na_2H_2EDTA, was used for the antimony speciation. However, it was found that the baseline was noisy with lots of small spikes. This might be due to the formation of the precipitate of $Na[Sb(OH)_6]$, known as the least soluble of all the alkaline metal salts [48], in the CE process. The problem was solved by using the potassium salt of EDTA and the pH adjustment was done using KOH.

5.3.2.2 Effect of the Addition of EDTA to Sample on Antimony Separation

Since EDTA is added to the sample to convert the Sb-tartrate complex to the Sb-EDTA complex, it is necessary to know what amount of EDTA is appropriate. In general, an excessive amount of EDTA added to the sample ensures the completeness of the transformation and stability of the $Sb(EDTA)^-$, but too large a concentration may substantially increase the conductivity of the sample, causing problems later on in the

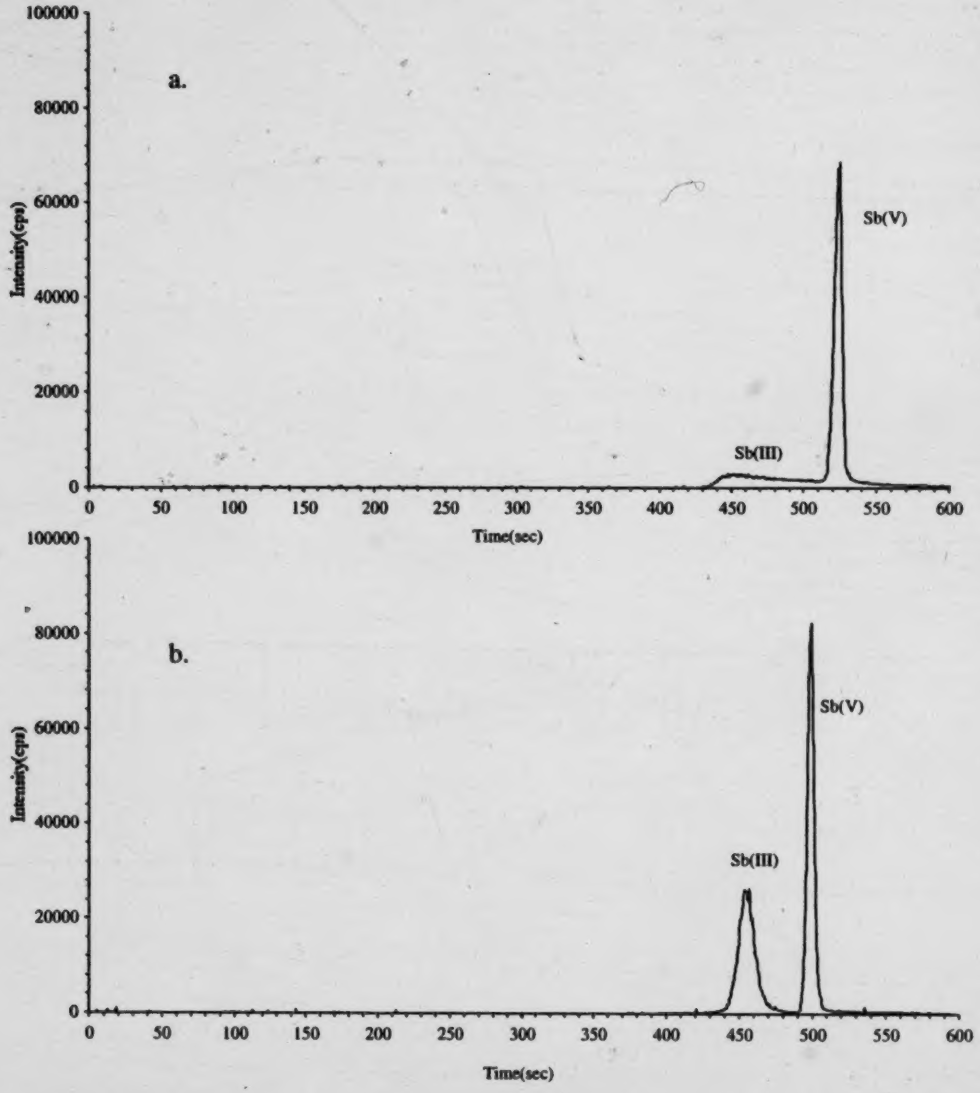

Figure 5.07 Electropherograms for sample solutions containing Sb(III) and Sb(V) (1 ppm each) and 0.4 mM EDTA using (a) 20 mM phthalate and (b) 15 mM plus 5 mM EDTA as the running buffer. Other conditions as in Fig. 5.06

sample stacking process. Therefore, the EDTA concentration in the sample should be controlled within an optimal range.

Figure 5.08 and Figure 5.09 demonstrate the effect of EDTA added in the sample on the separation of Sb(III) and Sb(V). The peak areas and peak heights for Sb(III) increase with increasing EDTA concentration until it reaches 0.20 mM. After which a stable peak area for Sb(III) is observed. At 0.20 mM the molar ratio between EDTA and Sb(III) is about 24 : 1. This is the minimum ratio to ensure the complete transformation from antimony tartrate complex to EDTA complex and to maintain the stability of the $Sb(EDTA)^-$ complex during the separation process. On the other hand, the peak areas for Sb(V) show no significant change with changing the EDTA concentration(Figure 5.09), indicating no chemical interaction between $Sb(OH)_6^-$ and EDTA, which is expected since $Sb(OH)_6^-$ is already six-coordinated and can not form complex with EDTA. An EDTA concentration of 0.40 mM in the sample was chosen in this study.

As seen from Figure 5.08, a desirable effect of adding EDTA to the sample and the running buffer is the good symmetrical peaks that are observed. This is probably a result of the similar mobility of analyte anions to that of EDTA anion. It is well known that peak distortion occurs when the mobility of the analyte ion is different from that of the buffer ion [49, 50].

The preferential complexation of Sb(III) with EDTA as compared to other organic ligands could be an advantage in quantitative speciation of the oxidation states of antimony in real samples. In real samples, Sb(III) may occur in different complex forms (e.g., with carbonic and fulvic acids), and all these will be converted to Sb(III)-EDTA complex when EDTA is used, therefore the Sb(III) oxidation state will come out as one peak.

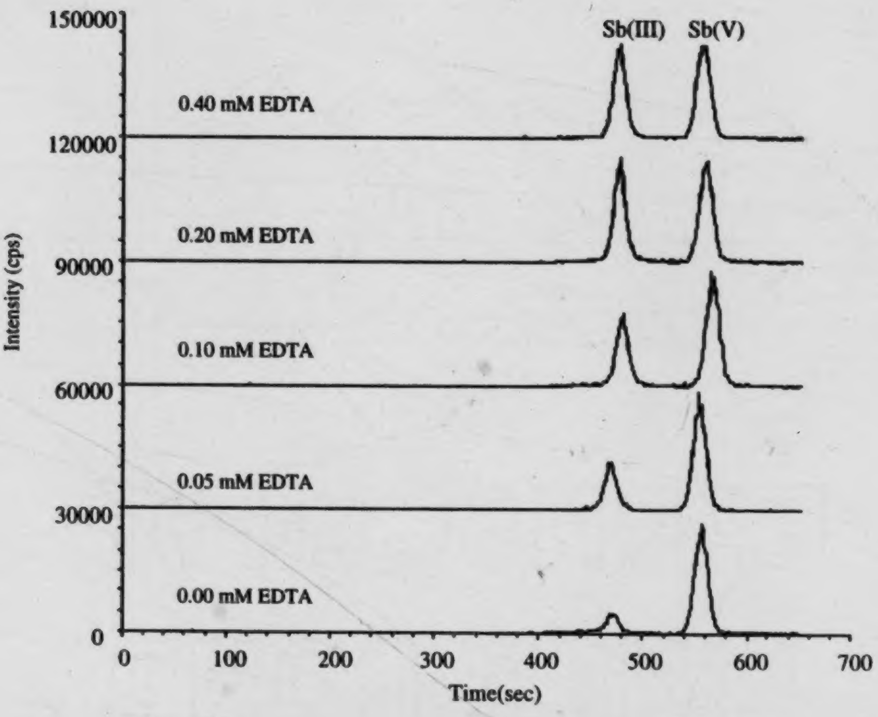

Figure 5.08 Electropherograms for sample solutions containing Sb(III) and Sb(V) (1 ppm each) with different EDTA concentration added in the sample. Other conditions as in Fig.5.06.

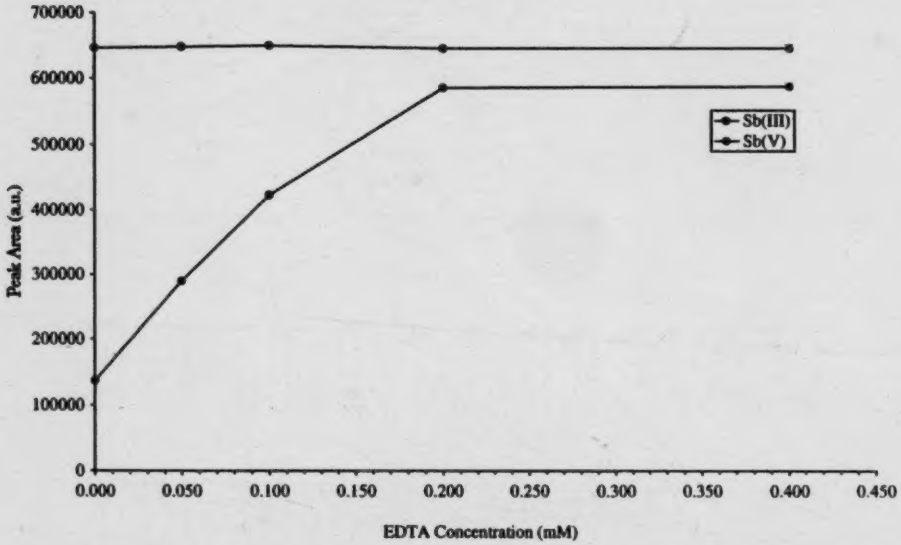

Figure 5.09 Plots of peak areas (arbitrary units) for Sb(III) and Sb(V) as a function of EDTA concentration added in the sample. Conditions as in Fig.5.06.

5.3.2.3 Effect of Stacking and Separation Voltage on Antimony Separation

The effects of stacking voltage on antimony speciation signals are summarized in Table 5.02. With an increase of the stacking voltage, no significant changes in peak area for Sb(III) and Sb(V) were observed. Although a high stacking voltage did shorten the time needed for analyte stacking and sample matrix removal, monitoring the current also became difficult because the current rise at the final stage of stacking was too fast. A voltage of -20 kV was therefore selected as the stacking voltage in this study.

According to Jorgenson and Lukacs [51], the resolution R between two peaks in CE is determined by the following equation:

$$R_s = 0.177(\mu_1 - \mu_2)\sqrt{\frac{U}{D\bar{\mu}_a}} \qquad (5.05)$$

where μ_1 and μ_2 are the electrophoretic mobility of the species 1 and 2, respectively, $\bar{\mu}_a$ is their average apparent mobility, D is the diffusion coefficient of the species, and U is the applied separation voltage.

Equation (5.05) suggests that increasing the voltage will improve the resolution. This was observed in this study. Figure 5.10 shows the effects of separation voltage on antimony separation. Increasing the separation voltage from 10 kV to 25 kV increases the peak separation. On the other hand, slight increases in migration time were observed when increasing the voltage from 10 to 20 kV. This may be explained from the following equation:

$$t_m = \frac{L}{[\upsilon_{suc} + (\mu_{eof} - \mu_{ep})E]} \qquad (5.06)$$

Table 5.02 Effect of stacking voltage on antimony speciation[a]

Stacking voltage (kV)	Stacking time[b] (min)	CE current[c] (μA)	Peak area ($\times10^5$) (a. u.)	
			Sb(III)	Sb(V)
-10	5.5	12	6.02	7.60
-15	3.6	20	5.89	7.58
-20	2.5	30	6.06	7.92
-25	2.0	42	6.07	7.97

[a] Solutions containing Sb(III) and Sb(V) (1 ppm each). Other conditions as in Fig.5.06.

[b] Time needed for completing the stacking and sample matrix removal.

[c] Current measured for the CE buffer at the stacking voltage.

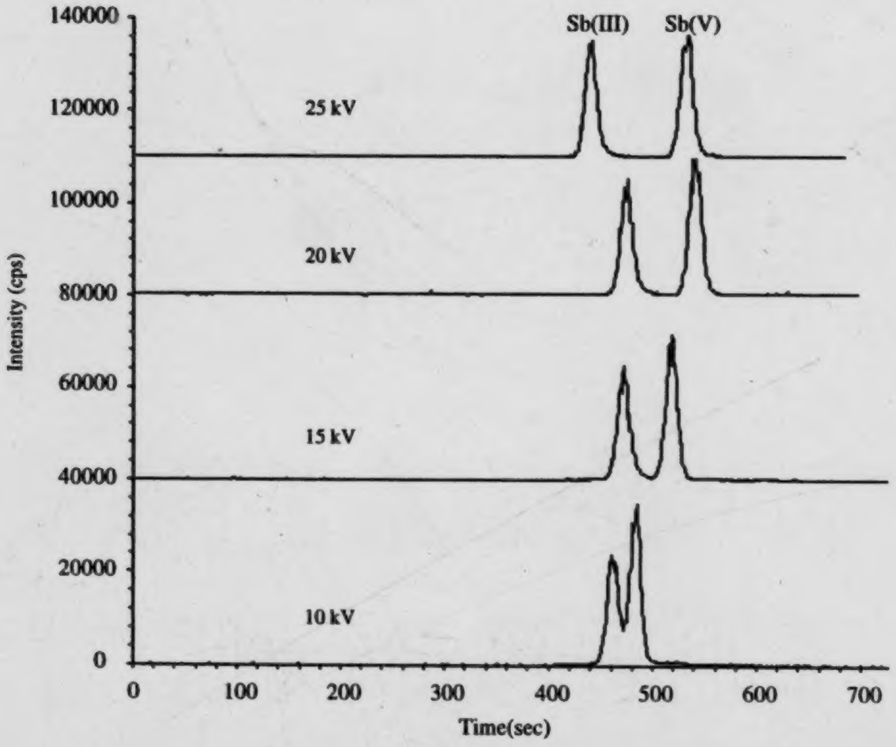

Figure 5.10 Electropherograms for sample solutions containing Sb(III) and Sb(V) (1 ppm each) and 0.4 mM EDTA with different separation voltage (15-25 kV) applied. Other conditions as in Fig.5.06.

where t_m is the migration time of species, L is the total length of capillary, υ_{suc} is suction-induced flow rate, μ_{eof} is the electroosmotic mobility, μ_{ep} is the electrophoretic mobility, and E is the field strength (E = U/L). Under the present experimental conditions it was found that $\mu_{eof} < \mu_{ep}$ and consequently the term $(\mu_{eof} - \mu_{ep}) < 0$ in Equation (5.06). Therefore increasing the voltage resulted in a slight increase in migration time. However, at 25 kV the migration time became shorter, probably due to Joule heating leading to a higher temperature and lower viscosity of the buffer, and thus faster υ_{suc}. Considering all these factors, 20 kV was chosen as the separation voltage in this study.

5.3.2.4 Effect of pH of Sample on Antimony Separation

Figure 5.11 shows a comparison of electropherograms obtained at five different sample pH conditions. The effects of the sample pH on migration time, peak area, peak width and peak separation are summarized in Table 5.03. The sample contains Sb(III) and Sb(V) (1 ppm each) and 0.4 mM EDTA. The separation buffer is 20 mM EDTA at pH4.6. Since the electropherograms were recorded after the sample matrix had been removed, the analyte ions migrate in a homogeneous buffer system, and the electric field strength and EOF are constant during the separation process. Consequently, one would expect that these electropherograms would be very similar regardless of the sample pH However, this turned out to be true only when the sample pH was in the range of 5.6-9.0. As seen from Figure 5.11 and Table 5.03, at sample pH 11.0, the peak for Sb(III) shows considerable broadening, the resolution becomes worse, and the migration time shifts downward. Another interesting case is at pH 3.2. In this case, a new peak is observed at the migration time of 684 sec, but the identification of this peak using standard injection is not as simple as one might initially anticipate. It can be seen from Figure 5.12 (a) and (b), when 1 ppm Sb(III) and 1 ppm Sb(V) standards are injected individually at sample pH 3.2, no peak at 684 sec is observed in either solution. However, when solution

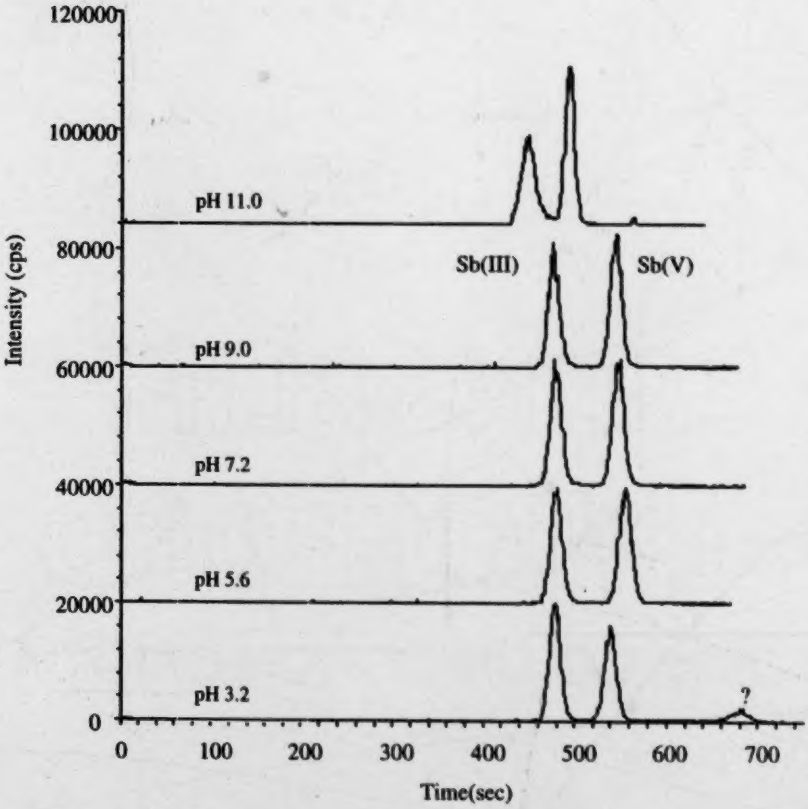

Figure 5.11 Electropherograms for solutions containing Sb(III) and Sb(V) (1 ppm each) and 0.4 mM EDTA with different sample pH (3.2-11.0). Other conditions as in Fig.5.06.

Table 5.03 Effect of sample pH on migration time, peak area, peak width, and peak separation [a]

sample pH	migration time (s)		peak area($\times 10^5$) (a.u.)		fwhm (s)		peak separation (s)
	Sb(III)	Sb(V)	Sb(III)	Sb(V)	Sb(III)	Sb(V)	
3.2	479	540[b]	4.92	4.39[c]	14	14[d]	61
5.6	480	556	4.92	5.20	14	15	76
7.2	479	549	4.93	5.28	13	15	70
9.0	476	545	4.66	5.40	12	14	69
11.0	449	493	4.75[e]	5.65[e]	15	12	44

[a] Conditions as in Fig.5.06.

[b] Contaning two peaks, the other peak has a migration time 684 (s).

[c] Containing two peaks, the other peak has an area of 0.82×10^5 (a.u.).

[d] Containing two peaks ,the other peak has an fwhm of 23 (s).

[e] Essentially baseline-resolved, peak area estimated.

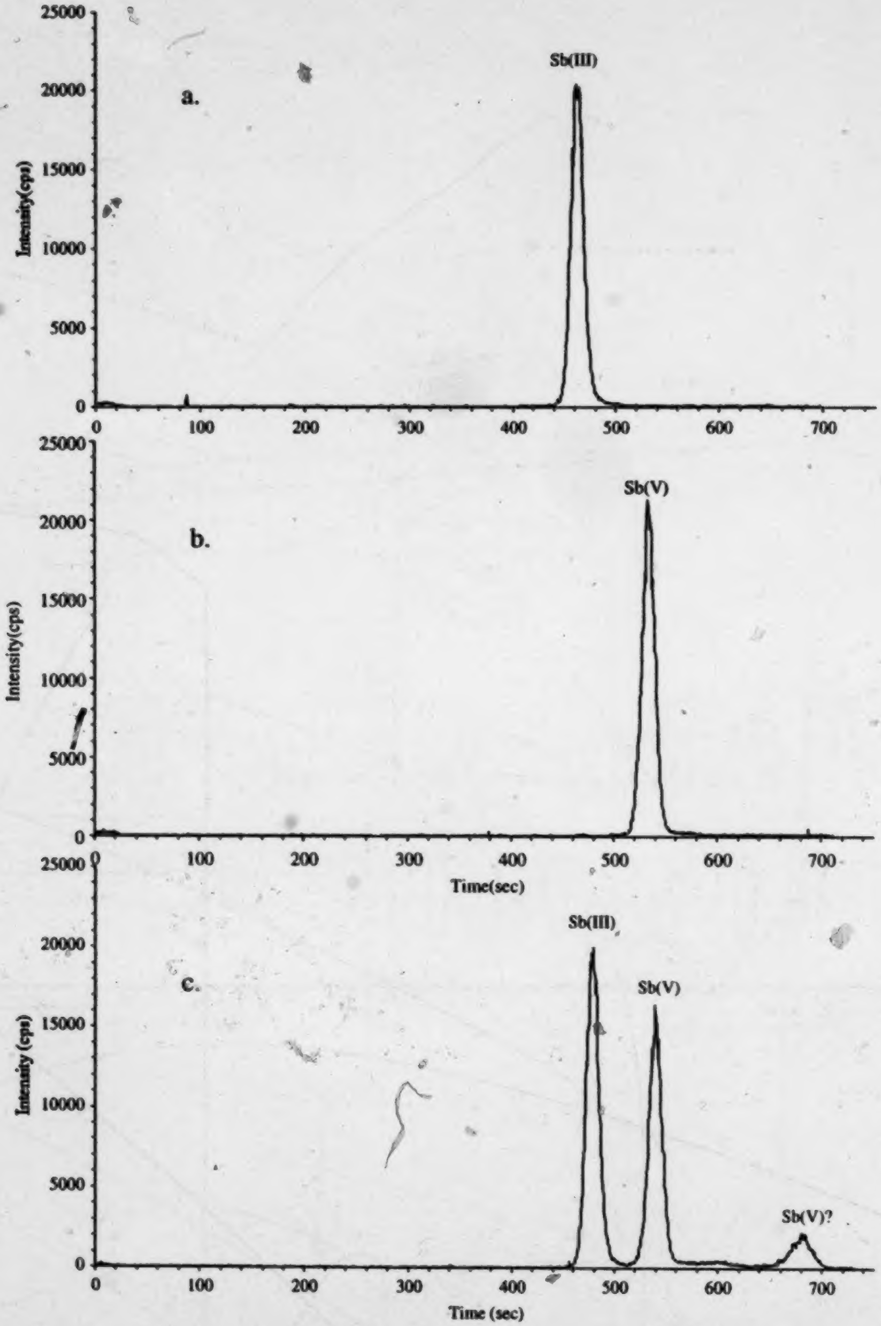

Figure 5.12 Electropherograms for solutions containing (a) 1 ppm Sb(III), (b) 1ppm Sb(V) , and (c) Sb(III) and Sb(V) (1 ppm each) at sample pH 3.2. Other conditions as in Fig.5.06.

containing 1 ppm Sb(III) and 1ppm Sb(V) is injected at pH 3.2, the peak at 684 sec appears. It is postulated that this peak might be a species of Sb(V). This postulation is based on the following two reasons. First, the sum of areas of the two peaks at 540 sec and 684 sec is equal to the peak area of 1ppm Sb(V) standard. Second, the longer migration time of this species indicates it probably bears more negative charge than $Sb(OH)_6^-$, and it is known that Sb(V) can form a series of polynuclear species $Sb_{12}(OH)_{64}^{4-}$ to $Sb_{12}(OH)_{67}^{7-}$ at acidic pH. On the other hand, $Sb(EDTA)^-$ would more likely protonate in acidic solution to form a less negatively charged complex. To verify this postulation, more work is definitely needed. But our purpose is to choose the best sample pH range for quantitative speciation, and knowing the above results is adequate for this purpose. To keep the peak integrity for Sb(V) for quantitative speciation, a sample pH of 3.2 or below should be avoided.

In all, species distribution depends on sample pH. To achieve effective separation, the sample pH should be carefully controlled. A pH of 5.6 was chosen as the optimal sample pH in this study.

5.3.2.5 Effect of pH of CE Buffer on Antimony Separation

The pH of the CE buffer is another important factor that needs careful consideration because if affects the stability of species during the separation and also the EOF. Figure 5.13 shows a comparison of the electropherograms of sample solutions containing 1 ppm Sb(III), 1 ppm Sb(V) and 0.4 mM EDTA at pH 5.6 with different buffered pH (3.6-6.6). Measured values of migration time (sec), peak area (arbitrary unit), peak width (s, full width at half maximum) and peak separation (s) are listed in Table 5.04. Increasing the buffer pH from 3.6 to 6.6 decreases the migration time for both Sb(III) and Sb(V), a result of the faster EOF at higher pH. At buffer pH 3.6, two peaks are observed for

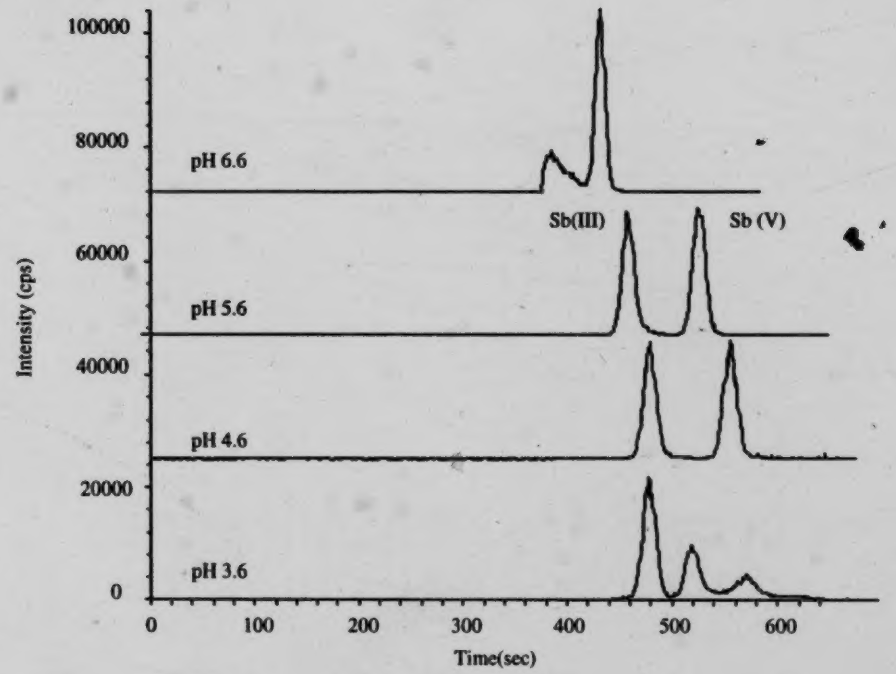

Figure 5.13 Electropherograms for sample solutions containing Sb(III) and Sb(V) (1 ppm each) and 0.4 mM EDTA with different running buffer pH (3.6-6.6). Other conditions as in Fig.5.06.

Table 5.04 Effect of buffer pH on migration time, peak area, peak width, and peak separation [a]

buffer pH	migration time (s)		peak area($\times10^5$) (a.u.)		fwhm (s)		peak separation (s)
	Sb(III)	Sb(V)	Sb(III)	Sb(V)	Sb(III)	Sb(V)	
3.6	479	518[b]	5.36		14	15[c]	39
4.6	480	556	4.82	5.12	13	14	76
5.6	467	533	4.99	5.46	13	14	66
6.6	386	433	2.67[d]	6.21[d]	19	11	47

[a] Conditions as in Fig.5.06.

[b] Contaning two peaks, the other peak has a migration time 571 (s).

[c] Containing two peaks, the other peak has a fwhm of 20 (s).

[d] Peaks are not baseline-resolved, and areas are estimated.

Sb(V), similar to that observed in Section 5.3.3.4 where the sample pH was 3.2, but they can not be baseline-resolved at this buffer pH. At buffer pH 6.6, the peak for Sb(III) shows significant broadening and the peak area is also smaller. This is somewhat unexpected since increasing the pH would supply more $EDTA^{4-}$ for complexation and therefore would enhance the stability of $Sb(EDTA)^-$ in the separation process. It is well known that many metal ions can form seven-coordinate EDTA complexes, with the seventh coordination position occupied by a water molecule [52]. It is thus assumed that the broadening of Sb(III) peak at higher pH may be the result of the hydrolysis of $Sb(EDTA)^-$ leading to a seven-coordinate complex $Sb(OH)(EDTA)^{2-}$, i.e., the following reaction may be responsible:

$$Sb(EDTA)^- + OH^- \Leftrightarrow Sb(OH)(EDTA)^{2-} \qquad (5.06)$$

During the study, we found that when the buffer pH was raised to 10.5, the order of migration time for Sb(III) and Sb(V) was reversed, i.e., Sb(III) came out later than Sb(V). This is consistent with the above idea that at higher pH Sb(III) may exist as the doubly charged species $Sb(OH)(EDTA)^{2-}$ having a higher electrophoretic velocity away from the detector.

To summarize, Sb(III) as the $Sb(EDTA)^-$ complex is stable in acidic buffer solution of pH 3.6, while Sb(V) as $Sb(OH)_6^-$ seems to form new species at this pH. On the other hand, $Sb(EDTA)^-$ complex may undergo hydrolysis at higher pH 6.6, while $Sb(OH)_6^-$ is stable at the same pH. The optimal pH range is around pH 4.6-5.6. In this study, pH 4.6 was chosen as the buffer pH.

5.3.2.6 Effect of Suction-induced Flow on Antimony Separation

The nebulizer used in the CE-ICP-MS interface is a pneumatic one that naturally causes a suction-induced flow in the capillary. Normally, this suction flow is considered undesirable because it has a parabolic flow profile that may lead to band broadening. But it can also be utilized in cases where the EOF is small and a proper suction flow toward the detector can significantly reduce the analysis time.

Figure 5.14 shows a comparison of the electropherograms of a sample solution containing 1 ppm Sb(III), 1 ppm Sb(V) and 0.4 mM EDTA at three different suction flow rates. All other conditions were kept the same. At the suction flow rate of 0.26 μL/min (Figure 5.14a), the migration times for Sb(III) and Sb(V) were shorter, and the peaks were narrower owing to less time available for diffusion controlled band broadening. But the time available for separation was also less so that they were not baseline-resolved. In contrast, at the suction flow rate of 0.16 μL/min (Figure 5.14c), the peaks were well separated, but the migration times were significantly longer and the peaks are much broader. It seems that a suction flow rate of 0.21 μL/min (Figure 5.14b) is a good compromise where baseline resolution and reasonable migration times were obtained. This flow rate was thus chosen as the optimal suction flow rate for antimony speciation. The presence of a suction flow did not cause significant peak broadening and in fact narrower peaks were observed with higher suction flow rates.

5.3.2.7 Effect of Injection Volume on Antimony Separation

In conventional CE separation, the injection volume is rather limited. For generating a maximum 10% broadening, the total length of the sample plug should be less than 1% of the capillary length [45,48]. In this study, a method of sample stacking with sample matrix removal is used. A large sample injection volume should not present any problem.

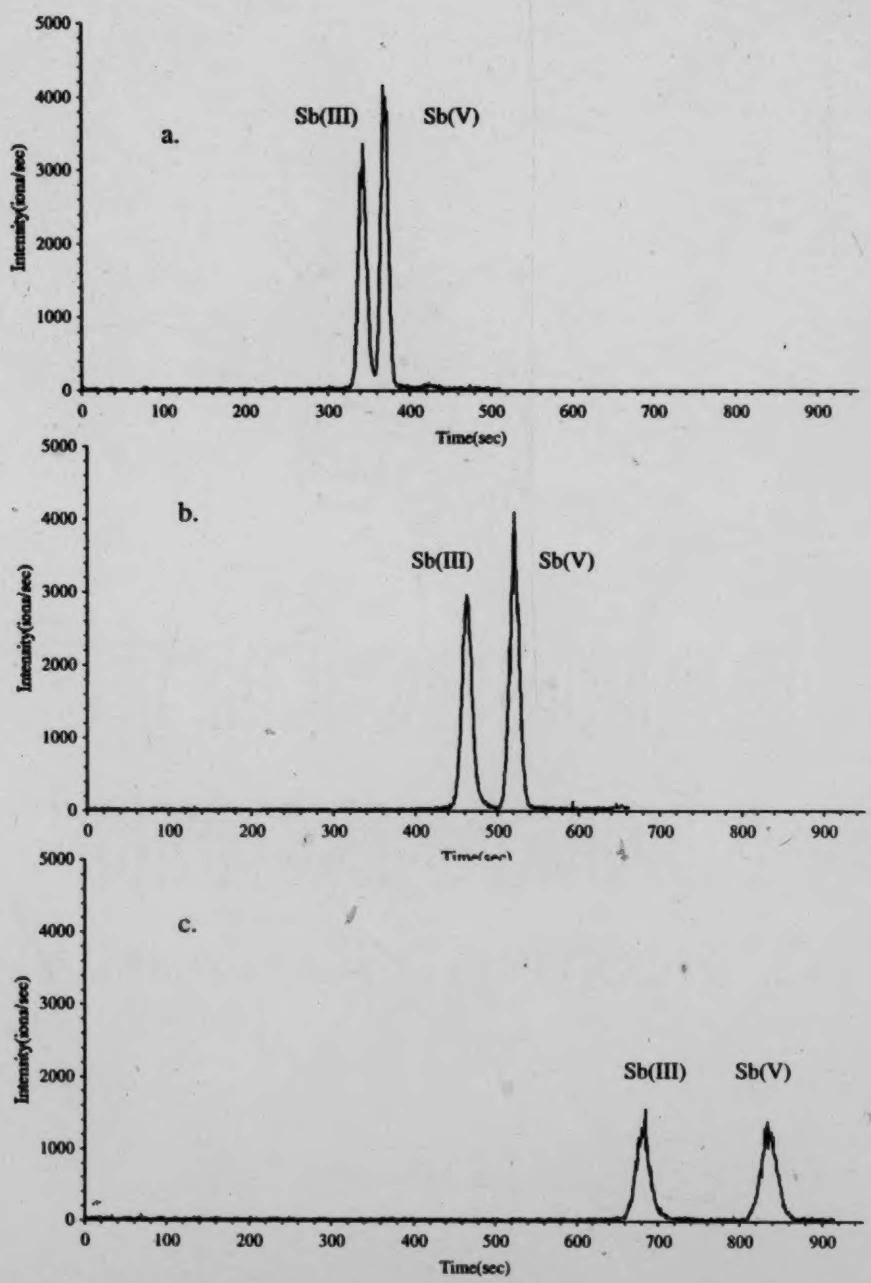

Figure 5.14 Electropherograms for sample solutions containing Sb(III) and Sb(V) (1 ppm each) in the presence of different suction flow rate: (a),0.26 μL/min; (b), 0.21 μL/min; (c), 0.16 μL/min. Other conditions as in Fig.5.06.

Figure 5.15 shows a comparison between six different injection volumes. All the electropherograms are plotted on the same scale in order to visualize the influence of increasing injection volumes. Injection volumes are estimated by calculation from the suction flow rate and injection time. The six injection volumes 0.11, 0.21, 0.42, 0.63, 0.84 and 1.05 μL correspond to 7.0%, 14%, 28%, 42%, 56% and 70% of the total capillary volume, respectively. Listed in Table 5.05 are the measured values of peak area, peak height, peak width (full width at half maximum), and peak separation as well as the injection time and volumes. As can be seen from Figure 5.15 and Table 5.05, both peak area and peak height for Sb(III) and Sb(V) increase with increasing injection volume. No significant band broadening or loss of efficiency is observed with increasing the injection volume. All peaks are symmetrical and baseline resolved. Since the sample matrix plug has been backed out from the capillary and the analyte ions are stacked up in a narrow zone at essentially the same point in capillary regardless of the initial sample volume injected, the migration times should be essentially the same for each run. As seen from Figure 5.15, the migration times are reasonably reproducible, the slight difference is probably due to the different amounts of water which are left in the capillary for each run.

Plots of peak areas for Sb(III) and Sb(V) versus injection volume are shown in Figure5.16. A good linear relationship between the peak area and the injection volume for Sb(V) is observed, but the plot for Sb(III) starts to show a negative deviation from linearity at an injection volume of 0.63 μL. This latter phenomenon was similar to that observed by Chien and Burgi [44] who offered an explanation using a simplified mathematical treatment. In order for the anions to stack up in the capillary without loss during the back-out process, the anion must have a higher electrophoretic velocity (υ_{epi}) than the bulk electroosmotic velocity (υ_b), i.e.,

$$-\upsilon_{epi} > \upsilon_b \qquad (5.07)$$

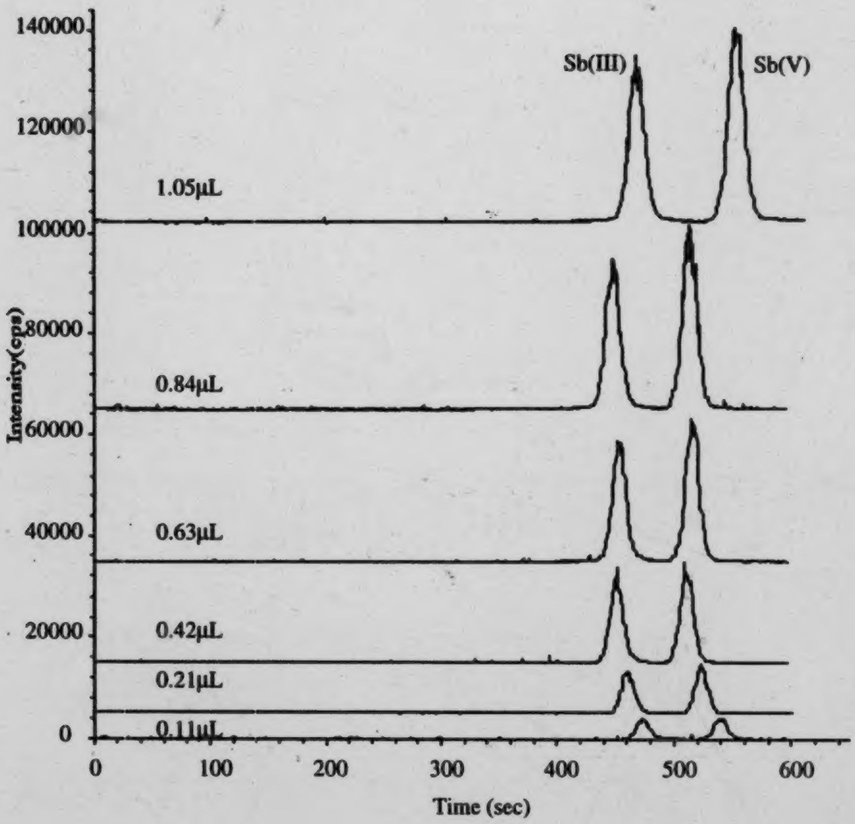

Figure 5.15 Electropherograms of Sb(III) and Sb(V) (1ppm each)solutions with different injection volume (0.11-1.1 µL). Conditions as in Fig.5.06

Table 5.05 Effect of injection volume on peak area, peak height, peak width, and peak separation [a]

injection time (sec)	injection volume (μL)	peak area($\times10^5$) (a.u.)		peak height($\times10^4$) (cps)		fwhm (s)		peak separation (s)
		Sb(III)	Sb(V)	Sb(III)	Sb(V)	Sb(III)	Sb(V)	
30	0.11	0.940	0.960	0.387	0.390	13	13	65
60	0.21	1.98	2.06	0.813	0.950	13	13	72
120	0.42	3.93	4.21	1.90	1.99	11	12	57
180	0.63	5.82	6.57	2.40	2.83	13	13	63
240	0.84	7.30	8.81	2.99	3.63	13	14	66
300	1.05	8.66	10.8	3.26	3.83	15	15	85

[a] Conditions as in Fig. 5.06.

The negative sign indicates the electrophoretic velocity must be in a direction opposite to the electroosmotic flow as the sample buffer is backed out of the capillary. The υ_{epi} can be expressed as

$$\upsilon_{ep_i} = \mu_{ep_i} \frac{E_0}{x} \tag{5.08}$$

where μ_{epi} is the electrophoretic mobility of species of interest, E_0 is overall field strength, and x is the fraction of the capillary length filled with the sample plug. The bulk electroosmotic velocity can be expressed approximately as

$$\upsilon_b = \mu_{eo} E_0 \tag{5.09}$$

where μ_{eo} is the electroosmotic mobility of the sample buffer. Combining Equations (5.07-5.09) yields

$$-\frac{\mu_{ep_i}}{x} > \mu_{eo} \tag{5.10}$$

Therefore, the maximum sample filled length (x_{max}) without loss of any analyte is:

$$x_{max} = -\frac{\mu_{epi}}{\mu_{eo}} \tag{5.11}$$

Equation (5.11) indicates that if the relative injected plug length exceeds x_{max}, the total injected sample will not be stacked and some of it will be lost in the sample matrix removal process. Under this situation, different analytes with different electrophoretic mobilities will not be stacked in the same way, resulting in a bias similar to that observed with electrokinetic injection, where the injected amount depends on the electrophoretic

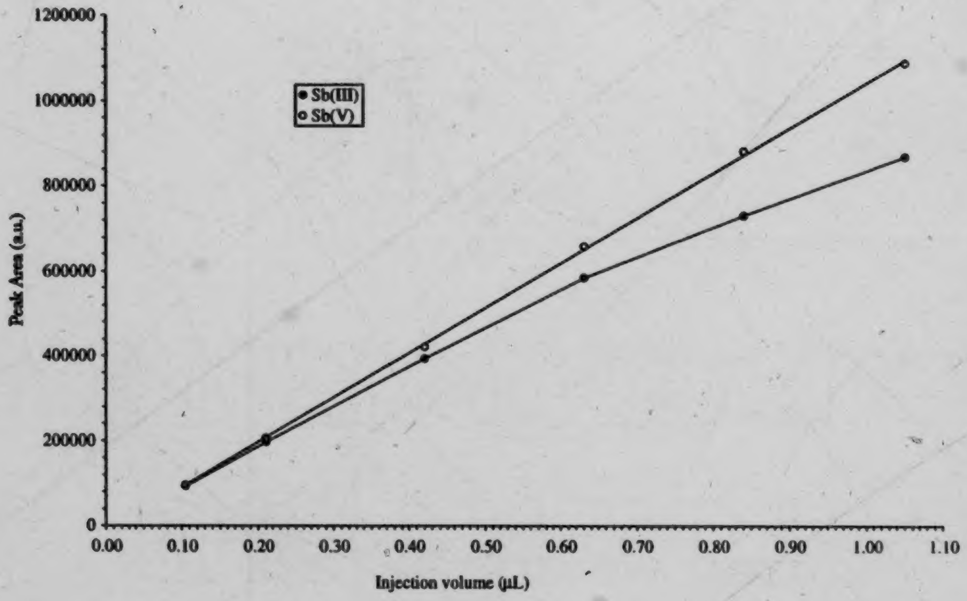

Figure 5.16 Plots of peak areas for Sb(III) and Sb(V) versus injection volume. Conditions as in Table 5.05

mobility of analyte [53]. This may account for the negative deviation from linearity for Sb(III) in Figure 5.16.

Although a larger injection volume leads to better sensitivity, discrimination of Sb(III) and Sb(V) may occur in the stacking process. Therefore, a sample volume of 0.63 μL was chosen as the appropriate injection volume in this study.

5.3.3 Quantitative Speciation

5.3.3.1 Calibration Curves

Under the optimized conditions, calibration curves for Sb(III) and Sb(V) were constructed over the concentration range 10-1000 ppb and are shown in Figure 5.17. Both Sb(III) and Sb(V) species exhibit a linear relationship between peak area and concentration over 2 orders of magnitude. The slopes of calibration curves on linear scales for Sb(III) and Sb(V) are 476.7±5.8 and 510.6±3.9 peak area (arbitrary units) per ppb Sb, respectively. The similar sensitivity indicates both species are efficiently converted to Sb^+ in the ICP regardless of the oxidation states, which is expected for such a high temperature ion source as ICP. The slight difference might be due to the bias nature of the sample stacking process (see Section 5.3.3.7). It may be interesting to note that slightly different sensitivities for Sb(III) and Sb(V) have also been observed in speciation studies using an HPLC-ICP-MS system [4, 29]. Lintschinger et al. [29] suggested that the difference in sensitivity might be caused by the different vaporization, atomization and/or ionization of the antimony compounds in the ICP.

5.3.3.2 Limits of Detection

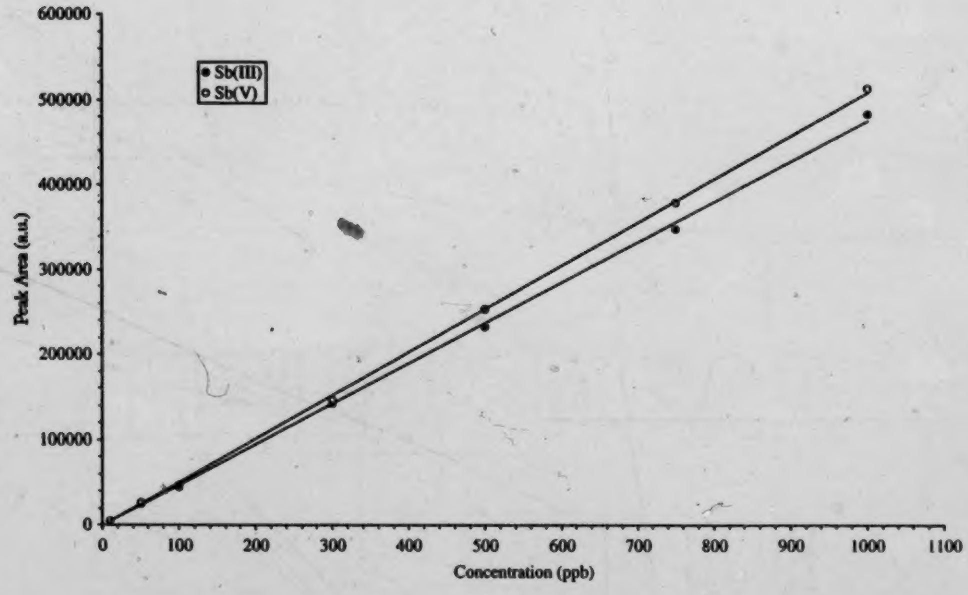

Figure 5.17 Calibration curves for Sb(III) and Sb(V). Conditions: running buffer, 20 mM EDTA at pH 4.6; sample, 0.4 mM EDTA at pH 5.6; injection volume, 0.63 μL; stacking voltage, -20 kV; separation voltage, +20 kV.

Detection limits were defined as the concentration that produces a net signal equivalent to three times the standard deviation of the blank signal. Peak area was used for quantification. Peak areas were obtained by integrating the intensities of the data points across the peak and were background corrected. To obtain the standard deviation of the background for peak area, five to seven electropherograms of the background were acquired. The intensities of the data points (equal in number to the points across the peak) from the baseline were added up for each electropherogram, and the standard deviation of the added baseline points was calculated. The detection limit was calculated as three times the standard deviation of the peak area of the background divided by the slope of the calibration curve (peak area vs. concentration). The repeatability was determined by making five consecutive injections of a standard solution containing 100 ppb each of Sb(III) and Sb(V). The relative standard deviations (RSDs) of the peak areas and migration times were calculated. The detection limits (concentration and absolute), along with slopes of log-log plot, linear dynamic range and repeatability are listed in Table 5.06.

Compared with the speciation method using CE-UV detection [37], the present method has concentration detection limits ~500 times lower. The detection limits are comparable to those reported by Michalke and Schramel [38] using CE-ICP-MS detection, but the resolution problem caused by the broad peak shape of Sb(III) tatrate was successfully solved in the present method. Compared with the HPLC methods (Table 5.01), the concentration detection limits of this method are either comparable or better depending on the detection system. But our absolute detection limits are generally better because of the much smaller sample loading in CE.

5.3.3.3 Speciation of Antimony in Synthetic Standard Mixtures

Table 5.06 Analytical figures of merit for the speciation of antimony (III) and antimony (V) by CE-DIN-ICP-MS[a]

Analyte	Sb(III)	Sb(V)
Linear dynamic range (ppb)	10-1000	10-1000
Slope of log-log plot	1.00	1.00
Correlation coefficient	0.999	0.999
Detection limit[b] concentration (ppb)	0.22	0.17
Detection limit[b] absolute (pg)	0.14	0.11
Repeatability (RSD%)[c] peak area	2.3	1.8
Repeatability (RSD%)[c] migration time	2.2	2.1

[a] Conditions as in Fig.5.18.

[b] Detection limits based on peak area.

[c] Repeatability based on 100 ppb solution.

Table 5.07 Quantitative speciation of Sb(III) and Sb(V) in synthetic standard mixtures

Concentrations of Sb in standard mixtures (ppb)		Found (ppb)[a]			
		with external standardization		with internal standardization[b]	
Sb(III)	Sb(V)	Sb(III)	Sb(V)	Sb(III)	Sb(V)
40.0	10.0	36.3±1.3	9.6±0.8	39.5±1.4	10.4±0.4
10.0	40.0	9.3±0.7	35.9±0.5	10.0±0.6	37.5±0.8
400.0	100.0	399.3±2.4	97.1±4.9	392.7±4.6	95.4±3.1
100.0	400.0	101.7±3.5	346.1±7.7	101.6±1.5	341.5±9.6

[a] Value expressed as mean ± standard deviation for three determinations.

[b] As(V) was used as the internal standard.

The validity of the proposed method was evaluated by determination of Sb(III) and Sb(V) in several synthetic standard mixtures since there is yet no certified reference material available. The results are listed in Table 5.07. The recoveries using external standardization are generally comparable to those using internal standardization (arsenate was used as the internal standard) although it may appear that better recovery was obtained at the 10 ppb level using internal standard. In both cases satisfactory results were obtained indicating that the proposed method is accurate and suitable for the speciation of Sb(III) and Sb(V) in water samples at the ppb level.

5.4 Conclusions

A method for quantitative speciation of inorganic antimony by CE-DIN-ICP-MS has been developed. The problem caused by the broad peak shape of the Sb(III)-tartrate complex was solved by converting it into the EDTA complex. On-line concentration by large volume sample stacking using polarity switching was shown to be an effective technique for sensitivity enhancement and for the simultaneous determination of Sb(III) and Sb(V). The optimal conditions for speciation of Sb(III) and Sb(V) were established by a systematic optimization of the various parameters. Good repeatability and linearity were observed. Linear dynamic ranges extended over two orders of magnitude. Concentration detection limits were obtained at the ~0.2 ppb level and absolute detection limits were at the ~0.1 pg level. Compared with the literature method for antimony speciation using a CE –UV system, the present method has a concentration detection limit two to three orders of magnitude lower. Compared with the HPLC methods for antimony speciation, the present method has concentration detection limits that are comparable or better, and absolute detection limits are generally better than those methods. The accuracy of the method was verified by determination of Sb(III) and Sb(V) in synthetic standard mixtures using both internal and external standardization.

5.5 References

1. Steinnes, E., Hvatum, O., and Bolviken, B., *Environ. Biogeochem. Eco. Bull.*, 1983, **35**, 351.
2. Groth, D. H., Stettler, L. E., Burg, J. R., Busey, W. E., Grant, G. C., and Wong, L. J., *J. Toxicol. Environ. Health*, 1986, **18**, 607.
3. Lide, D. R., Ed., *Handbook of Chemistry and Physics*, 78th Edition, CRC Press, New York, 1997-1998.
4. Smichowski, P., Madrid, Y., de la Calle Guntinas, M. B., and Camara, C., *J .Anal. At. Spectrom.*, 1995, **10**, 815.
5. Smichowski, P., Madrid, Y., and Camara, C., *Fresenius J. Anal. Chem.*, 1998, **360**, 623.
6. Subramanian, K. S., and Merangur, J. C., *Anal. Chim. Acta*, 1981, **124**, 131.
7. Chung, C.-H., Iwamoto, E., Yamamoto, M., Yamamoto, Y., *Spectrochim. Acta.*, 1984, **39B**, 459.
8. Sato, S., *Talanta*, 1985, **32**, 341.
9. de la Calle Guntinas, M. B., Madrid, Y., and Camara, C., *Anal. Chim. Acta*, 1991, **247**, 7.
10. Mori, I., Fujita, Y., Toyota, M., Kato, K., Fujita, K., and Okazaki, Y., *Talanta*, 1 991, **38**, 343.
11. Menendez Garcia, A., Perez Rodriguez, M.C., Sanchez Uria, J.E., Sanz-Medel, A., *Fresenius J. Anal. Chem.*, 1995, **353**, 128.
12. de la Calle Guntinas, M. B., Madrid, Y., and Camara, C., *J .Anal. At. Spectrom.*, 1993, **8**, 745.
13. Smichowski, P., de la Calle Guntinas, M. B., Madrid, Y., Cobo, M. G., and Camara, C., *Spectrochim. Acta,* Part B., 1994, **49**, 1049.

14. Madrid, Y., Cabrera, C., Perez-Corona, T., and Camara, C., *Anal. Chem.*, 1995, **6 7**, 750.

15. Garbos, S., Bulska, E., Hulanicki, A., Shcherbinina, N. I., and Sedykh, E.M., *Anal. Chim. Acta*, 1997, **342**, 167.

16. Garbos, S., Rzepecka, M., Bulska, E., and Hulanicki, A., *Spectrochim. Acta,* 1999, **54B**, 873.

17. Frank, T., and Neeb, R., *Fresenius J. Anal. Chem.*, 1987, **327**, 670.

18. Waller, P. A., and Pickering, W., *Talanta,* 1995, **42**, 197.

19. Wagner, W., Sander, S., and Henze, G., *Fresenius J. Anal. Chem.*, 1996, **354**, 11.

20. Nakashima, S., *Analyst*, 1980, **105**, 732.

21. Andreae, M. O., Asmode, J.-F., Foster, P., and Van't dack, L., *Anal. Chem.*, 1981, **53**, 1766.

22. Yamamoto, M., Urata, K., and Yamamoto, Y., *Anal. Lett.*, 1981, **14**, 21.

23. Yamamoto, M., Urata, K., Murashige, K., Yamamoto, Y., *Spectrochim. Acta,* 1981, **36B**, 671.

24. Nakahara, T., and Kikui, N., *Anal. Chim. Acta*, 1985, **172**, 127.

25. de la Calle Guntinas, M. B., Madrid, Y., and Camara, C., *Fresenius' J. Anal. Chem.*, 1992, **343**, 597.

26. Rondon, C., Burguera, J. L., ., Burguera, M., Brunetto, M. R., Gallignani, M., and Petit de Pena, Y., *Fresenius J. Anal. Chem.*, 1995, **353**, 133.

27. Hou, H.-B., and Narasaki, H., *Anal. Sci.*, 1998, **14**, 1161.

28. Feng, Y.-L., Narasaki, H., Chen, H.-Y., and Tian, L.-C., *Anal. Chim. Acta*, 1999, **386**, 297.

29. Lintschinger, J., Koch, I., Serves, S., Feldmann, J., and Cullen, W. R., *Fresenius J. Anal. Chem.*, 1997, **359**, 484.

30. Zhang, X., Cornelis, R., and Mees, L., *J. Anal. At. Spectrom.*, 1998, **13**, 205.

31. Ulrich, N., *Anal. Chim. Acta*, 1998, **359**, 245.

32. Ulrich, N., *Fresenius J. Anal. Chem.*, 1998, **360**, 797.

33. Lintschinger, J., Schramel, O., and Kettrup, A., *Fresenius' J. Anal. Chem.*, 1998, **361**, 96.

34. Lindemann, T., Prange, A., Dannecker, W., and Neidhart, B., *Fresenius' J. Anal. Chem.*, 1999, **364**, 462.

35. Dabek-Zlotorzynska, E., Lai, E. P. C., and Timerbaev, A. R., *Anal. Chim. Acta*, 1998, **359**, 1.

36. Timerbaev, A. R., Dabek-Zlotorzynska, E., and van den Hoop, M. A. G. T., *Analyst*, 1999, **124**, 811.

37. Casiot, C., Alonso, M. C. B., Biosson, J., Donard, O. F. X., and Potin-Gautier, M., *Analyst*, 1998, **123**, 2887.

38. Michalke, B., and Schramel, P., *J. Chromatogr. A*, 1999, **834**, 341.

39. de la Calle Guntinas, M. B., Madrid, Y., and Camara, C., *Fresenius J. Anal. Chem.*, 1992, **344**, 27.

40. Cotton, F. A., and Wilkinson, G., *Advanced Inorganic Chemistry*, 5th Edition, Wiley-Interscience, New York, 1988.

41. Baes, C. F., and Mesmer, R. E., *The Hydrolysis of Cations*, John Wiley and Sons, New York, 1976, pp. 370-374.

42. Gress, M. E., and Jacobson, R.A., *Inorg. Chim. Acta*, 1974, **8**, 209.

43. Burgi, D. S., and Chien, R. L., *Anal. Chem.*, 1991, **63**, 2042.

44. Chien, R. L., and Burgi, D.S., *Anal. Chem.*, 1992, **64**, 1046.

45. Chien, R. L., and Burgi, D.S., *Anal. Chem.*, 1992, **64**, 489A.

46. Albin, M., Grossman, P. D., and Moring, S. E., *Anal. Chem.*, 1993, **65**, 489A

47. Burton, L. L., and Horlick, G., *Spectrochim. Acta*, 1992, **47B**, 1627.

48. Blandamer, M. J., Burgess, J., and Peacock, R. D., *J. Chem. Soc. Dalton*, 1974, 1084.

49. Hjerten, S., *Electrophoresis*, 1990, **11**, 665.

50. Jandik, P., and Bonn, G., *Capillary Electrophoresis of Small Molecules and Ions*, VCH, New York, 1993, pp. 70-74.

51. Jorgenson, J. W., Lukacs, K. D., *Anal. Chem.*, 1981, **53**, 1298.

52. Harris, D. C., *Quantitative Chemical Analysis,* 3rd Edition, W. H. Freeman and Company, New York, 1991.

53. Huang, X., Gordon, M. J., and Zare, R.N., *Anal. Chem.*, 1988, **60**, 377.

Chapter 6

Quantitative Speciation of Arsenic

6.1 Introduction

Arsenic is an element that is ubiquitous in the natural environment and is commonly found in soil and rocks, waters, the atmosphere, plants and animals. Arsenic enters into the aquatic and terrestrial environments as a result of natural sources such as weathering and erosion of rock and soil, and through human activities. Anthropogenic sources include mining and refining of precious metals, the use of arsenical pesticides and herbicides, the burning of fossil fuels and the disposal of domestic and industrial waste [1]. Arsenic levels in Canadian surface waters are typically < 2 ppb. However, higher concentrations of arsenic (mean levels of about 45 ppb) have been reported in surface waters in the vicinity of gold-mining or ore-roasting operations [1].

The determination of arsenic species is of importance for environmental studies because its toxicity and biological activity are closely related to its chemical form and/or the oxidation states involved. It is well known that the toxicity of arsenic species decreases going from the purely inorganic forms, such as arsenite [As(III)] and arsenate [As(V)], to the more organometallic forms such as arsenobetaine $[(CH_3)_3As^+CH_2CO_2^-]$ and arsenocholine $[(CH_3)_3As^+CH_2CH_2OH]$. Arsenite and arsenate are the most toxic water-soluble species of arsenic, and arsenite is considered to be more toxic than arsenate. Arsenobetaine and arsenocholine, commonly found in marine organisms and seafood, are not bioavailable but rapidly excreted from the body and therefore are regarded as essentially non-toxic [2].

Canadians are exposed to inorganic arsenic in food, drinking water, soil and ambient air, with food representing the major source of intake [1]. While food contains both inorganic and organic arsenic species, primarily inorganic forms (arsenite and arsenate) are present in water [3-5]. Exposure to arsenic at high levels poses serious health effects, as it is a known human carcinogen. Studies suggest that exposure to drinking water that contains high level of arsenic increase the risk of skin cancer, and tumors of the bladder, kidney, liver and lung [1,6,7]. In the USA, the Maximum Contaminant Level (MCL) for total arsenic in drinking water is currently set at 50 ppb. The US EPA is considering lowering this MCL to as low as 2 ppb [8].

Given the diversity in toxicity of arsenic species, the determination of total arsenic concentration does not provide an adequate measure of its impact on the environment and human health. Quantitative arsenic speciation in water is required to provide valuable information for a meaningful exposure assessment and for the protection of human health. Arsenic speciation also plays an important role in development of effective methods for arsenic removal from drinking water as it has been shown that better removal efficiency is obtained when arsenic is in the As(V) form using the co-precipitation method [9].

Arsenic speciation has been the subject of extensive research for more than two decades. Numerous methods have been developed. Several review articles [3,10-13] and book chapters [2,14,15] dealing with arsenic speciation have been published. The most frequently used method is the hyphenation of HPLC with atomic spectrometry detection, such as AAS [16-21], AFS [22-25], ICP-AES [26-28], and ICP-MS [29-46]. The excellent sensitivity and element specificity of ICP-MS makes HPLC-ICP-MS one of the most promising techniques for arsenic speciation. Moreover, the sensitivity in the detection of arsenic species can be improved substantially by using hydride generation

(HG) as the sample introduction technique. HPLC-HG-ICP-MS has the best reported detection limits (1.1 ppt for arsenate and 0.5 ppt for arsenite) [46].

Capillary electrophoresis (CE) as a separation technique has several advantages: highly efficient separation, small sample and buffer volume requirements and fast analysis time. Compared with HPLC methods, CE has another important advantage: lack of a stationary phase, which exerts only minor disturbance on the existing equilibrium between different species [47,48]. These unique properties make CE an attractive technique for arsenic speciation.

Table 6.01 is a summary of the CE methods available to date for the determination of arsenic species. As seen from the table, arsenic speciation has been achieved using CE interfaced to a variety of detection systems, such as direct UV [50, 52-54, 58, 60, 61, 65, 66, 70], indirect UV [49, 51, 56, 63,], conductivity [58], indirect LIF [67], ICP-AES [69], ICP-MS [55, 57, 62, 64, 68, 71, 72,], and ESI-MS [73]. Although on-column detection schemes using UV, LIF, and conductivity are simple and easy to implement, they lack sufficient sensitivities to determine arsenic speciation in the ultra-trace level (1 ppb or below). In order to improve the sensitivity of UV detection for arsenic, some authors [54, 60, 61, 70] have utilized sample pre-concentration techniques (large volume sample stacking). Even with these techniques, the sensitivity of UV detection is still insufficient to detect arsenic species at the ppb level. Based on the available CE methods reported (Table 6.01), it can be reasonably concluded that ICP-MS is the only detection system that yields limits of detection at the ppb level or lower. The coupling of CE with ICP-MS requires an efficient interface. A number of different interfaces have been developed, most of which were based on modification of commercial nebulizers such as concentric [55,68], direct injection (DIN) [57], ultrasonic [64], or microconcentric nebulizers [71,72]. A hydride generation (HG) system was also developed to couple CE

Table 6.01 Summary of CE methods for speciation of As(III) and As(V)

CE method	Interfacing technique	Detection system	Detection limits (ppb)		References
			As(III)	As(V)	
CZE	On-column detection	Indirect UV (254 nm)	a	a	Wildman et al., 1991 [49]
CZE	On-column detection	Direct UV(190 nm)	a	a	Morin et al., 1992 [50]
CZE	On-column detection	Indirect UV(254 nm)	a	a	Vogt and Werner, 1994 [51]
CZE	On-column detection	Direct UV(190 nm)	a	a	Lopez-Sanchez et al., 1994 [52]
CZE	On-column detection	Direct UV(190 nm)	~1000	~1000	Albert et al., 1995 [53]
CZE (sample stacking with sample matrix removal)	On-column detection	Direct UV(195 nm)	–	25	Li and Li, 1995 [54]
CZE	Concentric nebulizer	ICP-MS	1	1	Olesik et al., 1995 [55]
CZE	On-column detection	Indirect UV(274 nm)	400-2000	400-2000	Lin et al., 1995 [56]
CZE	Direct injection nebulizer (modified Microneb 2000)	ICP-MS	0.1	0.02	Liu et al., 1995 [57]
CZE	On-column detection	Conductivity Direct UV(200 nm)	72 90	40 60	Schlegal et al., 1996 [58]
CZE(sample stacking with polarity switching)	On-column detection	Direct UV(195 nm)	a	~125	Albert et al., 1997 [60]
CZE(sample stacking without polarity switching)	On-column detection	Direct UV(195 nm)	a	a	Albert et al., 1997 [61]
CZE	Hydride generation	ICP-MS	0.017	0.017	Magnuson et al., 1997 [62]
CZE	On-column detection	Indirect UV(254 nm)	304	89	Casiot et al., 1998 [63]

Table 6.01 (continued)

CZE	Ultrasonic nebulizer (Cetac)	ICP-MS	95	84	Kirlew et al., 1998 [64]
CZE	On-column detection	Direct UV(185 nm)	100	150	Van den Broeck et al.,1998 [65]
CZE	On-column detection	Direct UV(200 nm)	~200	~200	Greschonig et al., 1998 [66]
CZE	On-column detection	Indirect LIF λ_{ex} (488 nm), λ_{em}(520 nm)	160	70	Huang and Whang, 1998 [67]
CZE with two step procedure	Modified Meinhard nebuliser	ICP-MS	15	15	Michalke and Schramel, 1998 [68]
CZE	Hydride generation	ICP-AES	320	320	Tian et al., 1998 [69]
CZE (sample stacking with sample matrix removal)	On-column detection	Direct UV(192 nm)	350	479	Gil et al., 1999 [70]
CZE	Microconcentric nebulizers (MCN-100 and MicroMist)	ICP-MS	2.1	1.3	Van Holderbeke, et al., 1999 [71]
CZE	Modified microconcentric nebulizers (MCN-100)	ICP-SFMS	~1	~1	Prange and Schaumloffel, 1999 [72]
CZE	Electrospray ionisation	MS	1600	51000	Schramel et al., 1999 [73]

[a] Not reported.

With ICP-MS for arsenic speciation [62]. It appears that DIN and HG have the best detection limits reported (Table 6.01).

In this study, the quantitative speciation of As(III) and As(V) in water using CE-ICP-MS with a laboratory-constructed direct injection nebulizer interface is presented. To increase the sensitivity and resolution, a method of on-line concentration by sample stacking with sample matrix removal was used. The method of field-amplified electrokinetic injection with suction flow balanced EOF was also studied. Several CE operating parameters such as sample size, buffer pH, stacking and separation voltage and injection volume were optimized. The analytical performance of the method, in terms of linear dynamic range, detection limits and repeatability, were evaluated.

In aqueous solution arsenic mainly exists in the III or V oxidation states. The pentavalent state is predominant and stable in air-saturated water, while the trivalent state is predominant under moderate reducing conditions common in ground water [74]. In dilute solutions (< 0.1 M), As(III) exists probably as several mononuclear species $As(OH)_3$, $As(OH)_2O^-$, $As(OH)O_2^{2-}$, and AsO_3^{3-} based on Raman evidence [74,75]. The ionization behavior of arsenious acid resembles that of boric acid, a monobasic acid, the ionization equilibrium can be represented as [74]:

$$As(OH)_3\,(aq) + H_2O \Leftrightarrow As(OH)_4^- + H^+ \qquad \log K_1 = -9.29 \qquad (6.01)$$

It should be noted there has been disagreements over the formulas of arsenious acid and arsenite in literature. Some authors use $HAsO_2$ to represent arsenious acid and AsO_2^- to represent arsenite. But Raman studies found no evidence of the presence of such species in aqueous solution [75]. However, the use of $As(OH)_4^-$ to represent arsenite is uncommon in the literature, so in this study, $As(OH)_2O^-$ or $H_2AsO_3^-$ have been used to represent arsenite species in water. A graphical representation of the species distribution of Equation (6.01) between the pH ranges of 1 and 14 is shown in Figure 6.01a.

Arsenic (V) forms arsenic acid (H_3AsO_4) whose properties resemble those of phosphoric acid (H_3PO_4). Arsenic acid is tribasic and dissociates in solution to give species $H_2AsO_4^-$, $HAsO_4^{2-}$, and AsO_4^{3-}. The dissociation equilibria along with acid dissociation constants [76] are summarized below:

$$H_3AsO_4 \Leftrightarrow H_2AsO_4^- + H^+ \qquad pK_1 = 2.26 \qquad (6.02)$$

$$H_2AsO_4^- \Leftrightarrow HAsO_4^{2-} + H^+ \qquad pK_2 = 6.76 \qquad (6.03)$$

$$HAsO_4^{2-} \Leftrightarrow AsO_4^{3-} + H^+ \qquad pK_3 = 11.29 \qquad (6.04)$$

Based on Equation (6.02-6.04), the species distribution under different pHs can be calculated and the resulting composition diagram for arsenic (V) is shown in Figure 6.01b.

6.2 Experimental

6.2.1 Chemical Reagents

All chemicals were of analytical reagent grade and were used as received. De-ionized water (18 MΩ cm) was obtained by purifying distilled water with a Milli-Q water purification system (Millipore, Bedford, MA). Standard stock solutions (1000 ppm) of As(III) were prepared by dissolving appropriate amounts of sodium arsenite ($NaAsO_2$) (BDH, Poole, UK) in de-ionized water. Standard stock solutions (1000 ppm) of As(V) were prepared by dissolving appropriate amounts of sodium arsenate ($Na_2HAsO_4 \cdot 7H_2O$)

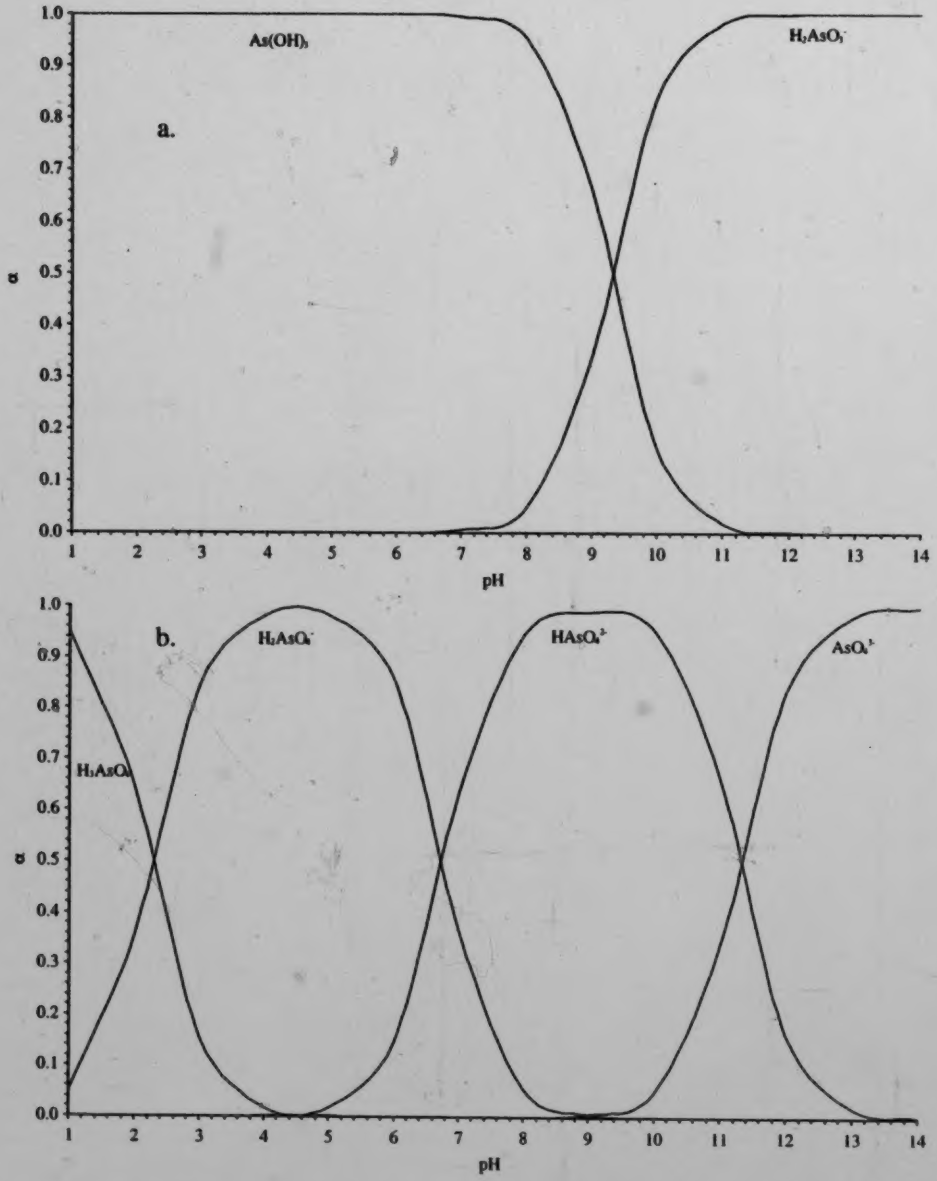

Figure 6.01 Fractional composition diagrams for (a) arsenic(III) and (b) arsenic(V) as a function of pH in dilute aqueous solution.

(Fischer Scientific, Fair Lawn, NJ) in de-ionized water. Both standard stock solutions of arsenic were stored refrigerated in polyethylene bottles at 4°C in the dark. Fresh working standard solutions were prepared daily by appropriate mixing and diluting of the stock standard solutions. Stock buffer solutions of $Na_2B_4O_7 \cdot 10H_2O$ (BDH, Poole, UK), $NH_4H_2PO_4$ (BDH, Toronto, ON), and potassium hydrogen phthalate (BDH, Toronto, ON) were prepared by dissolving appropriate amounts of each in de-ionized water. All buffer solutions were de-aerated before use.

6.2.2 Instrumentation

A laboratory-constructed CE system was used. A 76-cm long fused silica capillary (Polymicro Technologies, Phoenix, AZ) with an inner diameter of 50 μm and an outer diameter of 182 μm was used as the electrophoresis capillary. A Model CZE1000R high voltage power supply (Spellman, Hauppauge, NY) was used to provide the stacking and separation voltage. With this power source, polarity switching can be completed within 1.5 seconds at the 20 kV level. The capillary outlet end was grounded by means of a sheath flow liquid (2% HNO_3). A 74900 series syringe pump (Cole-Parmer, Niles, IL) was used to deliver the sheath liquid.

A laboratory-constructed direct injection nebulizer was used as the interface to connect CE to ICP-MS. The design and optimization of this interface has been described in detail in Chapter 2.

A Perkin-Elmer SCIEX ELAN 5000A ICP-MS instrument (Thornhill, ON, Canada) was used as the detector. The arsenic isotope m/z 75 was monitored as a function of time in the graphic mode of the instrument. Electropherogram data were collected using a 200 ms dwell time and one point per peak. Data analysis was performed after the data were copied to a Microsoft Excel spreadsheet. Peak areas were calculated using a program written in Visual Basic. The ICP-MS operating parameters and optimization have been described in Chapter 2.

An ORION Model 420A pH Meter (Orion Research Inc., Beverly, MA) was used to measure pH. The pH probe (Orion Triode Combination Electrode) was calibrated just before use using three buffer solutions (Fisher, Nepean, ON) with pH 4, 7 and 10.

6.2.3 Sample Injection

Sample solutions were injected using either hydrodynamic or electrokinetic injection. Hydrodynamic injections were obtained by nebulizer suction. Sample injection volume was estimated by the method as described previously (Chapter 3). In the electrokinetic injection mode, a high voltage (-20 kV) was applied to the inlet end of the capillary for 60 seconds to force the anions into capillary. However, since EOF is directed toward the inlet buffer reservoir, the introduced ions would be pushed out from the injection end of the capillary by EOF. This problem can be solved by application of the suction-induced flow toward detector to counterbalance the EOF. The applications will be discussed in Section 6.3.5.

6.3 Results and Discussion

6.3.1 Choice of pH of Sample and Buffer

As can be seen from Figure 6.01, the arsenic species distribution depends strongly on the pH of the sample solution. At pH higher than about 11, As(III) exists mainly as the singly charged anionic species $H_2AsO_3^-$, while at pH below about 7 it exists mainly as the uncharged species $As(OH)_3$. Since there is no electrostacking effect for uncharged species in CE, sample pH 11 appears to be necessary for effective sample pre-concentration of As(III) by electrostacking. At pH 11, As(V) exists primarily as the double charged anion $HAsO_4^{2-}$. The different apparent charges of the As(III) and As(V) lead to different electrophoretic mobilities, which should allow their separation in CE. Experiments confirmed that a sample pH of 10-11 is the optimum pH range for the CE separation of As(III) and As(V). There is a stability concern associated with the analysis of As(III) in alkaline pH range, because in alkaline solutions As(III) as $H_2AsO_3^-$ is a moderate reducing agent that can be converted to As(V) by air oxidation. Therefore samples were immediately analyzed after the pH adjustment.

The pH of the buffer is an important factor that affects the separation of As(III) and As(V). The apparent charges and thus, the electrophoretic mobility of arsenic anions depend on pH. The charges on the silica surface and thus, the electroosmotic flow also depend on pH. In this study pH 10-11 was chosen as the buffer pH for arsenic speciation.

6.3.2 Sample Stacking without Removal of Sample Matrix

In order to improve the sensitivity, a method of on-line concentration by large volume stacking was used. Figure 6.02 is an electropherogram for a solution containing 1 ppm As(III) and 1 ppm As(V) dissolved in de-ionized water, with the pH adjusted to 11.0 using NaOH. The running buffer is 20 mM phosphate at pH 11.0. A volume of 0.63 μL of the sample was injected into the capillary. A positive voltage of +20 kV was applied to the capillary inlet end. In order to visualize the sample plug, VO_3^- was added to the running buffer and the ^{51}V signal was monitored. Since no VO_3^- was added to the sample, the signal drop of VO_3^- indicates the location of the sample plug in the capillary. As seen from Figure 6.02, both As(III) as $H_2AsO_3^-$ and As(V) as $HAsO_4^{2-}$ were stacked up at the

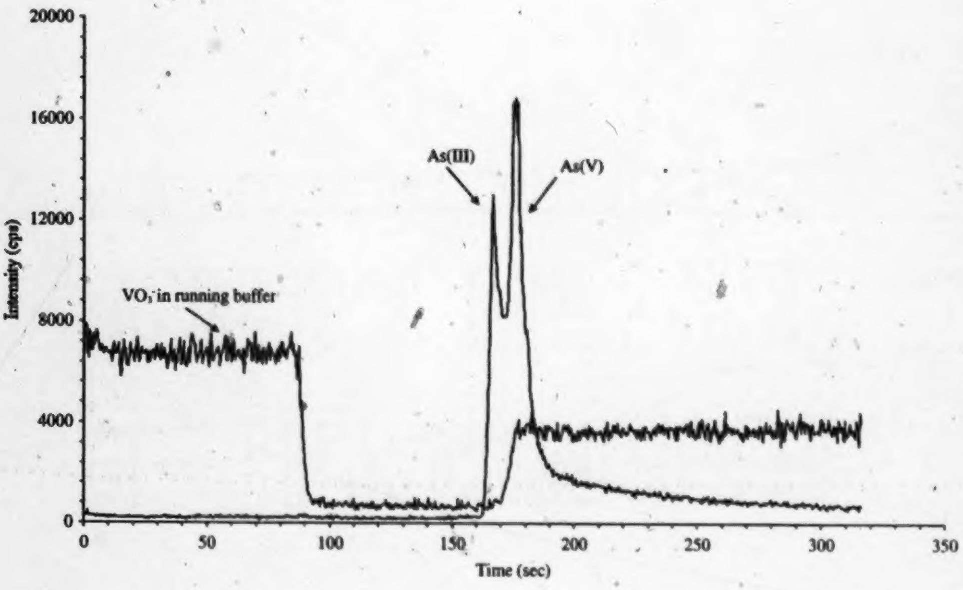

Figure 6.02 Electropherogram for a sample solution containing As(III) and As(V) at 1 ppm each. Conditions: running buffer, 20 mM phosphate at pH 11.0; sample pH, 11.0; applied voltage, +20 kV; injection volume, 0.63 µL.

rear of the sample plug as predicted by the model described in Chapter 3. However, without removal of the sample matrix, the As(III) and As(V) can not be baseline resolved. This is because when the low conductivity sample plug is in the capillary, almost all the separation potential is dropped across the sample plug, and the field strength over the buffer region approaches zero. When analyte ions migrate out of the sample plug into the buffer, their electrophoretic velocities will be zero. Consequently, all analyte ions will move only with the bulk flow, and no further separation can occur. The different signal levels of VO_3^- before and after the sample plug is also a result of this field strength re-distribution. The signal level of VO_3^- is determined by the bulk flow rate (υ_b) which can be expressed as

$$\upsilon_b = \upsilon_{suc} + \upsilon_{eof} - \upsilon_{ep} \tag{6.05}$$

where υ_{suc} is suction flow rate, υ_{eof} is the electroosmotic flow, and υ_{ep} is the electrophoretic velocity of VO_3^- whose direction is opposite to the bulk flow. When the low conductivity sample plug is in the capillary, υ_{ep} of VO_3^- in the buffer is so small that $\upsilon_b = \upsilon_{suc} + \upsilon_{eof}$. After the low conductivity sample matrix exits the capillary, all the voltage is dropped across the buffer, υ_{ep} of VO_3^- becomes higher so that $\upsilon_b < \upsilon_{suc} + \upsilon_{eof}$, resulting in lower signal level of VO_3^-. From the above discussion, it is evident that in order to increase the separation efficiency, the low conductivity sample matrix must be removed from the capillary to eliminate the field strength inhomogeneity before CE separation can occur. This can be achieved by sample stacking with polarity switching.

6.3.3 Sample Stacking with Removal of Sample Matrix

The technique of sample stacking with removal of sample matrix by polarity switching has been described in Chapter 5, so here it will be only briefly reviewed. First, a long sample plug with low conductivity is injected into the capillary. Then a negative voltage (–15 kV) is applied to the injection side. The sample matrix is pushed out by EOF at the same time as the anions stack up at the sample-buffer interface. The current initially remains low as the more conductive running buffer is replacing the low conductivity sample plug. When most of the sample plug has been removed, the current increases rapidly to the normal value of the buffer solution. The polarity should be switched just before the current plateau is reached to avoid loss of the stacked analytes. In the experiment, the optimum switching point was found to be when the current reached 90% of the normal value.

Figure 6.03a is a demonstration of the separation of As(III) and As(V) using this technique. The test solution contained 100 ppb each As(III) and As(V) at pH 10.0. The buffer was 20 mM $Na_2B_4O_7$ at pH 10.0. Borate buffer was used instead of phosphate because it was found that phosphate buffer generally contains significant arsenic impurities. A volume of 0.63 μL of the sample was injected into the capillary. Good resolution and peak shape for As(III) and As(V) were obtained (Fig.6.03a). Compared with the individual standard injections under the same experimental conditions shown in Fig. 6.03b and c, the peaks in Fig. 6.03a can be easily identified. That As(III) as $H_2AsO_3^-$ came out earlier than As(V) as $HAsO_4^{2-}$ is expected because the former has smaller apparent charge and thus slower electrophoretic velocity toward the injection side.

6.3.3.1 Effect of Stacking and Separation Voltage on the Arsenic Separation

The effects of stacking voltage on arsenic separation were investigated. With an increase of the stacking voltage from –5 kV to –20 kV, no significant effect on peak areas for As(III) and As(V) was observed. On the other hand, increasing the stacking voltage did shorten the time needed for completing of the analyte stacking and sample matrix

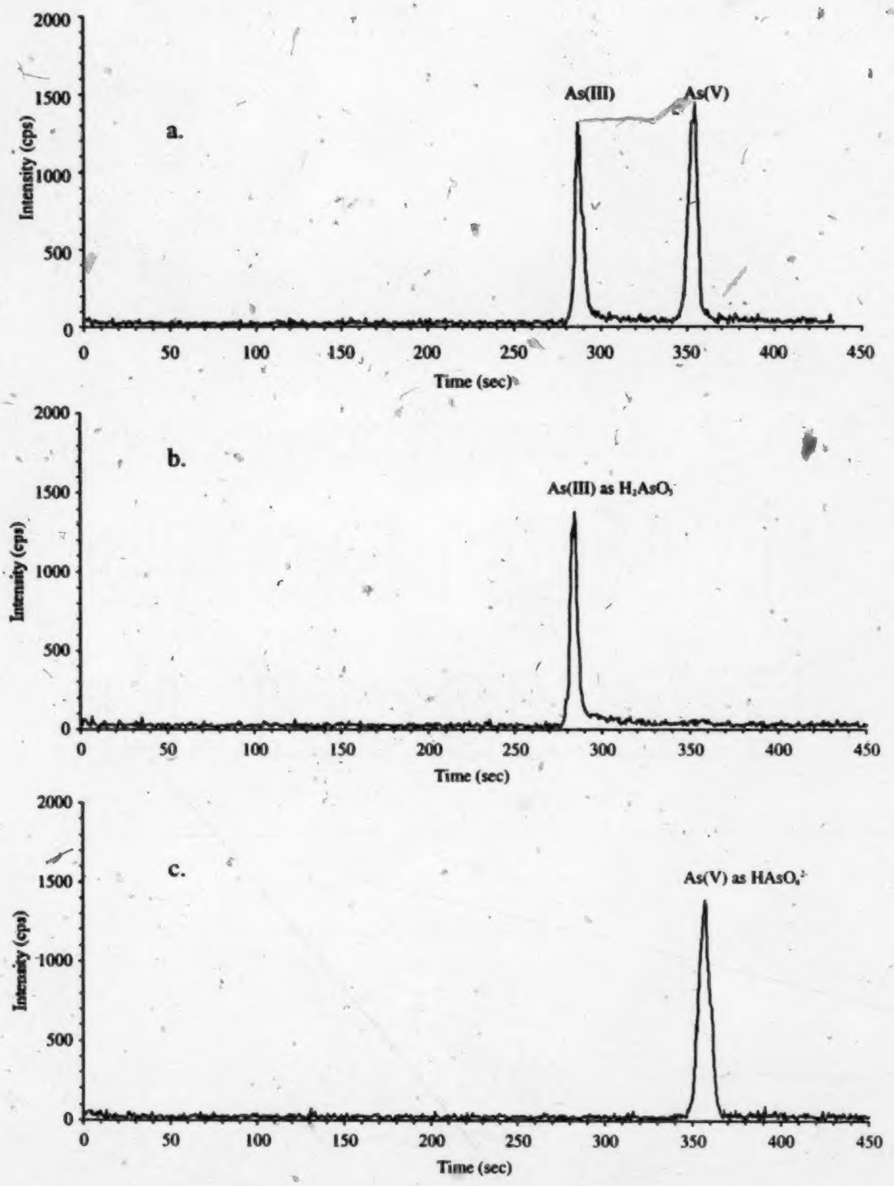

Figure 6.03 Electropherograms for solutions containing (a) 100 ppb each As(III) and As(V), (b) 100 ppb As(III), and (c) 100 ppb As(V). Conditions: running buffer, 20 mM $Na_2B_4O_7$ at pH 10.0; sample pH, 10.0; stacking voltage, -15 kV; separation voltage, +20 kV; injection volume, 0.63 μL.

removal. However, monitoring the current also became more difficult because the current rise at the final stage of stacking was too fast. A voltage of –15 kV was therefore selected as the stacking voltage in this study.

The effects of separation voltage on arsenic separation were also studied. Figure 6.04 shows the influence of separation voltage on the arsenic separation. Increasing the separation voltage from 10 kV to 25 kV decreased the migration times for both As(III) and As(V). The migration time (t_m) can be expressed as

$$t_m = \frac{L}{[\upsilon_{suc} + (\mu_{eof} - \mu_{ep})E]} \qquad (6.06)$$

where L is the total length of capillary and E is the field strength (E = V/L). Under the present experimental conditions it was found that $\mu_{eof} > \mu_{ep}$ and consequently the term $(\mu_{eof} - \mu_{ep}) > 0$ in Equation (6.06). Therefore increasing the voltage resulted in shorter migration times. Increasing the separation voltage from 10 kV to 20 kV increased peak resolution. However, the resolution of peaks was reduced at 25 kV. As a compromise, 20 kV was chosen as the separation voltage in this study.

6.3.3.2 Effect of Injection Volume on the Arsenic Separation

Six different injection volumes were studied: 0.11, 0.21, 0.42, 0.63, 0.84 and 1.05 μL corresponding to 7.0%, 14%, 28%, 42%, 56%and 70% of the total capillary volume, respectively. The samples were injected hydrodynamically. Injection volumes are estimated by calculation from the suction flow rate and injection time. The effects of injection volume on the arsenic separation are summarized in Figure 6.05 and Table 6.02. By increasing the injection volume (up to 0.84 μL), increases in peak area and peak height for both As(III) and As(V) were observed. The more the amount of sample

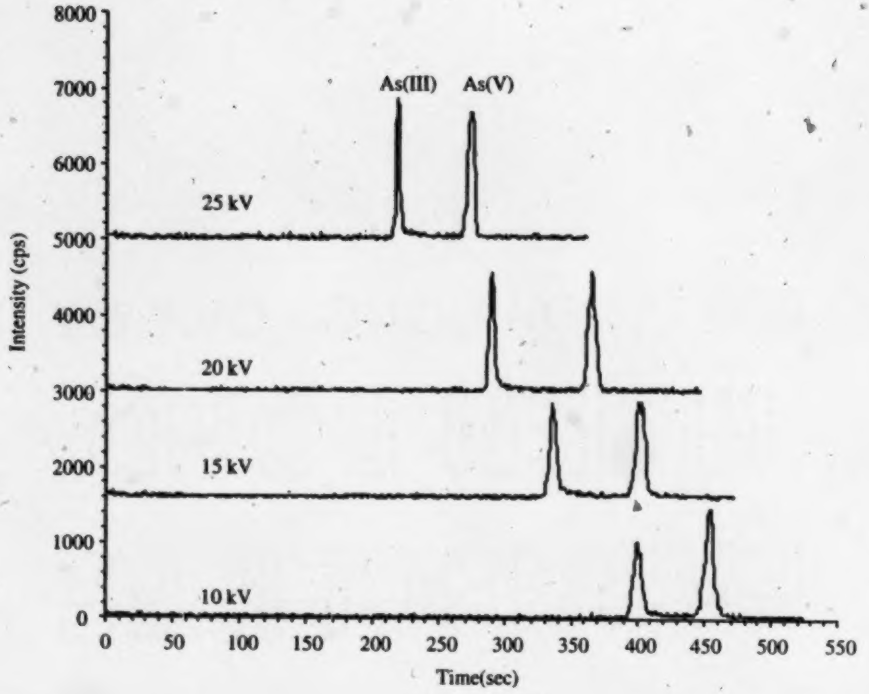

Figure 6.04 Electropherograms for a test solution containing 100 ppb each As(III) and As(V) with different separation voltages (10-25 kV) applied. Other conditions as in Fig. 6.03.

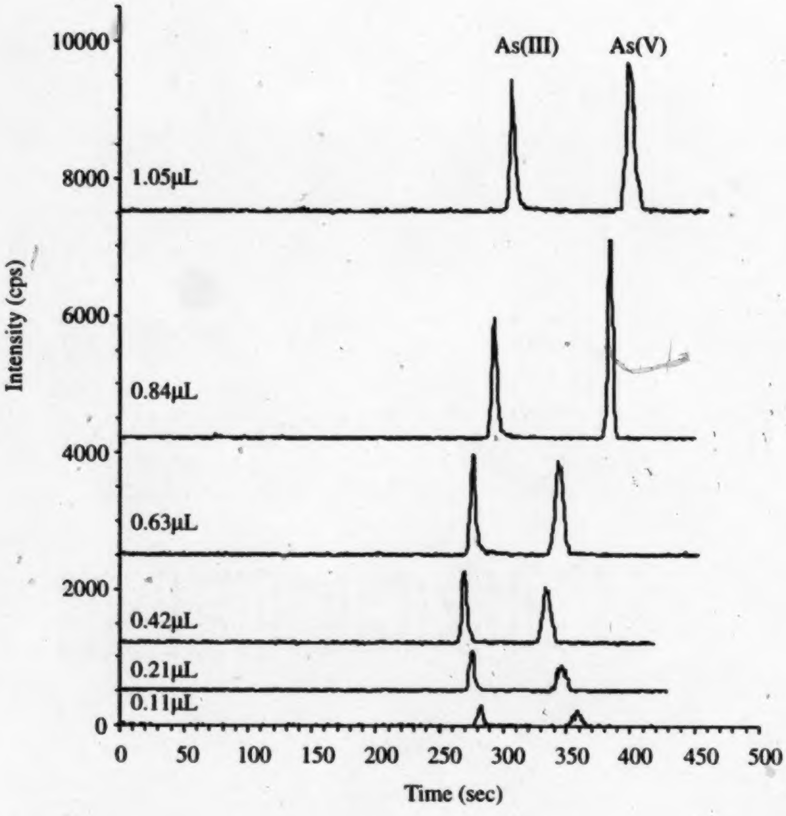

Figure 6.05 Electropherograms for a test solution containing 100 ppb each As(III) and As(V) with different injection volumes (0.11-1.05 μl). Other conditions as in Fig. 6.03.

Table 6.02 Effect of injection volume on peak area, peak height, peak width, and peak separation [a]

Injection time (sec)	injection volume (μL)	peak area($\times 10^4$) (a.u.)		peak height($\times 10^5$) (cps)		fwhm (s)		peak separation (s)
		As(III)	As(V)	As(III)	As(V)	As(III)	As(V)	
30	0.11	0.256	0.278	0.277	0.217	5	8	76
60	0.21	0.534	0.549	0.593	0.370	4	8	70
120	0.42	0.992	1.14	1.05	0.817	5	8	64
180	0.63	1.44	1.73	1.45	1.36	4	7	67
240	0.84	1.64	2.21	1.73	2.88	5	4	91
300	1.05	1.66	2.87	1.91	2.18	4	8	92

[a] Conditions as in Fig. 6.03.

injected, the greater the sensitivity of the analysis, as would be expected. No significant band broadening or loss of efficiency was observed with increasing the injection volume. The peaks for As(III) and As(V) were well resolved for each run. Since most of the sample matrix plug has been removed from the capillary, the migration times should be essentially the same for each run. As seen from Figure 6.05, the migration times are reasonably reproducible for injection volumes up to 0.63 µL, the slight difference is probably due to the different amounts of water which are left in the capillary for each run. However, at larger injection volumes (0.84 µL and 1.05 µL), the migration times were significantly longer. The reason for this upward shift in migration times is yet to be explained, but the entrance of the make up liquid (2% HNO_3) into the capillary during the sample plug back-out process is a possibility. When the acid enters the capillary from the outlet end, it will discharge the capillary wall, thereby reducing the EOF resulting in increased migration times.

Plots of peak areas for As(III) and As(V) versus injection volume are shown in Figure 6.06. A good linear relationship between the peak area and the injection volume for As(V) is observed, but the plot for As(III) starts to level off at about 0.63 µL injection volume. A similar phenomenon for Sb(III) and Sb(V) was observed in Chapter 5. The explanation there likely applies here. A sample volume of 0.63 µL was therefore chosen as the injection volume in this study.

6.3.3.3 Calibration Curves

Under the optimized experimental conditions, calibration graphs for As(III) and As(V) were obtained by plotting the peak areas against the concentration of each species in the range 10-1000 ppb and are shown in Figure 6.07. Both As(III) and As(V) species demonstrate a linear relationship between peak area and concentration over 2 orders of

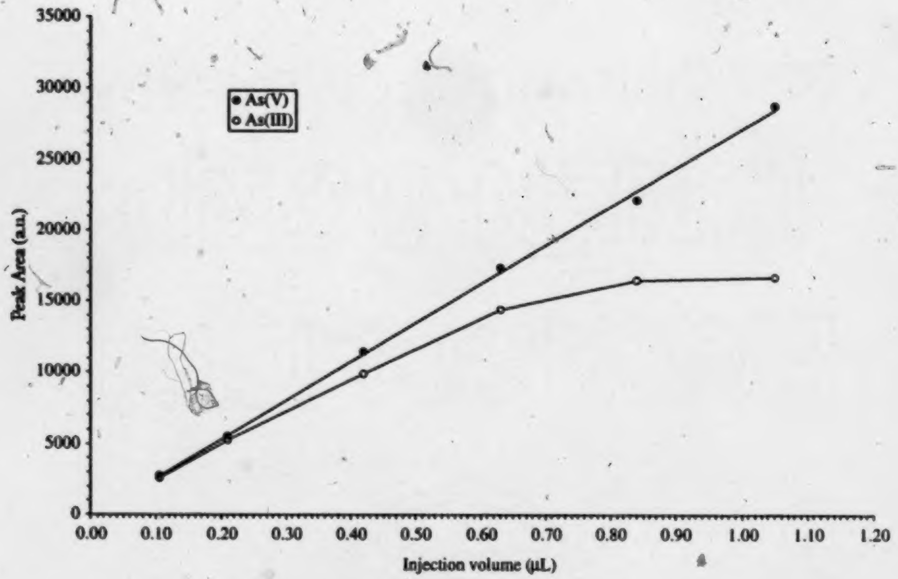

Figure 6.06 Plots of peak areas for As(III) and As(V) versus injection volumes. Conditions as in Fig. 6.05.

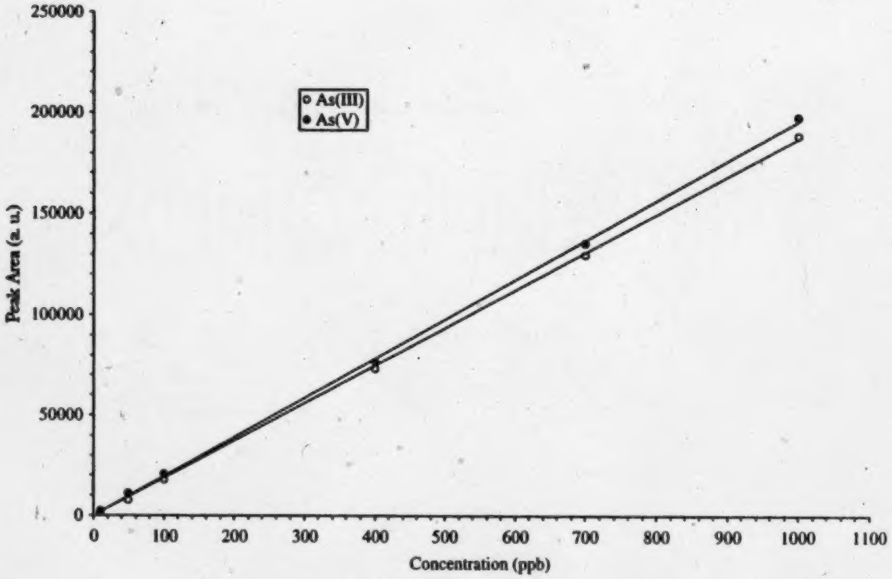

Figure 6.07 Calibration curves for As(III) and As(V). Conditions as in Fig.6.03.

magnitude. The slopes of calibration curves on linear scales for As(III) and As(V) are 188.2±1.0 and 194.9±1.8 peak area (arbitrary units) per ppb As, respectively. The similar sensitivity indicates both species are converted to As^+ with similar efficiency in the ICP regardless of the oxidation states, as would be expected for such a high temperature ion source as the ICP. The slight difference might be due to the bias nature of the sample stacking process.

6.3.3.4 Limits of Detection

Detection limits were defined as the concentration that produces a net signal equivalent to three times the standard deviation of the blank signal. Peak area was used for quantification. The standard deviation of peak areas of the blank was obtained from seven replicated injections of the blank. The detection limit was calculated as three times the standard deviation of the peak area of the blank divided by the slope of the calibration curve (peak area vs. concentration). The relative standard deviations (RSDs) of the peak areas and migration times were evaluated by making five consecutive injections of a standard solution containing 100 ppb each of As(III) and As(V). The detection limits (concentration and absolute), along with slopes of the log-log plot, linear dynamic range and repeatability (peak area and migration time) are listed in Table 6.03.

Compared with the arsenic speciation methods using CE-UV detection (Table 6.01), the present method has concentration detection limits 2 to 3 orders of magnitude lower. Compared with the CE-ICP-MS methods reported (Table 6.01), the detection limits of this method are either comparable or better.

6.3.4 On-line Concentration by Field-amplified Electrokinetic Injection

Table 6.03 Analytical figures of merit for arsenic speciation by CE-DIN-ICP-MS after sample stacking with sample matrix removal[a]

Analyte	As(III)	As(V)
Linear dynamic range (ppb)	10-1000	10-1000
Slope of log-log plot	1.05	0.95
Correlation coefficient	0.999	0.999
Detection limit[b] concentration (ppb)	0.23	0.22
Detection limit[b] absolute (pg)	0.14	0.14
Repeatability (RSD%)[c] peak area	4.4	4.5
Repeatability (RSD%)[c] migration time	0.6	0.9

[a] Conditions as in Fig.5.18.

[b] Detection limits based on peak area.

[c] Repeatability based on 100 ppb solution.

Electrokinetic injection is a well-known sample introduction technique in capillary electrophoresis [64,77-79]. In this technique, analyte ions are injected into the capillary under the influence of an electric field produced by the injection voltage applied to the sample reservoir. The major advantage of electrokinetic injection is that the sensitivity of the method can be several orders of magnitude higher than using hydrodynamic injection. The concepts of sample stacking discussed in previous chapters can also be applied to electrokinetic injection, leading to a method known as field-amplified sample injection [77]. In this section the preliminary results of the quantitative speciation of As(III) and As(V) are presented using a modified method of field-amplified sample injection.

The modified method of field-amplified sample injection is illustrated in Figure 6.08. First, a short plug of water is hydrodynamically injected into the capillary filled with high-conductivity buffer. This water plug is to ensure a high electric field at the point of injection (step a). Next anions are injected electrokinetically into the capillary by the application of a negative voltage (-20 kV) to the sample reservoir (step b). Since the electric field within the water plug is much higher than in the running buffer, the anions move quickly through the water plug and stack up at the water-buffer interface (step c). In the mean time, the negative injection voltage produces a bulk flow that is contributed from EOF of the water zone and EOF of the buffer zone. Since the direction of the EOF is toward the injection side of the capillary, water is moving out the capillary from the injection end. Consequently, there is a time limit for electrokinetic injection. The injection must stop before the injected ions are flushed back into the sample reservoir by EOF. To solve this problem, a suction flow opposite to the direction the EOF is applied during the electrokinetic injection. The EOF slows down as the water plug moves out of the capillary because the contribution to the EOF from the water plug is greater than that from the buffer. Eventually, the EOF is balanced with the suction flow, no further change in the water plug length can occur. When this occurs, the injection time can be arbitrarily

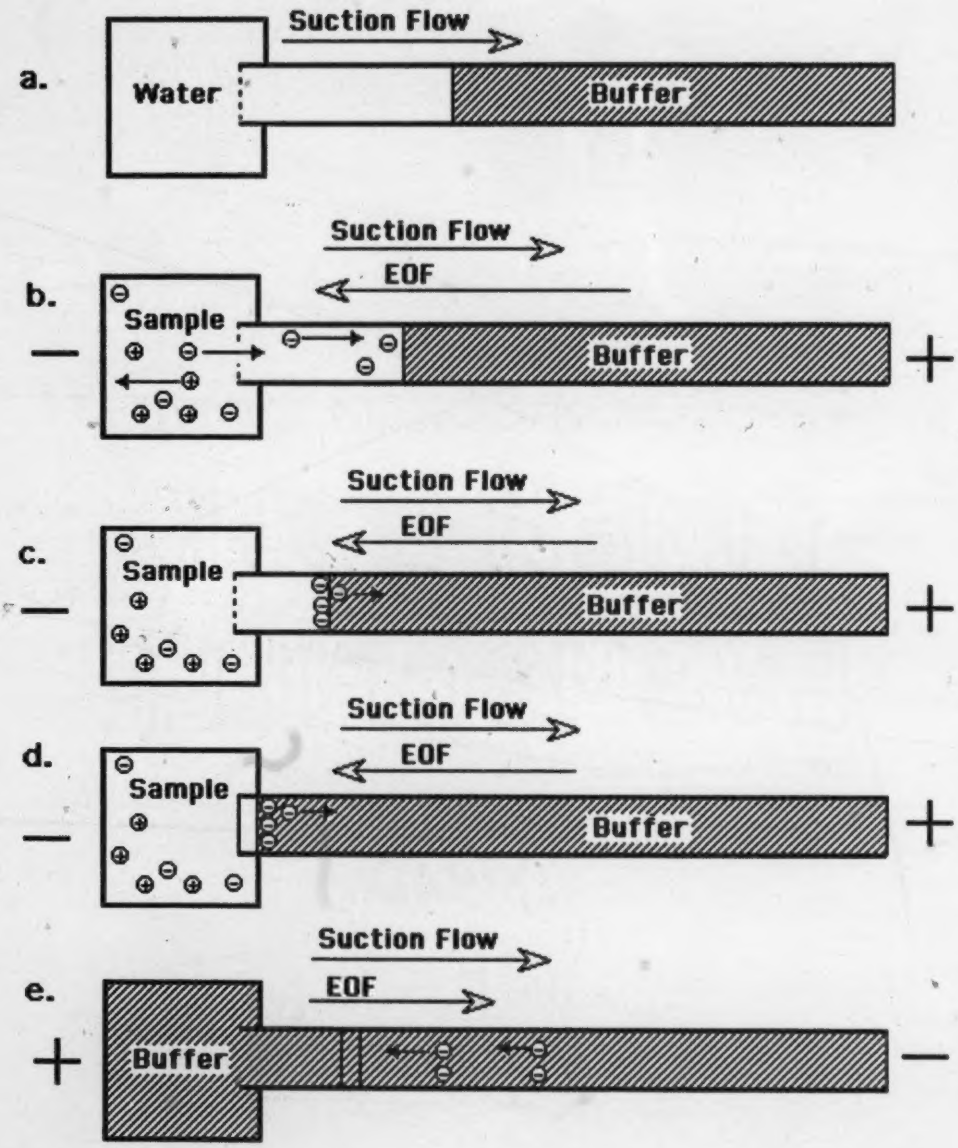
a.
Suction Flow
Water
Buffer
b.
Suction Flow
EOF
Sample
Buffer
−
+
c.
Suction Flow
EOF
Sample
Buffer
−
+
d.
Suction Flow
EOF
Sample
Buffer
−
+
e.
Suction Flow
EOF
Buffer
+
−

Figure 6.08 Schematic diagram showing the modified field-amplified sample injection: (a) hydrodynamic injection of water plug, (b) electrokinetic injection of sample, (c) pumping water plug out of capillary by EOF while the anions stack up at the boundary, (d) EOF balanced with suction flow, (e) normal CE separation after polarity switching.

chosen, without worrying about the loss of the injected ions (step d). Finally, the polarity of applied voltage is switched to positive (-20 kV→ +20 kV), the anion separation occurs under normal CE conditions (step e).

The final water plug left in the capillary has a significant effect on the CE separation. The water plug length must be sufficiently short otherwise the separation resolution will be degraded (Section 6.3.3). For a running buffer of 20 mM $Na_2B_4O_7$ at pH 10.0 and suction flow rate of 0.21 μL/min, good peak resolution for As(III) and As(V) was observed.

The quantitative speciation of As(III) and As(V) using the above method was evaluated. Calibration graphs for As(III) and As(V), linear over 2 orders of magnitude, were obtained and are shown in Figure 6.09. The slopes of calibration curves on linear scales for As(III) and As(V) are 541.0±4.6 and 846.9±6.7 peak area (arbitrary units) per ppb As, respectively. The different sensitivities of As (III) and As(V) are consistent with the nature of mobility bias of electrokinetic injection with which ions of high mobility are introduced into the capillary at higher rate than ions of low mobility [78,79] and do not appear to be due to the ionization efficiency in ICP.

The analytical figures of merit including detection limits, slope of log-log plot, linear dynamic range and repeatability (peak area and migration time) are summarized in Table 6.04. Compared to the method of sample stacking with sample matrix removal (hydrodynamic injection) discussed in Section 6.3.4, the present method of field-amplified electrokinetic injection has detection limits 3 to 5 times lower. Further improvement of the detection limits may be possible after systematic optimization of the latter method. The major limitation of the latter method is that its precision and accuracy are more strongly affected by experimental conditions than the former method.

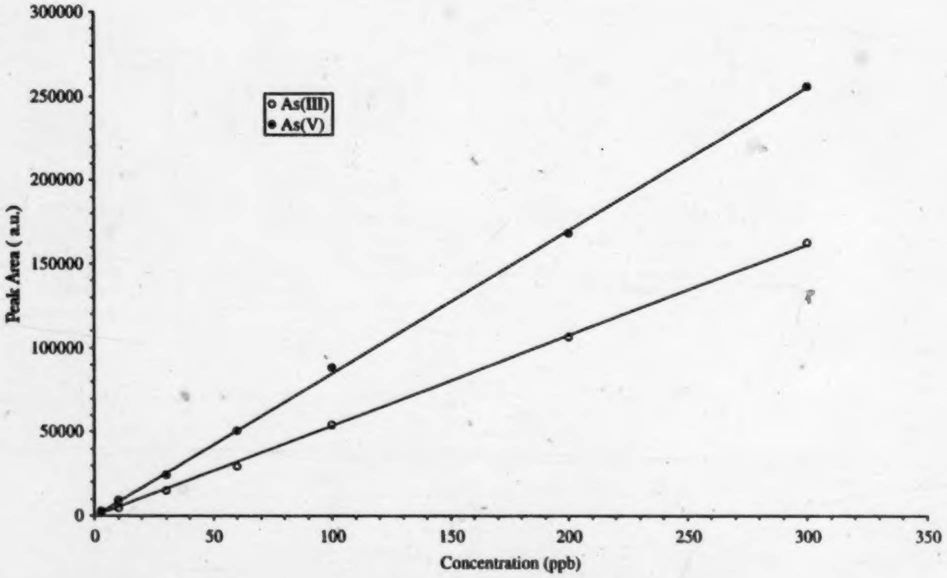

Figure 6.09 Calibration curves for As(III) and As(V) with the modified field-amplified electrokinetic injection. Conditions: running buffer, 20 mM Na_2B_4O, at pH 10.0, sample pH, 10.0; suction flow rate, 0.21 µL/min; injection voltage, -20 kV; injection time, 60 s; separation voltage, +20 kV.

Table 6.04 Analytical figures of merit for arsenic speciation by CE-DIN-ICP-MS with field-amplified electrokinetic injection[a]

Analyte	As(III)	As(V)
Linear dynamic range (ppb)	3-300	3-300
Slope of log-log plot	1.00	0.96
Correlation coefficient	0.998	0.999
Detection limit[b] concentration (ppb)	0.077	0.049
Repeatability (RSD%)[c] peak area	6.0	6.8
Repeatability (RSD%)[c] migration time	3.4	4.0

[a] Conditions as in Fig. 6.09

[b] Detection limits based on peak area.

[c] Repeatability based on 30 ppb solution.

6.4 Conclusions

The quantitative speciation of As(III) and As(V) in water using CE-ICP-MS with a laboratory-constructed direct injection nebulizer interface has been presented. The results demonstrate that CE-DIN-ICP-MS combined with sample stacking with sample matrix removal is an effective technique for the determination of inorganic arsenic speciation in water at ultra-trace level. Good linearity and good precision of peak areas and migration times were obtained. Linear dynamic ranges extended over two orders of magnitude. Concentration detection limits were at the ~0.2 ppb level and absolute detection limits were at the ~0.1 pg level. The detection limits can be reduced further to the low ppt level by using a modified method of field-amplified electrokinetic injection.

6.5 References

1 *Arsenic and its compounds*, Priority Substance List Assessment Report, Canadian Environmental Protection Act, Environment Canada, Ottawa, 1993.

2. Caoli, S., La Torre, F., Petrucci, F., and Violante, N., in *Element Speciation in Bioinorganic Chemistry*, Ed., Caroli, S., John Wiley & Sons, New York, 1996, pp.445-463.

3. Cullen, W. R., and Reimer, K. J., *Chem. Rev.,* 1989, **89**, 713.

4. Masscheleyn, P. H., Delaune, R. D., and Patrick Jr., W. H., *Environ. Sci. Technol.*, 1991, **25**, 1414.

5. Korte, N., *Environ. Geol. Water Sci.*, 1991, **18**, 137.

6. Chen, C. J., Chuang, Y., Lin, T. M., and Wu, H. T., *Cancer Res.*, 1985, **45**, 5895.

7. Smith, A. H., Duggan, H. M., Wood, R., Kosnett, M. J., and Smith, M.T., *Environ. Health Perspect.*, 1992, **97**, 259.

8. Frey, M. M., Owen, D. M., Chowdhury, Z. K., Raucher, R. S., and Edwards, M. A. *J. AWWA*, 1998, **90**, 89.

9. Brewster, M., *Water Environ.Technol.,* 1992, **11**, 54.

10. Morita, M., and Edmonds, J. S., *Pure Appl. Chem.,* 1992, **64**, 575.

11. Burguera, M., and Burgurea, J. L., *Talanta*, 1997, **44**, 1581.

12. Goessler, W., Schlagenhaufen, C., Kuehnelt, D., Greschonig, H., and Irgolic, K. I., *Appl. Organomet. Chem.*, 1997, **11**, 327.

13. Larsen, E. H., *Spectrochim. Acta,* Part B, 1998, **53**, 253.

14. Irgolic, K. J., in *Hazardous Metals in the Environment*, Ed., Stoeppler, M., Elsevier, Amsterdam, 1992, pp.287-350.

15. Dedina, J., and Tsalev, D. L., *Hydride Generation Atomic Absorption Spectrometry*, John Wiley & Sons, Chichester, 1995, pp.182-245.

16. Liu, Y. M., Fernadez-Sanchez, M. L., Blanco-Gonzalez, E. B., and Sanz-Medel, A., *J. Anal. At. Spectrom.*, 1993, **8**, 815.
17. Zhang, X., Cornelis, R., De Kimple, J., and Mees, L., *Anal. Chim. Acta*, 1996, **319**, 177.
18. Velez, D., Ybanez, N., and Montoro, R., *J. Anal. At. Spectrom.*, 1996, **11**, 271.
19. Howard, A. G., *J. Anal. At. Spectrom.*, 1997, **12**, 267.
20. Tsalev, D. L., Sperling, M., and Welz, B., *Analyst*, 1998, **123**, 1703.
21. Hsieh, C.-J., Yen, C.-H., and Kuo, M.-S., *Anal. Sci.*, 1999, **15**; 669.
22. Woller, A., Mester, Z., and Fodor, P., *J. Anal. At. Spectrom.*, 1995, **10**, 609.
23. Le, X. C., Ma, M., and Wong, N. A., *Anal. Chem.*, 1996, **68**, 4501.
24. Gomez-Ariza, J. L., Sanchez-Rodas, D., Beltran, R., Corns, W., and Stockwel, P., *Appl. Organomet. Chem.*, 1998, **12**, 439.
25. Ma, M., and Le, X. C., *Clin. Chem.*, 1998, **44**, 539.
26. Rauret, G., Rubio, R., Padro, A., *Fresenius J. Anal. Chem.*, 1991, **340**, 157.
27. Costa-Fernadez, J., Lunzer, F., Pereiro-Garcia, R., Sanz-Medel, A., and Bordel-28. Garcia, N., *J. Anal. At. Spectrom.*, 1995, **10**, 1019.
28. Elmoll, A., Heimburger, R., Lagarde, F., Leroy, M. J. F., and Maier, E., *Fresenius J. Anal. Chem.*, 1996, **354**, 550.
29. Larsen, E. H., Pritzl, D., and Hansen, S. H., *J. Anal. At. Spectrom.*, 1993, **8**, 557.
30. Larsen, E. H., Pritzl, D., and Hansen, S. H., *J. Anal. At. Spectrom.*, 1993, **8**, 1075.
31. Demesmay, C., Olle, M., and Porthault, M., *Fresenius J. Anal. Chem.*, 1994, **348**, 205.
32. Branch, S., Ebdon, L., and O'Neill, P., *J. Anal. At. Spectrom.*, 1994, **9**, 33.
33. Thomas, P., and Sniatecki, K., *J. Anal. At. Spectrom.*, 1995, **10**, 615.
34. Larsen, E. H., *Fresenius J. Anal. Chem.*, 1995, **352**, 582.
35. Guerin, T., Astruc, M., Batel, A., and Borsier, M., *Talanta*, 1997, 44, 2201.

36. Saverwyns, S., Zhang, X., Vanhaecke, F., Cornelis, R., Moens, L., and Dams, R., *J. Anal. At. Spectrom.*, 1997, **12**, 1047.

37. Thomas, P., Finnie, J. K., and Williams, J.G., *J. Anal. At. Spectrom.*, 1997, **12**, 1367.

38. Van den Broeck, K., Vandecasteele, C., and Geuns, J. M. C., *Anal. Chim. Acta*, 1998, **361**, 101.

39. Woller, A., Garraud, H., Boisson, J., Dorthe, A. M., Fodor, P. and Donard, O. F. X., *J. Anal. At. Spectrom.*, 1998, **13**, 141.

40. Moldovan, M., Gomez, M. M., Palacios, M. A., and Camara, C., *Microchem. J.*, 1998, 59, 89.

41. Zheng, J., Goessler, W., Kosmus, W., Mikrochim. Acta, 1998, 130, 71.

42. Lintschinger, J., Schramel, P., Hatalak-Rauscher, A., Wendler, I., and Michalke, B., *Fresenius J. Anal. Chem.*, 1998, **362**, 313.

43. Le, X. C., and Ma, M., *Anal. Chem.*, 1998, **70**, 1926.

44. Le, X. C., Li, X.-F., Lai, V., Ma, M., Yalcin, S., and Feldmann, J., *Spectrochim. Acta*, Part B., 1998, **53B**, 899.

45. Londesborough, S., Mattusch, J., and Wennrich, R., *Fresenius J. Anal. Chem.*, 1999, **363**, 577.

46. Taniguchi, T., Tao, H., Tominaga, M., and Miyazaki, A., *J. Anal. At. Spectrom.*, 1999, **14**, 651.

47. Dabek-Zlotorzynska, E., Lai, E. P. C., and Timerbaev, A. R., *Anal. Chim. Acta*, 1998, **359**, 1.

48. Timerbaev, A. R., Dabek-Zlotorzynska, E., and van den Hoop, M. A. G. T., *Analyst*, 1999, **124**, 811.

49. Wildman, B. J., Jackson, P. E., Jones, W. R., and Alden, P. G., *J. Chromatogr.*, 1991, **546**, 459.

50. Morin, P., Amram, M. B., Favier, S., Heimburger, R., and Leroy, M., *Fresenius J. Anal. Chem.*, 1992, **342**, 357.

51. Vogt, C., and Werner, G., *J. Chromatogr. A* , 1994, **686**, 325.

52. Lopez-Sanchez, J. F., Amram, M. B., Lakkis, M .D., Lagarde, F., Rauret, G., and and Leroy, J. F., *Fresenius J. Ana. Chem.*, 1994, **348**, 810.

53. Albert, M., Demesmay, C., and Rocca, J. L., *Fresenius J. Ana. Chem.*, 1995, **351**, 426.

54. Li, K., and Li, S. F. Y., *Analyst*, 1995, **120**, 361.

55. Olesik, J. W., Kinzer, J. A., and Olesik, S. V., *Anal. Chem.*, 1995, **67**, 1.

56. Lin, L., Wang, J., and Caruso, J., *J. Chromatogr. Sci.*, 1995, **33**, 177

57. Liu, Y., Lopez-Avila, V., Zhu, J. J., Wiederin, D. R., and Beckert, W. F., Anal. Chem., 1995, 67, 2020.

58. Schlegel, D., Mattusch, J., and Wennrich, R., *Fresenius J. Ana. Chem.*, 1996, **354**, 535.

59. Magnuson, M. L., Creed, J. T., and Brockhoff, C. A., *Analyst*, 1997, **122**, 1057.

60. Albert, M., Debusschere, L., Demesmay, C., and Rocca, J. L., *J. Chromatogr. A*, 1997, **757**, 281.

61. Albert, M., Debusschere, L., Demesmay, C., and Rocca, J. L., *J. Chromatogr. A*, 1997, **757**, 291.

62. Magnuson, M. L., Creed, J. T., and Brockhoff, C. A., *J. Anal. At. Spectrom.*, 1997, **12**, 689.

63. Casiot, C., Alonso, M. C. B., Biosson, J., Donard, O. F. X., and Potin-Gautier, M., *Analyst*, 1998, **123**, 2887.

64. Kirlew, P. W., Castillano, M. T. M. and Caruso, J. A., *Spectrochim. Acta,* 1998, **53B**, 221.

65. Van den Broeck, K., and Vandecasteele, C., *Mikrochim. Acta*, 1998, **128**, 79.

66. Greschonig, H., Schmid, M.G., and Gubitz, G., *Fresenius J. Ana. Chem.*, 1998, **362**, 218.

67. Huang, Y. M., and Whang, C. W., *Electrophoresis*, 1998, **19**, 2140.

68. Michalke, B., and Schramel, P., *Electrophoresis*, 1998, **19**, 2220.

69. Tian, X.-D., Zhuang, Z.-X., Chen, B., and Wang, X.-R., *Analyst*, 1998,**123**, 899.

70. Gil, E. P., Ostapczuk, P., and Emons, H., *Anal. Chim. Acta,* 1999, 389, 9.

71. Van Holderbeke, M., Zhao, Y., Vanhaecke, F., Moens, L., Dams, R., and Sandra, P., *J. Anal. At. Spectrom.*, 1999, **14**, 229.

72. Prange, A., and Schaumloffel, D., *J. Anal. At. Spectrom.*, 1999, **14**, 1329.

73. Schramel, O., Michalke, B., and Kettrup, A., *J. Anal. At. Spectrom.*, 1999, **14**, 1339.

74. Baes, C. F., and Mesmer, R. E., *The Hydrolysis of Cations*, John Wiley and Sons, New York, 1976, pp.366-370.

75. Loehr, T. M., and Plane, R. A., *Inorg. Chem.,* 1968, **7**, 1708.

76. Lide, D. R., Ed., *Handbook of Chemistry and Physics*, 78th Edition, CRC Press, New York, 1997-1998.

77. Chien, R.-L., and Burgi, D. S., *Anal. Chem.*, 1992, **64**, 489A.

78. Huang, X., Gordon, M. J., and Zare, R.N., *Anal. Chem.*, 1988, **60**, 377.

79. Krivacsy, Z., Gelencser, A., Hlavay, J., Kiss, G., and Sarvari, Z., *J. Chromatogr. A*, 1999, **834**, 21.

Chapter 7

Summary and Future Work

7.1 Summary

The combination of CE with ICP-MS has become an attractive technique for trace elemental speciation. The key to the successful hyphenation is the development of an efficient interface to couple CE with ICP-MS. A new Direct Injection Nebulizer (DIN) was designed and used for coupling CE with ICP-MS. Methods of speciation of chromium, vanadium, antimony and arsenic were developed and presented in this thesis.

7.1.1 DIN Interface for CE-ICP-MS

The design and optimization of the DIN interface for CE-ICP-MS was addressed in Chapter 2. A DIN is a microconcentric pneumatic nebulizer placed directly inside the ICP torch without using a spray chamber. Compared to conventional nebulizers using spray chambers, the DIN has several major advantages: 100% analyte transport efficiency, low sample consumption rate, low dead volume, fast sample washout and minimal memory effects. Although an expensive DIN system is now available commercially (CETAC Technologies), it can not be used directly for coupling CE with ICP-MS without modification [1]. We developed an inexpensive DIN interface for coupling CE with ICP-MS. Compared with the DIN interface reported previously [1], our DIN interface has two notable features. First, the positioning of the sheath flow capillary tip relative to the nozzle tip of the nebulizer tube is adjustable by turning a nut, therefore making it possible to optimize the aerosol generation and to achieve the maximum sensitivity. Second, there is a sheath gas (make-up) flow around the nebulizer tube, which helps to cool the sensitive nebulizer tip, protecting it from possible damage by the high temperature plasma. As a result of these features, a robust and efficient DIN interface was successfully built. In order to achieve the best performance, the interface was carefully optimized prior to CE separations. It has been demonstrated that the DIN interface is capable of providing stable nebulization and reproducible operations under different CE conditions such as different CE buffer systems and applied voltages, which ensures its successful application in speciation studies.

7.1.2 Speciation of Chromium and Vanadium

The quantitative speciation of Cr(III) and Cr(VI) using CE-DIN-ICP-MS was presented in Chapter 3. The separation of Cr(III) and Cr(VI) is based on the fact that they bear the opposite charges under certain pH conditions (e.g. pH 3) and migrate to the opposite directions in an electrical field. Separation can be achieved using sample stacking technique to focus the two species of opposite polarity to the opposite ends of a sample plug. It was found that a sample volume up to 54% of total capillary volume can be injected into the capillary without significant band broadening and both sensitivity and resolution of the Cr(III) and Cr(VI) peaks increased with increasing the length of the sample plug. The presence of a suction-induced flow toward the detector did not cause any significant band broadening; rather it allowed the simultaneous separation of both species in a single run in less than 8 min, without the need for sample pre-complexation or conversion. Linear calibration plots were established for both Cr(III) and Cr(VI) with dynamic ranges over at least four orders of magnitude. Good repeatability was observed. Concentration detection limits at the ppb levels and absolute detection limits at the pg levels were realized. Peak tailing of Cr(III) due to adsorption on the capillary wall is a potential problem but can be minimized by controlling the pH of the background electrolyte and sample within the acetic range (pH 2-3). Peak broadening due to high conductivity of sample matrix was observed but not extensively studied. Some methods that may help to reduce this matrix effect have been reported [2,3].

The aforementioned technique of CE-DIN-ICP-MS combined with sample stacking was also successfully applied to the quantitative speciation of vanadium, which was reported in Chapter 4. It was found that at sample pH ~3.0, vanadium (IV) exists primarily as the cationic species VO^{2+} and vanadium (V) exists mainly as the anionic species $H_2VO_4^-$. The opposite polarity allowed the separation of V(IV) and V(V) to be achieved using sample stacking technique. The method showed good repeatability and linearity in addition to wide linear dynamic range. Compared to other CE methods for vanadium speciation, the present method offers several advantages: lower detection limits, shorter analysis time and no sample pre-complexation or conversion necessary. The method was also successfully applied for multi-element speciation.

7.1.3 Speciation of Antimony and Arsenic

For element speciation where different oxidation forms are oppositely charged, the aforementioned technique, CE-DIN-ICP-MS combined with sample stacking, has been proved to be effective. However, for element speciation involving oxidation forms of similar charges, the application of the above technique is unsatisfactory because separation of similar charged ions in a stacked analyte band can not occur as long as the plug of low conductivity sample matrix remains in capillary. To separate Sb(III) and Sb(V), both of which exist as anions, a new technique of sample stacking with removal of sample matrix was introduced in Chapter 5. A problem associated with the use of Sb(III)-tartrate complex, $[Sb_2(C_4H_2O_6)_2]^{2-}$, as a standard for Sb(III) was the seriously broadened peak shape. The problem can be solved by converting it into the EDTA complex, $Sb(EDTA)^-$. The optimal conditions for speciation of Sb(III) as $Sb(EDTA)^-$ and Sb(V) as

$Sb(OH)_6^-$ were established by a systematic optimization of the various parameters. Concentration detection limits as low as ~0.2 ppb were obtained and the absolute detection limits were at the ~0.1 pg level. Those detection limits were improved by 2 – 3 orders of magnitude, relative to those obtained with the literature methods using CE–UV systems. Repeatability and linearity tests showed good results. The accuracy of the method was verified by determination of Sb(III) and Sb(V) in synthetic standard mixtures using both internal and external standardization.

The aforementioned technique, CE-DIN-ICP-MS combined with sample stacking with sample matrix removal, was also successfully applied to the quantitative speciation of inorganic arsenic, which was the focus of the research presented in Chapter 6. The analytical figures of merit obtained were generally comparable to those obtained with antimony speciation presented in Chapter 5. The detection limits can be reduced further to the lower ppt level by using a modified method of field-amplified electrokinetic injection.

7.2 Future Work

Extension of the speciation techniques developed in this thesis to the speciation of other elements is of great interest for future work. The immediate example is selenium, which is recognized as an essential element at low concentrations and toxic at higher concentrations for humans. Selenium may exist in the environment in several oxidation states in a variety of inorganic (e.g., selenite and selenate) and organic forms (e.g., seleno-amino acids) with different toxicological and biological properties. Therefore, there is a need for species selective quantification of selenium [4]. In aqueous solution of pH 5, selenite exists mainly as the single-charged anion $HSeO_3^-$, while selenate exists as the double-charged anion SeO_4^{2-}[4]. Therefore, they should be able to be separated using the method developed in Chapter 5. The speciation of other elements of environmental interests such as tin, iron, lead, mercury should also be pursued in the future. Modifications of existing methods would possibly need to be considered. For instance, to speciate the cationic species Sn(II) and Sn(IV) or Fe(II) and Fe(III), the method developed in Chapter 5 would need to be modified. In this case, positive voltage should be applied to the capillary inlet, and the direction of EOF should be reversed using a cationic surface modifier added to the CE buffer.

Modification of the CE-ICP interface to increase the nebulization efficiency and to lower the detection limits should be studied further. The effects of the interface design, the CE capillary length, and the CE capillary inner diameter on the suction-induced flow should be investigated in detail in order to control the suction flow rate to achieve the best compromise between resolution and analysis time. Finally the application of the developed methods to real-world samples such as environmental and biological samples should be pursued in future work.

CE-ICP-MS as a speciation technique has a major limitation. ICP-MS as an element specific detector is unable to directly detect molecular forms. Species identification is based solely on comparison of CE migration times with those of available standards. Cases in which the electrophoretic peaks are not successfully identified are possible (an example can be found in Chapter 5). A solution to this problem might be the development of a complementary technique, which is capable of providing both elemental and molecular detection capabilities. An example of such a technique is the hyphenation of CE to electrospray mass spectrometry (ES-MS) [5]. The combination of both CE-ICP-MS and CE-ES-MS systems for speciation analysis would be of great interest for future investigation.

7.3 References

1. Liu, Y., Lopez-Avila, V., Zhu, J. J., Weiderin, D. R., and Beckert, W. F., *Anal. Chem.*, 1995, **67**, 2020.
2. Ding, W., Thornton, M. J. and Fritz, J. S., *Electrophoresis*, 1998, **19**, 2133.
3. Gil, E. P., Ostapczuk, P., and Emons, H., *Anal. Chim. Acta*, 1999, **389**, 9.
4. Barnett, D., *PhD Thesis,* University of Alberta, Edmonton, Alberta, 1999.
5. Michalke, B., Schramel, O., and Kettrup, A., *Fresenius J. Ana. Chem.*, 1999, **363**, 456.